PETROLEUM RESEARCH JOURNAL

TECHNICAL PAPERS

ENGINEERING

Equation of state application to predict MMC and MMP for Raguba oil field, Libya.....
A.H. Al-Khafaji, M.M. Alswieh, S.T. Abuzbeda and S.O. Alabani 1

EXPLORATION

Tertiary – Quaternary alkaline – subalkaline magmatism in Gharyan area-field aspects and petrography.....
M.T. Busrewil and W.J. Wadsworth 13

Foraminiferal study of the Miocene from well D2-NC41, northwestern offshore, Libya..... *Ahmed K. Abusrewil* 25

The Pre-Cretaceous (Triassic) sequence in the subsurface of Maradah trough, eastern Sirt Basin, Libya.....
R.N. Sinha and H.B. Eland 49

CHEMISTRY

Models for the hydrogen-bonded water molecules to the chemisorbed oxyhydroxyl layer on the chromium surface..... *A.S. Al-Taie* 61

Evaluation of Sedra and Hamada crude oils for manufacturing of lube base stocks..... *Iftikar Ahmad, Adel Tuwil and Salem Debbah* 67

Production of glycerine by tungstate catalyzed oxidation of allyl alcohol by hydrogen peroxide: a kinetic and mechanistic study.....
Iftikar Ahmad and Masood Degam 75

VOLUME 8 - (1425)/(1996)

Petroleum Research Centre
P.O. Box 6431 Tripoli
Great Socialist People's Libyan Arab Jamahiriya

PRJ, Vol. 8 (January 1996); P. 1–11, 24 FIGS. 4 TABLES.

Equation of State Applieation to Predict MMC and MMP for Raguba Oil Field, Libya

A.H. Al-Khafaji*, M.M. Alswieh*, S.T. Abuzbeda*, and S.O. Alabani*

تطبيق معادلة الحالة للتنبؤ بالتركيب الإمتزاجي الأدنى والضغط الإمتزاجي الأدنى لنفط حقل الراقوبة ، ليبيا

علي حبيب الخفاجي ، محمد مسعود السويح ، صلاح الدين أبو زبيدة و سالم عمران العباني

تم في هذا البحث تمثيل عينتين من النفط المكمني بواسطة معادلة الحالة EOS لـ (بنك روبنسن) واستعمال منظومة (CMG-Prop). لقد طورت خصائص معادلة الحالة لكل من العينتين النفطيتين بهدف استنباط تراكيب المحاليل المثلى. أي الحد الأدنى للتركيب الإمتزاجي (MMC) لخليط محاليل الغاز السائل — الغاز الجاف والضغط الإمتزاجي الأدنى (MMP) لغاز ثاني أكسيد الكربون في الإفاضة المتجانسة. وجرى تنعيم عوامل معادلة الحالة لكي تتوافق مع البيانات الإختبارية للضغط والحجم والحرارة بالإضافة إلى اللزوجة لكلا العينتين النفطية. وعليه تم الحصول على الشكل البياني الطوري. والشكل الثلاثي الإجمالي والشكل لعلاقة الضغط — التركيب لكلا العينتين النفطية الملامسة مع تراكيب مختلفة من محاليل الغاز السائل — الغاز الجاف وكذلك غاز ثاني أوكسيد الكربون وفي درجة حرارة المكمن النفطي 206° ف.

وجد بأن الدفع المكثف هو الميكانيكية الرئيسة في استخراج النفط لكلا العينتين عند التركيب الإمتزاجي الأدنى للمحلول ، وحصل التجانس لهاتين العينتين مع ثاني أكسيد الكربون عند ضغط يعتبر عال نسبياً.

لقد ساعدت المعلومات أعلاه على تصميم اختبارات الإمتزاجية باستعمال الأنبوب الرفيع وكذلك اختبارات عملية الإنتفاخ.

Abstract *In this investigation, Peng-Robinson equation of state (EOS) modelling for two recombined reservoir oil samples is represented using the Computer Modelling Group (CMG PROP) software. EOS characterizations for these oils were developed to predict optimum solvent compositions-minimum miscibility composition (MMC) for LPG-Dry Gas mixtures, and minimum miscibility pressure (MMP) for CO_2 in miscible flooding. EOS parameters were tuned to match the experimental PVT data besides viscosity data for both oils. Accordingly, phase diagrams, pseudoternary diagrams and pressure-composition diagrams for both oils in contact with several LPG-Dry Gas compositions and/or CO_2 were generated at reservoir temperature of 206 °F.*

It was found that the main mechanism of oil recovery is a condensing drive for both oils at minimum miscibility composition. Miscibility of these oils with CO_2 was achieved at a pressure considerably high. These foundings were used to help design slim tube experiments as well as swelling experiments.

INTRODUCTION

Study of miscibility of different solvents and gases with reservoir oil is one of the most important processes to enhance oil recovery. Literatures on theoretical studies,[1,2,3,4,5] experimental laboratory investigations[6,7,8,9] and field applications[10,11] of miscibility are available. Miscibility is achieved at certain conditions of pressure and temperature depending on the composition of both the reservoir oil and the injected gases or solvents. There are generally two types of miscible processes, the first contact miscible (FCM),

* Petroleum Research Centre, P.O. Box 6431, Tripoli, G.S.P.L.A.J.

where solvent (LPG) mix directly with reservoir oil in all proportions and their mixtures always remain in a single phase. The second process is the multiple contact miscible (MCM) process-dynamic miscibility processes, where gases or solvents are not directly miscible with reservoir oil, but under a appropriate conditions of pressure, temperature and oil-gas or oil-solvent compositions, *in-situ* miscibility could be achieved through repeated contacts of the injected material with reservoir oil. The MCM is of three kinds: the vaporizing, the condensing and condensing/vaporizing miscible processes.

In the present investigation, equation of state (EOS) characterizations of two recombined oils (1800R & 2030R) were developed in order to predict the minimum miscibility composition (MMC) for rich-gas and minimum miscibility pressure (MMP) for CO_2 in miscible flooding processes. Peng-Robinson[12,13] cubic equation of state was applied for both oils. Equation of state parameters were tuned to match all available experimental data for these oils. Then, pseudoternary diagrams and pressure-composition diagrams for the oils in contact with several rich gas compositions and/or CO_2 were generated to figure out the mechanisms of oil recovery and the optimum compositions and pressures for gas injection with rich gas and/or CO_2. This information was used to help design slim tube experiments as well as swelling experiments. Once these experiments were completed then the EOS characterization can be revised and compositional simulation could be undertaken.

EXPERIMENTAL DATA

Experimental data were available for two recombined oils 1800R and 2030R with bubble point pressures of 1800 psia and 2030 psia respectively.[14,15] These oils were directly recombined from the separator gas and oil at a specific gas oil ratio (GOR). The two oils are essentially the same except that 2030R has a greater amount of solution gas. Thus, it should be possible to characterize the C_{7+} for the oils with the same pseudocomponents. For each oil the experimental data available include bubble point pressure-flash liberation, direct flash, recombination of separator oil and gas and differential liberation data.

SPLITTING OF C_{7+}

Since both oils are derived from the same source except for a difference in the amount of the solution gas, it should be possible to use one set of plus fraction components for both oils. In order to split the plus fraction of the two oils the molecular weight and specific gravity of the plus fraction are required. The molecular weight of the plus fraction can be calculated from the extended chromatographic analysis. The molecular weight of the plus fraction for both oils 1800R and 2030R were about 155. Specific gravity of the plus fraction for oil 1800R was estimated to be about 0.85 by using specific gravity of the stock tank oil that was 0.8201. This information was used to split the plus fraction into two pseudocomponents. The properties of the two pseudocomponents. The properties of the two pseudocomponents are shown on Table 1 for oil sample 1800R and 2030R. It was found that two pseudocomponents were adequate to model these oils because of the large amount of components present between C_7 and C_{13}.

TUNING OF EOS PARAMETERS

In order to assure the accuracy of EOS predictions of miscibility conditions for these two oils, the EOS parameters must first be tuned to match experimental data, then a more reliable analysis of recovery mechanism and miscibility conditions may be made. The tuning is accomplished using the regression option in CMG PROP. The regression variables are critical pressure and temperature, the volume shifts of methane, and the C_{7+} components. Also, the binary interaction coefficient exponent and the molecular weights of the C_{7+} components were used as regression variables as represented in Table 1. These variables were adjusted to match the experimental data for both oils including the bubble point pressures, the flash liberation data, the differential liberation data, and the separator flash data. A high weight was given to matching the bubble point pressure data since the match of all the other experiments depended on having an accurate bubble point pressure. After several different regression runs, a good match of the experimental data was achieved. The final values of the regression variables and the match of the experimental data are shown on Tables 3 & 4. An acceptable match of the results for both oils was achieved (Figs. 1–13).

GENERATION OF PHASE DIAGRAMS AND DETERMINATION OF MISCIBILITY CONDITIONS

Using the tuned EOS parameters, the conditions for miscibility and the mechanism of oil recovery can be analyzed using multiple contact ternary diagrams as well as pressure-composition and pressure-temperature diagrams. First, the pressure-temperature diagrams were generated for both oils (Fig. 14). These diagrams are consistent with the typical diagrams for black oils with the reservoir temperature much lower

Table 1. EOS components properties for reservoir oils 1800R and 2030R at 206 F, Raguba oil field, Well No. E40.

Component	*MW*	*Critical Pressure*	*Critical Temperature*	*Critical Volume*	*Acentric Factor*	*Volume Shift*	*Interaction Coefficient* Hydrocarbon and*		*Critical Volume***		*Oil Composition Mole Fraction*	
									1800R	*2030R*		
		Pc, Atm.	*Tc, K*	*Vc, l/gmol*	*AC*		*N2*	*CO2*	*Vc, l/gmol*	*Vc, l/gmol*	*1800R*	*2030R*
N2	28.01	33.50	126.20	8.950E-02	4.000E-02	−1.284E-01		−2.08E-02	8.950E-02	8.950E-02	2.08E-03	2.57E-03
CO_2	44.01	72.80	304.20	9.400E-02	2.250E-01	−9.435E-02	−2.08E-02		9.400E-02	9.400E-02	5.89E-03	6.34E-03
C1	16.04	46.73	164.73	9.900E-02	8.000E-03	−1.237E-01	3.10E-02	1.03E-01	9.900E-02	9.900E-02	2.08E-01	2.31E-01
C2	30.07	48.20	305.40	1.480E-01	9.800E-02	−1.021E-01	4.20E-02	1.30E-01	1.480E-01	1.480E-01	7.53E-02	7.80E-02
C3	44.10	41.90	369.80	2.030E-01	1.520E-01	−7.330E-02	9.10E-02	1.35E-01	2.030E-01	2.030E-01	7.53E-02	7.50E-02
iC4	58.12	36.00	408.10	2.630E-01	1.760E-01	−5.707E-02	9.50E-02	1.30E-01	2.630E-01	2.630E-01	2.49E-02	2.44E-02
nC4	58.12	37.50	425.20	2.550E-01	1.930E-01	−5.706E-02	9.50E-02	1.30E-01	2.550E-01	2.550E-01	6.85E-02	6.65E-02
iC5	72.15	33.40	460.40	3.060E-01	2.270E-01	−3.446E-02	9.50E-02	1.25E-01	3.060E-01	3.060E-01	3.46E-02	3.34E-02
nC5	72.15	33.30	469.60	3.040E-01	2.510E-01	−3.443E-02	9.50E-02	1.25E-01	3.040E-01	3.040E-01	3.80E-02	3.66E-02
FC6	86.00	30.26	563.61	3.440E-01	2.750E-01	−4.227E-03	1.20E-01	1.50E-01	3.440E-01	3.440E-01	5.37E-02	5.15E-02
C7–C13	138.85	23.72	706.99	4.755E-01	3.403E-01	2.258E-01	1.20E-01	1.50E-01	5.706E-01	5.706E-01	3.20E-01	3.12E-01
C14+	301.90	14.84	956.18	8.384E-01	6.436E-01	8.824E-02	1.20E-01	1.50E-01	8.569E-01	6.707E-01	9.24E-02	8.21E-02

OMEGA = 0.45723553 in the EOS
OMEGB = 0.07796074 in the EOS
MIXVC = 0.82733389, exponent coefficient used in viscosity calculations, for Oil 1800R, (see Appendix A)
MIXVC = 0.80000000, exponent coefficient used in viscosity calculations, for Oil 2030R, (see Appendix A)
PVC3 = 2.000, binary interaction coefficient exponent for hydrocarbon–hydrocarbon component pairs
*binary interaction coefficient for hydrocarbon–non-hydrocarbon component pairs
**Component pseudo-critical volume used to compute the mixture critical volume used in viscosity calculations

than the critical temperature. Next, series of pseudoternary diagrams were generated for oil 1800R at 1850 psia contacted by various solvents made up by blending LPG with dry gas in different molar ratios (from 30% to 60% LPG). The compositions of these various solvents, LPG and dry gas are represented in Table 2. Figure 15 shows the ternary diagram for oil 1800R contacted by solvent with LPG ratios of 55%. From this diagram, evidently miscibility is achieved when the solvent composition is around 55% LPG or greater. The pressure-composition diagrams for oil 1800R with different solvents is shown in Fig. 16. From this figure, it is evident that until the LPG ratio is 50% the principal mechanism of recovery will be via vaporizing mechanism. However, at higher LPG ratios, the mechanism becomes principally a condensing mechanism. Thus, miscibility is achieved with a solvent with LPG of 55% or greater by a condensing mechanism where the liquid phase becomes enriched with intermediates to the point that it becomes miscible with the injected gas.

The pseudoternary diagrams for oil 2030R at pressure of 2100 psia show that miscibility is achieved for a solvent with 50% LPG or greater (Fig. 17). To analyze the mechanism of recovery we examine the pressure composition diagrams for these systems (Fig. 18) just as we did for oil 1800R. From this diagram, it appears that up to 40% LPG in the solvent of the principal mechanism of recovery is a vaporizing mechanism but for more LPG in solvent the mechanism becomes primarily a condensing mechanism.

Ternary diagrams[16,17] for oil 1800R contacted with CO_2 at several different pressures were generated to determine the miscibility pressure for this oil with CO_2. The ternary diagram for pressures of 1850, 3000, and 4400 psia is shown in Fig. 19. For all these

Table 2. Solvents composition of the blended LPG/Dry gas samples.

Component	*Dry Gas*	*0.40 LPG**	*0.45 LPG*	*0.5 LPG*	*0.55 LPG*	*0.6 LPG*	*LPG*
	Mole%	*Mole%*	*Mole%*	*Mole%*	*Mole%*	*Mole%*	*Mole%*
N2	1.358	0.815	0.747	0.679	0.611	0.543	
CO_2							
C1	86.419	51.851	47.530	43.210	38.889	34.568	
C2	8.354	6.000	5.706	5.412	5.117	4.823	2.469
C3	2.831	13.560	14.901	16.243	17.584	18.925	29.654
IC4	0.389	9.444	10.576	11.708	12.839	13.971	23.026
NC4	0.649	18.330	20.540	22.750	24.960	27.170	44.850

*0.40 LPG: Molar Ratio of 0.40 LPG to 0.60 Dry Gas.

Table 3. Comparison of experimental data with EOS predicted values before and after regression analyses, reservoir oil sample of Pb = 1800 psia at 206F, Raguba oil field, Well No. E40.

Exper. Processes	*Data Type*	*Pressure psig*	*Exper. Values*	*Predicted Values*		*Error* Reduction*	*Error** After*	*Weight Factor*
				Before	*After*			
	Pb Psia	—	1800	1378.9	1805.8	0.2307	0.0032	200
Differential	Solution	1785	674.50	1358.20	716.95	0.9508	0.0629	12
Liberation	GOR	1500	588.60	1358.20	642.62	1.2158	0.0918	12
	Scf/bbl	1200	494.84	1253.20	567.63	1.3855	0.1471	12
		900	400.51	1067.60	493.17	1.4344	0.2314	12
		600	309.93	886.29	416.43	1.5160	0.3436	12
		300	206.31	687.19	325.85	1.7515	0.5794	12
		0	0.00	0.00	0.00	0.0000	0.0000	12
	Liberated	1785		0.844	0.897	0.0526	0.1029	0
	Gases	1500	0.813	0.836	0.900	−0.0778	0.1066	2.5
	Z-factor	1200	0.842	0.853	0.904	−0.0611	0.0741	2.5
		900	0.856	0.871	0.911	−0.0468	0.0644	2.5
		600	0.886	0.892	0.920	−0.0310	0.0380	2.5
		300	0.917	0.917	0.930	−0.0144	0.0145	2.5
		0	1.000	0.982	0.986	0.0039	0.0137	2.5
	Liquid	1785	0.675	0.772	0.669	0.1356	0.0087	4
	Densities	1500	0.685	0.776	0.676	0.1184	0.0139	4
	g/cc	1200	0.696	0.785	0.682	0.1084	0.0196	4
		900	0.708	0.809	0.690	0.1171	0.0259	4
		600	0.720	0.836	0.698	0.1295	0.0309	4
		300	0.736	0.868	0.708	0.1415	0.0377	4
		0	0.750	1.009	0.755	0.3386	0.0060	4
	Oil FVF	1785	1.457	2.005	1.495	0.3499	0.0259	2.5
	Bbl/stb	1500	1.414	1.997	1.462	0.3779	0.0340	2.5
		1200	1.367	1.948	1.429	0.3802	0.0450	2.5
		900	1.320	1.848	1.394	0.3436	0.0562	2.5
		600	1.274	1.747	1.357	0.3062	0.0652	2.5
		300	1.215	1.629	1.308	0.2643	0.0766	2.5
		0	1.080	1.077	1.051	−0.0239	0.0266	2.5
Direct	API	0	41.039	6.333	50.074	0.6255	0.2202	0.1
Flash	FVF	0	1.413	1.593	1.362	0.0914	0.0358	0.1
Liberation	GOR	0	762.40	821.58	547.25	−0.2046	0.2822	0.1
Constant	Relative	5000	0.9596	0.9283	0.9555	0.0284	0.0043	1
Composition	Oil	4000	0.9697	0.9429	0.9667	0.0245	0.0031	1
Liberation	Volume	3000	0.9817	0.9607	0.9800	0.0197	0.0017	1
		2500	0.9885	0.9711	0.9878	0.0169	0.0007	1
		2000	0.9961	0.9829	0.9964	0.0130	0.0003	1
		1900	0.9970	0.9855	0.9982	0.0104	0.0012	1
		1850	0.9977	0.9868	0.9992	0.0095	0.0015	1
		1785	1.0000	0.9885	1.0045	0.0071	0.0045	1
		1770	1.0058	0.9889	1.0078	0.0149	0.0020	1
		1700	1.0207	0.9908	1.0242	0.0259	0.0035	1
		1600	1.0461	0.9936	1.0509	0.0456	0.0046	1
		1500	1.0773	0.9964	1.0822	0.0706	0.0045	1
		1300	1.1649	1.0419	1.1630	0.1039	0.0016	1
		1000	1.4097	1.2838	1.3611	0.0549	0.0345	1
		700	1.9991	1.8016	1.7733	−0.0142	0.1130	1
Reservoir	Oil	5000	0.8522	0.1466	0.8720	0.8048	0.0232	1
Oil	Viscosity	4500	0.8235	0.1427	0.8382	0.8089	0.0179	1
Viscosity	cp	4000	0.7948	0.1386	0.8037	0.8144	0.0112	1
Meas.		3500	0.7661	0.1344	0.7685	0.8214	0.0032	1
		3000	0.7369	0.1301	0.7325	0.8176	0.0060	1
		2500	0.7081	0.1256	0.6957	0.8051	0.0176	1
		2200	0.6909	0.1228	0.6731	0.7964	0.0258	1
		2100	0.6852	0.1219	0.6655	0.7933	0.0288	1
		2050	0.6822	0.1214	0.6617	0.7919	0.0301	1
		2015	0.6804	0.1211	0.6590	0.7906	0.0315	1
		1785	0.6682	0.1189	0.6413	0.7818	0.0402	1
		1500	0.6725	0.1204	0.6730	0.8202	0.0008	1
		1200	0.6813	0.1219	0.7094	0.7798	0.0412	1
		900	0.6916	0.1235	0.7513	0.7353	0.0862	1
		600	0.7469	0.1250	0.8016	0.7594	0.0732	1
		300	0.9688	0.1268	0.8717	0.7689	0.1002	1
		0	1.2089	0.1294	1.1963	0.8825	0.0104	1

*Error Reduction = Error before Regression − Error after Regression

**Error after = (Experimental − Calculated)/Experimental

Table 4. Comparison of experimental data with EOS predicted values before and after regression analyses, reservoir oil sample of Pb = 2030 psia at 206F, Raguba oil field, Well No. E40.

Exper. Processes	*Data Type*	*Pressure psig*	*Exper. Values*	*Predicted Values*		*Error* Reduction*	*Error** After*	*Weight Factor*
				Before	*After*			
Differential Liberation	Pb Psia	—	2030	1534.7	2027.8	0.2429	0.0011	200
	Solution	2015	780.26	1511.40	800.34	0.9113	0.0257	12
	GOR	1800	703.64	1511.40	742.40	1.0928	0.0551	12
	Scf/bbl	1500	603.16	1497.50	662.79	1.3839	0.0989	12
		1200	508.23	1292.90	585.12	1.3926	0.1513	12
		900	414.91	1100.70	508.09	1.4282	0.2246	12
		600	326.62	913.24	428.75	1.4833	0.3127	12
		300	215.63	707.85	335.07	1.7288	0.5539	12
		0	0.00	0.00	0.00	0.0000	0.0000	12
	Liberated	2015		0.837	0.896	0.0592	0.1041	0
	Gases	1800	0.859	0.826	0.896	−0.0049	0.0436	2.5
	Z-factor	1500	0.851	0.838	0.899	−0.0408	0.0566	2.5
		1200	0.894	0.853	0.904	0.0352	0.0110	2.5
		900	0.919	0.871	0.911	0.0433	0.0092	2.5
		600	0.944	0.892	0.919	0.0288	0.0264	2.5
		300	0.970	0.917	0.930	0.0136	0.0413	2.5
		0		0.982	0.986	0.0040	0.0137	0
	Liquid	2015	0.648	0.756	0.662	0.1453	0.0221	4
	Densities	1800	0.656	0.763	0.667	0.1464	0.0167	4
	g/cc	1500	0.666	0.758	0.674	0.1264	0.0117	4
		1200	0.676	0.782	0.681	0.1491	0.0072	4
		900	0.686	0.806	0.688	0.1720	0.0035	4
		600	0.697	0.833	0.697	0.1949	0.0004	4
		300	0.710	0.866	0.708	0.2165	0.0035	4
		0	0.749	1.009	0.755	0.3395	0.0081	4
	Oil FVF	2015	1.570	2.097	1.537	0.3148	0.0208	2.5
	Bbl/stb	1800	1.527	2.079	1.512	0.3517	0.0098	2.5
		1500	1.478	2.090	1.477	0.4130	0.0008	2.5
		1200	1.430	1.979	1.442	0.3758	0.0083	2.5
		900	1.383	1.875	1.406	0.3387	0.0168	2.5
		600	1.337	1.770	1.368	0.3012	0.0229	2.5
		300	1.275	1.648	1.317	0.2600	0.0327	2.5
		0	1.079	1.079	1.052	−0.0245	0.0247	2.5
Direct Flash Liberation	API	0	41.631	5.838	49.684	0.6663	0.1935	0.1
	FVF	0	1.551	1.665	1.403	−0.0221	0.0954	0.1
	GOR	0	878	941.53	626.41	−0.2142	0.2866	0.1
Constant Composition Liberation	Relative	5000	0.9596	0.9283	0.9555	0.0284	0.0043	1
	Oil	4000	0.9716	0.9426	0.9681	0.0262	0.0036	1
	Volume	3000	0.9844	0.9618	0.9826	0.0211	0.0018	1
		2500	0.9916	0.9732	0.9911	0.0180	0.0005	1
		2300	0.9948	0.9782	0.9947	0.0167	0.0001	1
		2200	0.9964	0.9808	0.9966	0.0155	0.0002	1
		2100	0.9981	0.9834	0.9986	0.0142	0.0005	1
		2050	0.9992	0.9848	0.9996	0.0141	0.0004	1
		2015	1.0000	0.9857	1.0024	0.0119	0.0024	1
		2000	1.0031	0.9862	1.0053	0.0147	0.0022	1
		1950	1.0137	0.9876	1.0153	0.0242	0.0016	1
		1900	1.0252	0.9890	1.0260	0.0345	0.0008	1
		1800	1.0512	0.9919	1.0497	0.0550	0.0014	1
		1700	1.0815	0.9949	1.0770	0.0760	0.0041	1
		1500	1.1598	1.0156	1.1455	0.1120	0.0124	1
		1300	1.2716	1.1272	1.2404	0.0890	0.0245	1
		1000	1.5519	1.4072	1.4715	0.0414	0.0518	1
		760	1.9769	1.8362	1.8175	−0.0094	0.0806	1
Reservoir Oil Viscosity Meas.	Oil	5000	0.6589	0.1459	0.7304	0.6700	0.1085	1
	Viscosity	4500	0.6474	0.1417	0.7054	0.6917	0.0895	1
	cp	4000	0.6355	0.1373	0.6795	0.7147	0.0692	1
		3500	0.6260	0.1329	0.8528	0.7450	0.0428	1
		3000	0.6109	0.1282	0.6251	0.7668	0.0233	1
		2500	0.5982	0.1235	0.5965	0.7906	0.0029	1
		2200	0.5907	0.1206	0.5787	0.7756	0.0203	1
		2100	0.5882	0.1196	0.5727	0.7703	0.0264	1
		2050	0.5870	0.1191	0.5697	0.7676	0.0295	1
		2015	0.5861	0.1187	0.5676	0.7658	0.0317	1
		1785	0.5936	0.1200	0.5845	0.7827	0.0153	1
		1500	0.6088	0.1215	0.6080	0.7990	0.0013	1
		1200	0.6348	0.1232	0.6353	0.8050	0.0008	1
		900	0.6900	0.1250	0.6663	0.7845	0.0344	1
		600	0.7720	0.1268	0.7026	0.7459	0.0899	1
		300	0.8540	0.1289	0.7510	0.7284	0.1206	1
		0	0.9360	0.1329	0.9241	0.8453	0.0128	1

*Error Reduction = Error before Regression − Error after Regression

**Error after = (Experimental − Calculated)/Experimental

pressures no miscibility was achieved at pressure less than 4400 psia and the mechanism of recovery seemed to be a condensing/vaporizing mechanism. However, the results do not seem correct because CO_2 should be able to achieve miscibility with most black oils at pressures lower than 3000 psia. The MMP of CO_2 with this oil was calculated using Glaso[2] correlation for pure CO_2 and found 2572 psia. Similar results were achieved for oil 2030R contacted with CO_2 at several different pressures, 2100, 3000 and 4400 psia, as shown in Fig. 20. The MMP of CO_2 with this oil was calculated using Glaso[2] correlation for pure CO_2 and found 2669 psia. The results obtained by EOS may be misleading because the EOS was tuned only with black-oil data and not data for oil mixed with CO_2 that is not available.

VISCOSITY MATCHING OF OILS 1800R AND 2030R

Using the tuned EOS parameters obtained previously, the viscosity of the oil 1800R and 2030 psia were matched using regression on the parameters on the Jossi, Stiel, and Thodos[18] viscosity equation (see Appendix-A). A comparison of the experimental data and the calculated viscosity using the viscosity correlation is shown on Figs. 6 & 12 showing a good match at reservoir conditions above and below bubble point pressure. The final values of the viscosity parameters are shown in Table 1.

MINIMUM MISCIBILITY COMPOSITION DETERMINATION BY THE SLIM TUBE TECHNIQUE

When conducting slim tube experiments, it is essential that any solvent be a single phase at injection conditions. To check this, the pressure-temperature diagrams for solvents with varying amounts of LPG from 10% to 90% were generated. All solvents were found a single phase at the reservoir temperature of 206°F and the injection pressures of 1850 and 2100 psia. Figure 21 represents the pressure-temperature diagram for 40% to 60% LPG solvent.

The two oils were displaced, at reservoir temperature by different solvents made up by blending LPG and Dry Gas,[19,20,21] in a slim tube of 40 feet length, 40.5% porosity and the total pore volume of the system was 99 cc. Figure 22 illustrates the schematic diagram for the slim tube apparatus. Five slim tube experiments were conducted on each oil. For oil 1800R, the injection pressure was 1850 psia while for 2030R the injection pressure was 2100 psia. The first series of experiments were conducted on oil 1800R at 1850 psia by various solvents made up by blending LPG with dry gas in different molar ratios (15%, 25%, 35%, 45% and 55% LPG). The oil recovery in percent was plotted as a function of the LPG% in the solvent as shown in Fig. 23. The oil recovery was calculated when a solvent volume of 1.2 of the total system volume was injected. The intercept of the two straight lines in Fig. 23 shows that the minimum miscibility composition of the solvent was 40% LPG and 60% dry gas for the oil 1800R. In the same manner, the oil 2030R was displaced by solvents of 15%, 20%, 30%, 35% and 40% LPG and the results were plotted in Fig. 24. It was found that a minimum miscibility composition of 35% LPG was required to achieve miscibility with the oil 2030R. From the above experiments, obviously the minimum miscibility composition was over estimated by the EOS for both oils. The slim tube data will be combined with the swelling data when it is ready to re-tune the EOS.

CONCLUSIONS

1. The phase behaviour of both oils 1800R and 2030R were matched using one set of EOS parameters.
2. Using the tuned EOS parameters analysis indicates that miscibility will be achieved for oil 1800R at 1850 psia for LPG ratios of 55% or more. The main mechanism of recovery is a condensing drive.
3. For oil 2030R at 2100 psia miscibility will be achieved via a condensing mechanism for solvent with LPG content of 50% or greater.
4. Minimum miscibility composition for both oils was over estimated using EOS.
5. Any solvent composition will always be single phase at 206°F and 1850 or 2100 psia.
6. Minimum miscibility pressure predicted by EOS for both oils with CO_2 was also over estimated.

ACKNOWLEDGEMENT

Our thanks are expressed to the management of Sirte Oil Company for permission to publish this paper. Thanks are also extended to the management of the Petroleum Research Centre for their support.

APPENDIX A

The viscosity model used in obtaining oil viscosity values is the following

$$[(\eta-\eta^0)\zeta+1]^{0.25} = \text{viscoeff (1)}^* + \text{viscoeff (2)}\ \rho_r + \text{viscoeff (3)}\ \rho_r^2 + \text{viscoeff (4)}\ \rho_r^3 + \text{viscoeff (5)}\ \rho_r^4$$

where

η = phase viscosity, cp
η^0 = low pressure fluid viscosity, cp, calculated

internally from the Jossi, Stiel and Thodos equation, cp

ζ $= T_c^{1/6}\ MW^{1/2}\ P_c^{2/3}$

T_c = fluid pseudo-critical temperature, °K

MW = fluid molecular weight, gm/mol

P_c = fluid pseudo critical pressure, atm

ρr = fluid reduced molar density $= (\rho \times V_C)$

ρ = fluid molar density, kmol/m^3, and

$V_C^{mixvc} = \Sigma(z(i) \times visvc(i)^{mixvc})$

with

$z(i)$ = the mole fracture of component i.

*viscoeff (1–5) for oil 1800R:
1.227600E-01, 2.803680E-02, 7.023960E-02, −4.492087E-02 and 1.119888E-02

*viscoeff (1–5) for oil 2030R:
1.119912E-01, 1.869120E-02, 7.023960E-02, −3.260640E-02 and 7.465920E-03

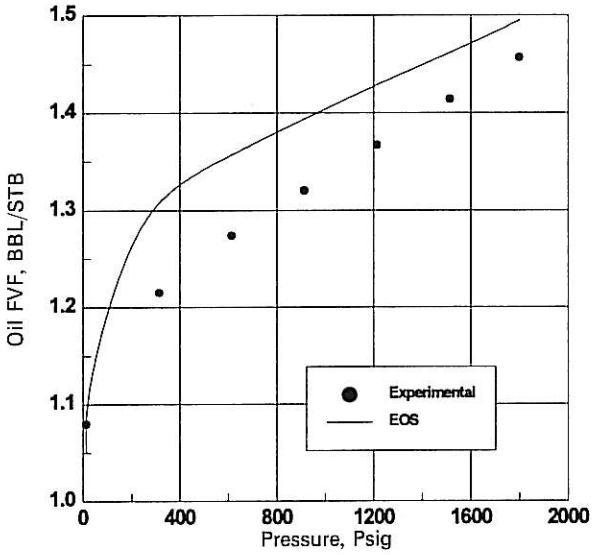


Fig. 1. EOS Match, Oil FVF vs Pressure, Pb = 1800 Psia, Raguba Oil Field – Well No. E40.

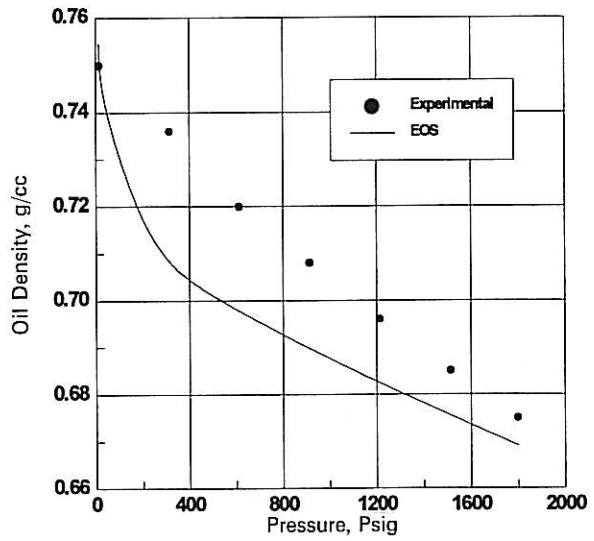


Fig. 2. EOS Match, Oil Density vs Pressure, Pb = 1800 Psia, Raguba Oil Field – Well No. E40.

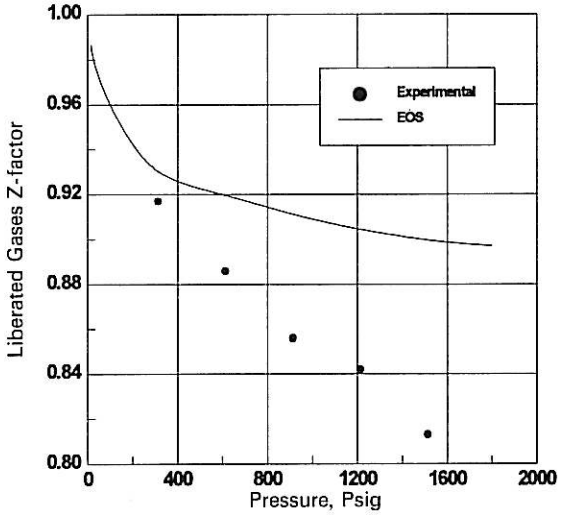


Fig. 3. EOS Match, Liberated Gases Z-factor vs Pressure, Pb = 1800 Psia, Raguba Oil Field – Well No. E40.

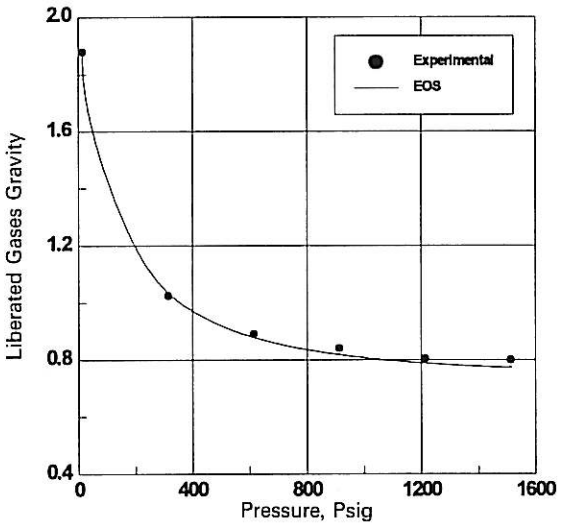


Fig. 4. EOS Match, Liberated Gases Gravity vs Pressure, Pb = 1800 Psia. Raguba Oil Field – Well No. E40.

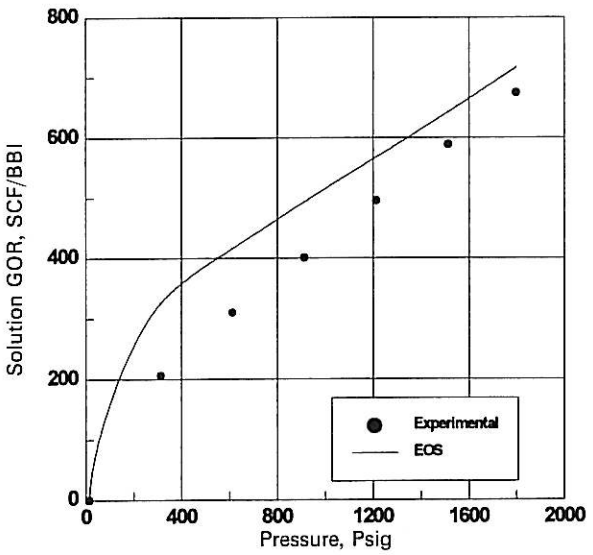


Fig. 5. EOS Match, Solution GOR vs Pressure, Pb = 1800 Psia, Raguba Oil Field – Well No. E40.

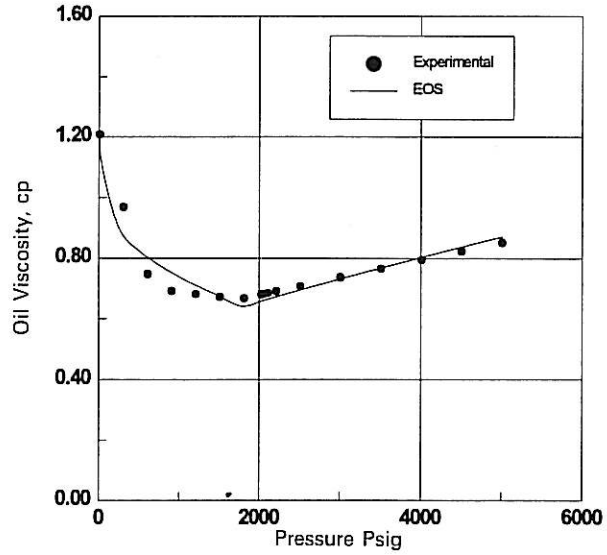


Fig. 6. EOS Match, Oil Viscosity vs Pressure, Pb = 1800 Psia, Raguba Oil Field – Well No. E40.

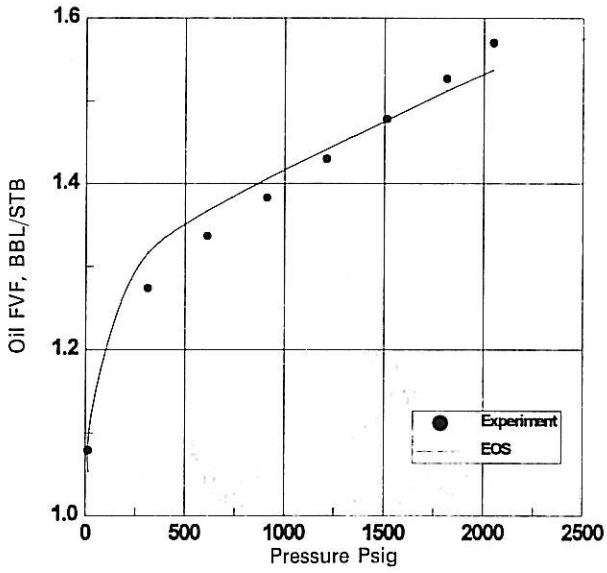


Fig. 7. EOS Match, Oil FVF vs Pressure, PB = 2030 Psia, Raguba Oil Field – Well No. E40.

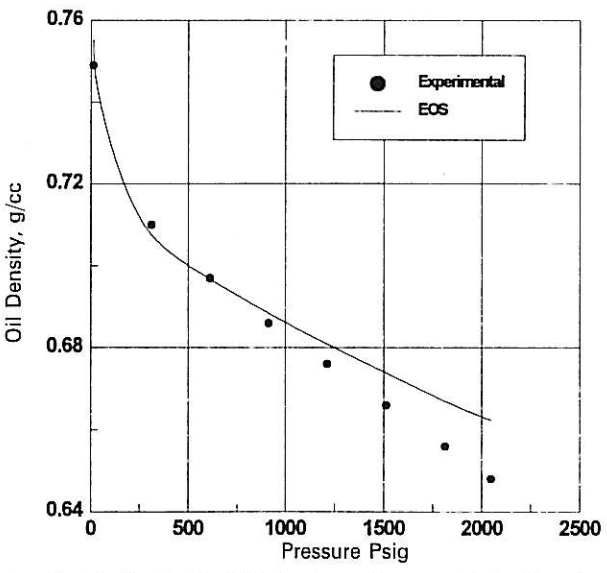


Fig. 8. EOS Match, Oil Densit vs Pressure, Psia, Raguba Oil Field – Well No. E40.

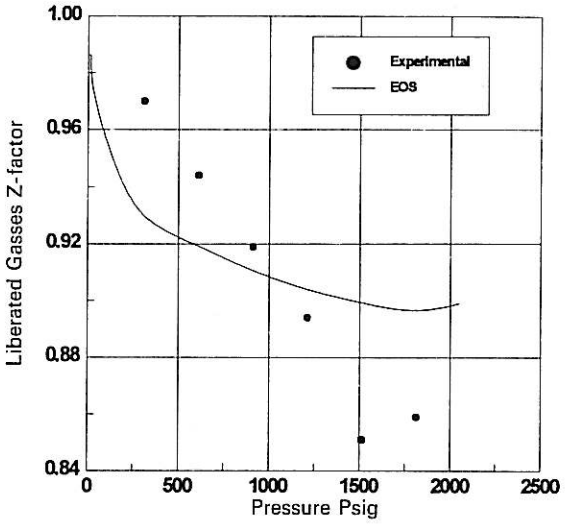


Fig. 9. EOS Match, Liberated Gases Z-factor vs Pressure, Pb = 2030 Psia, Raguba Oil Field – Well No. E40.

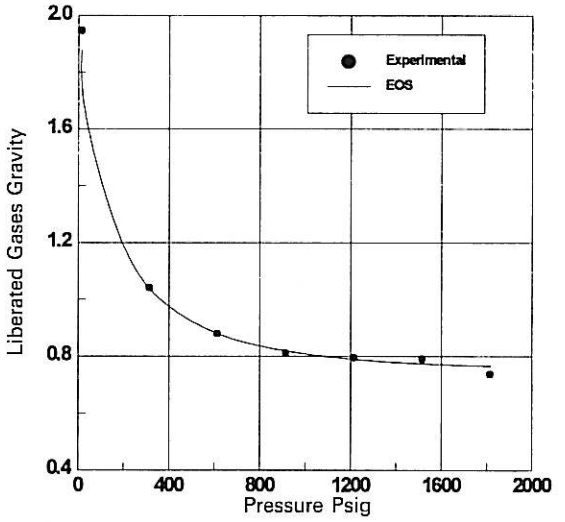


Fig. 10. EOS Match, Liberated Gases Gravity vs Pressure, Pb = 2030 Psia, Raguba Oil Field – Well No. E40.

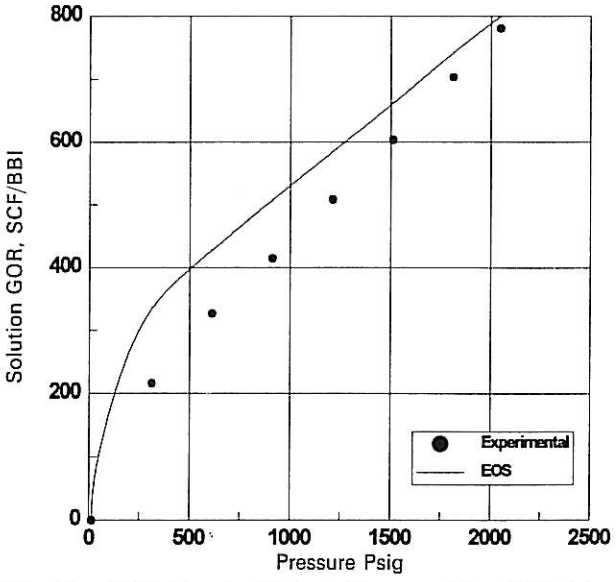


Fig. 11. EOS Match, GOR vs Pressure, Pb = 2030 Psia, Raguba Oil Field – Well No. E40.

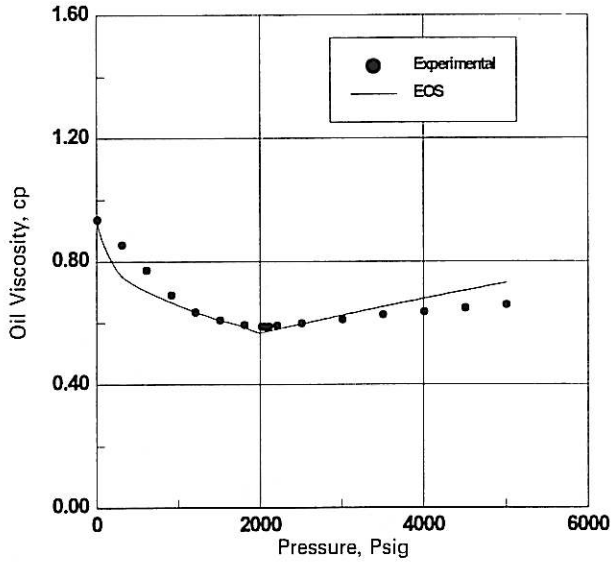


Fig. 12. EOS Match, Oil Viscosity vs Pressure, Pb = 2030 Psia, Raguba Oil Field – Well No. E40.

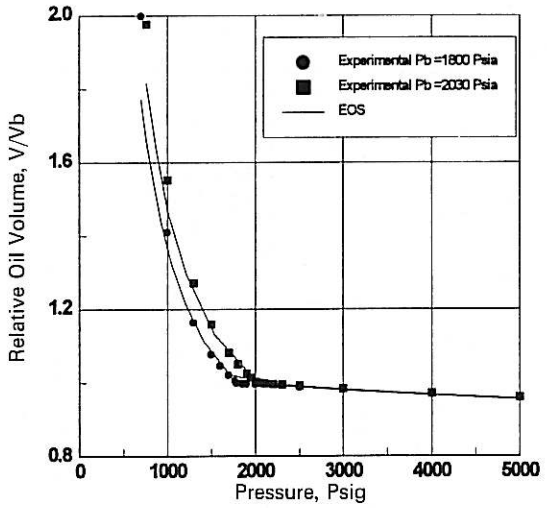


Fig. 13. EOS Match, Relative Oil Volume vs Pressure, Pb = 1800 & 2030 Psia, Raguba Oil Field – Well No. E40.

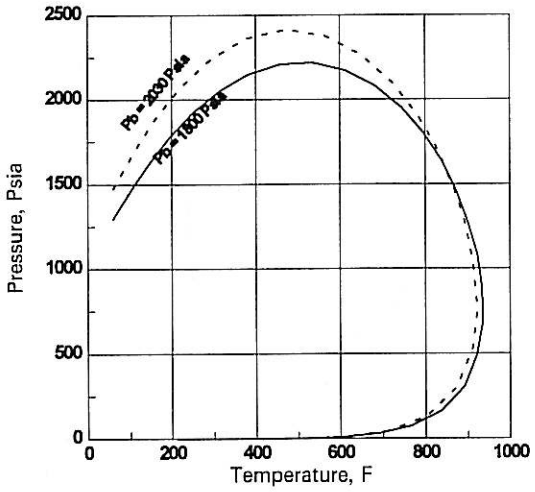


Fig. 14. EOS Generated, Pressure-Temperature Diagram Pb = 1800 & 2030 Psia, Raguba Oil Field – Well No. E40.

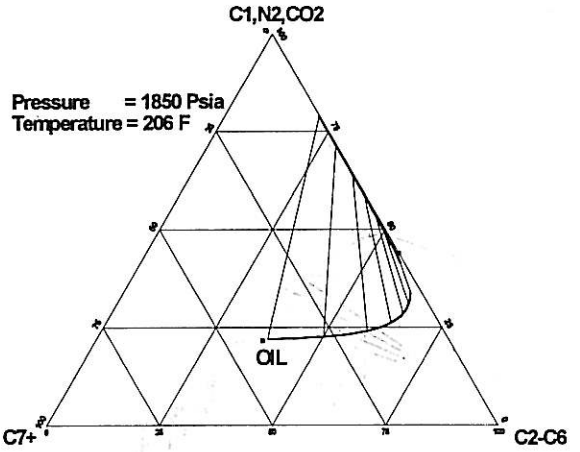


Fig. 15. Ternary Diagram for Solvent LPG/Dry Gas Ratio 55/45 and Resservoir Oil of Pb = 1800 Psia at 206 F. Raguba Oil Field – Well No. E40.

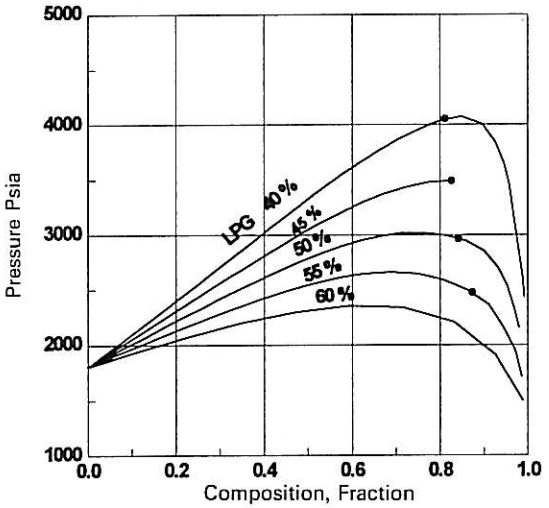


Fig. 16. EOS Generated Pressure-Composition Diagram for Oil 1800R and 5 Mixtures of LPG and Dry Gas, Raguba Oil Field – Well No. E40.

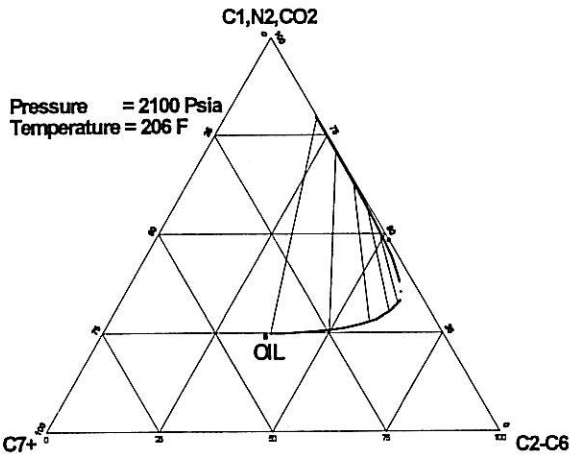


Fig. 17. Temary Diagram for Solvent LPG/Dry Gas Ratio 50/50 and Reservoir Oil of Pb = 2030 Psia at 2030 Psia at 206 F, Raguba Oil Field – Well No. E40.

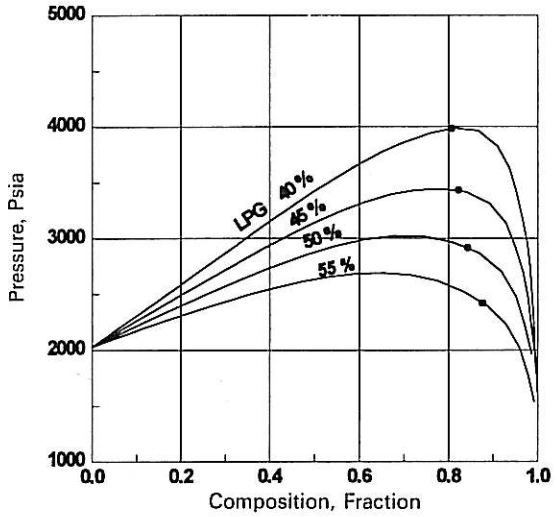


Fig. 18. EOS Generated, Pressure-Composition Diagram for Oil 2030R and 4 Mixtures of LPG and Dry Gas. Raguba Oil Field – Well No. E40.

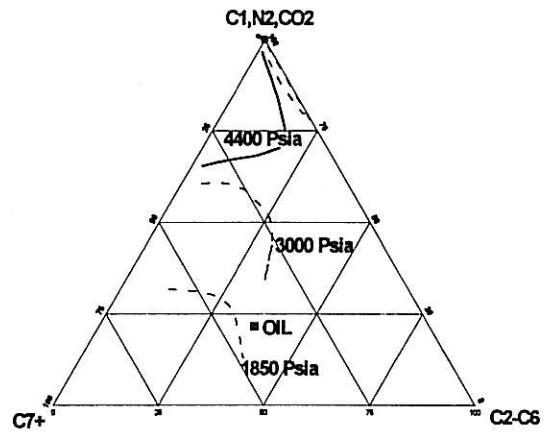


Fig. 19. Ternary Diagram for CO_2 and Reservoir Oil of Pb = 1800 Psia at 206 F, Raguba Oil Field – Well No. E40.

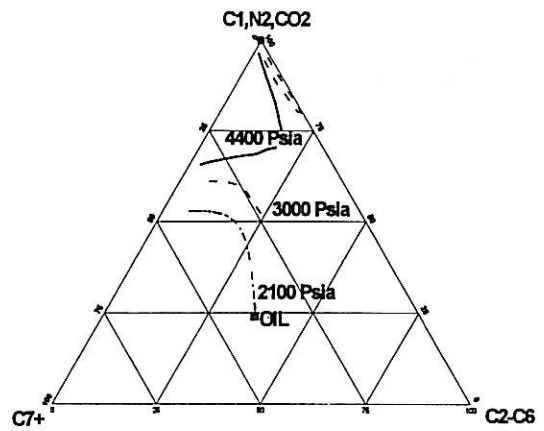


Fig. 20. Ternary Diagram for CO_2 and Reservoir Oil of Pb = 2030 Psia at 206 F, Raguba Oil Field – Well No. E40.

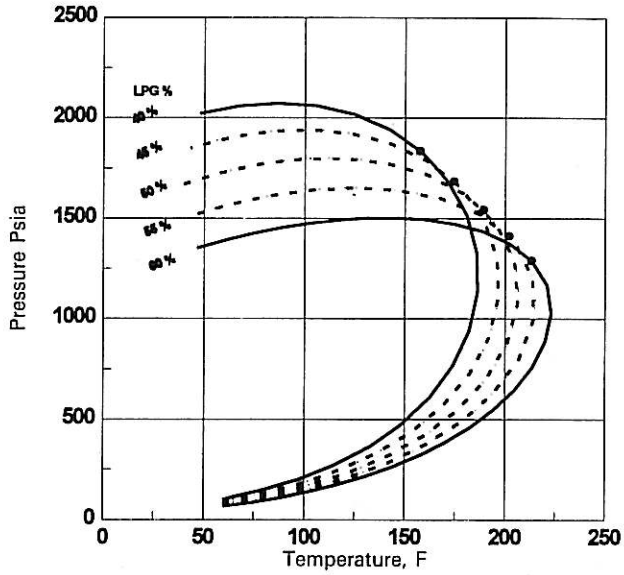


Fig. 21. EOS Generated, Pressure-Temperature Diagram for Different-Mixtures of LPG and Dry Gas, Raguba Oil Field – Well No. E40.

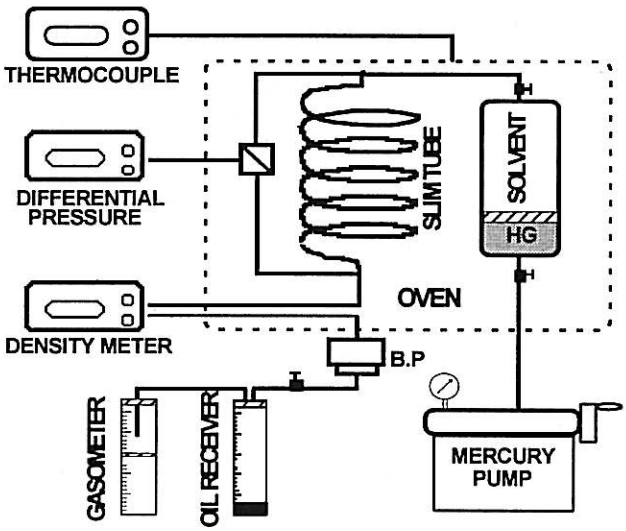


Fig. 22. SLIM TUBE APPARATUS.

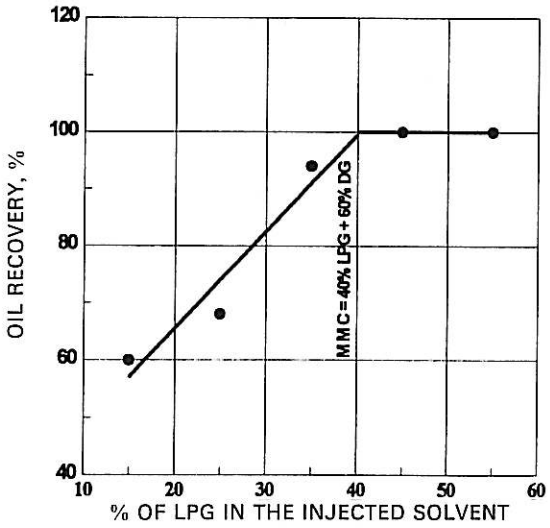


Fig. 23. Oil Recovery as a Function of % LPG in the Injected Solvent, for BPP = 1800 psia, Raguba Oil Field, Well No. E40.

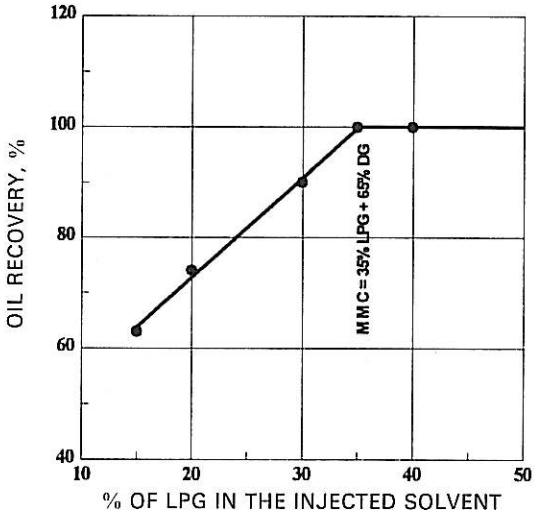


Fig. 24. Oil Recovery as a Function of % LPG in the Injected Solvent, for Oil Sample of BPP = 2030 psia, Raguba Oil Field, Well No. E40.

REFERENCES

[1] Benham, A.L., Dowden, W.E. and Kunzman, W.J., 1960. Miscible fluid displacement prediction of miscibility. *Trans., AIME* **219**, 229–237.

[2] Al-Khafaji, A.H., Al-Dulaimy, S.N. and Al-Doury, M.M., 1989. Correlation for minimum miscibility pressure, hydrocarbon gas-oil systems. *J. Petrol. Res.* **1**, 15–23.

[3] Glaso, O., Dec. 1985. Generalized minimum miscibility pressure correlation. *Soc. Pet. Eng. J.*, 927–934.

[4] Short course prepared and presented by Hycal Research Laboratories LTD, 1990. Design, interpretation and use of experimental laboratory data for miscible flood processes. Second Edition.

[5] Luks, K.D., Turek, E.A. and Baker, L.E., November 1987. Calculation of minimum miscibility pressure. *SPERE*, 501–506.

[6] Thomas, F.B., Bennlon, D.B., Bennlon, D.W., 1991. Recent development in laboratory data sets for determination of miscibility limits, Paper CIM/AOSTRA 91-4 Presented at the CIM/AOSTRA Technical Conference in Banff, (April 21–24) 1–24.

[7] Brigham, W.E., Reed, P.W. and Dew, J.N., March 1961. Experiments on mixing during miscible displacement in porous media, *Soc. Pet. Tech. J.*, 1–8; *Trans., AIME*, 222.

[8] Nutakki, R., Hamoodi, A.N., Li, Y.K., and Nghiem, L.X., 1991. Experimental analysis, modelling, and interpretation of recovery mechanisms in enriched-gas processes, Paper SPE 22634 presented at the 66th annual technical conference and exhibition of the Society of Petroleum Engineering held in Dallas, TX, October 6–9.

[9] Orr, F.M., Jr., Silva, M.K., Lien, C.L. and Pelletier, M.T., April 1982. Laboratory experiments to evaluate field prospects for CO_2 flooding. *J. Pet. Tech.*, 889–898.

[10] DesBrisay, C.L., Gray, J.W. and Spivak, A., August 1975. Miscible flood Performance of the Intisar (D) Field. Libya Arab Republic, *J. Pet. Tech.*, 935–943.

[11] Frazier, G.D. and Todd, M.R., 1982. Alvord (3000-ft Strawn) LPG-design and performance evaluation, Paper SPE/DOE 10692, presented at the SPE/DOE third joint symposium on enhanced oil recovery of the Society of Petroleum Engineering held in Tulsa, Ok, (April 4–7).

[12] Willimanns, C.A., Zana, E.N., and Humphrys, G.E., 1980. Use of Peng-Robinson equation of state to predict hydrocarbon phase behaviour and miscibility of fluid displacement, Paper SPE 8817 presented at the SPE/DOE Enhanced Oil Recovery Symposium, Tulsa, April 20–23.

[13] Benmekkl, E.H., and Mansoori, G.A., May 1988. Minimum miscibility pressure prediction with equation of state, SPERE 559–564.

[14] Enhanced oil recovery project-phase I: PVT studies, Raguba Oil Field, Well No. E40, prepared for Sirte Oil Co., 1994, prepared by Petroleum Research Centre, Tripoli, Libya.

[15] Enhanced oil recovery project-phase II: Equation of state modelling-part (1), Raguba Oil Field, Well No. E40, prepared for Sirte Oil Co., 1994, prepared by Petroleum Research Centre, Tripoli, Libya.

[16] Alston, R.B., Kokolis, G.P. and James, C.F., April 1985. CO_2 minimum miscibility pressure: A correlation for impure CO_2 streams and live oil systems, *Soc. Pet. Tech. J.*, 268–274.

[17] Holum, L.W. and Josendal, V.A., Feb. 1982. Effect of oil composition on miscible-type displacement by carbon dioxide. *Soc. Pet. Tech. J.*, 87–98.

[18] Reid, R.C., Prautsnitz, J.M. and Sherwood, T.K., 1977. *The Properties of Gases and Liquids*, 3rd Edition, McGraw-Hill, New York.

[19] Yarborough, L. and Smith, R., Sept. 1970. Solvent and driving gas compositions for miscible slug displacement. *Soc. Pet. Eng. J.*, 298–310.

[20] Flock, D.L. and Nouar, A., Sept.-October 1984. Parametric analysis on the determination of the minimum miscibility pressure in slim tube displacements. *J. Canadian Pet. Tech.*, 80–88.

[21] Arnold, C.W., Sotne, H.L. and Luffel, D.L., Displacement of oil by rich-gas banks, miscibility processes, SPE reprint series No. 8.

PRJ, Vol. 8 (January 1996); P. 13–23, 8 FIGS. 3 TABLES.

Tertiary-Quaternary Alkaline-Subalkaline Magmatism in Gharyan Area-Field Aspects and Petrography

M.T. Busrewil*, and W.J. Wadsworth**

السمات الحقلية والبتروغرافية لصهير الحينين الثالث والرابع القلوية والتحتقلوية بمنطقة غريان

الميروك أبو سريويل و جون وودسوورث

تظهر ملامح النشاط البركاني التابع للحينين الثالث والرابع واضحة على طول الجهة الشرقية من جبل نفوسة حيث تجلت هذه الملامح بتوضع سلسلتي اللابا القديمة والحديثة والبراكين المخروطية الشكل والفونولايت ذو المظهر القبابي وصخور البيروكلاستيك. تمثل اللابا القديمة أكثر الصخور البركانية إنتشاراً حيث تشكل سلسلة مستمرة عند منتصف المنطقة بينما تظهر اللابا الحديثة جلياً في صور الأقار الصناعية عند الحواف. كما وجدت مدفونة في مسارات بعض الوديان القديمة ، وبالرغم من أن العلاقات الحقلية والعمر المطلق يشير إلى أن اللابا تنتمي إلى أكثر من نشاط بركاني إلا أنه قد وجد أن بتروغرافية جميع هذه الصخور متشابهة مما يشير إلى أنه قد تم إشتقاق جميع اللابا من مصدر متشابه. إن إقتراح اللابا القديمة كأقدم نشاط بركاني بالمنطقة قابل للنقاش.

تتكشف صخور الفونولايت في أماكن محدودة بالمنطقة وتشير الأدلة الحقلية ومعلومات العمر المطلق إلى أن هذه الصخور أقل حداثة من صخور البراكين البيزانيتية المتكشفة حيث أن صخور هذه البراكين والصخور المتباينة منها كانت حصيلة نشاط بركاني من براكين مركزية وجذذ وأنها تمثل كميات بسيطة من نتاج النشاط البركاني داخل حقل اللابا وخارجه.

تم التعرف بالمنطقة على رواسب رديئة الفرز سوداء اللون تتكون من شظايا بركانية وكتل متماسكة بمادة لاحمة نتجت عن إنفجارات بركانية كانت قد لامست المياه السطحية وأن جزءاً من هذه الشظايا قد تعرض إلى إعادة نقل.

هذا وقد تم تقسيم هذه الصخور البيروكلاستيلية إلى سحنة الفتحات البركانية وسحنة الصخور قريبة المصدر وسحنة الصخور بعيدة المصدر.

Abstract *Tertiary – Quaternary volcanic activity is conspicuous along the eastern scarp of Jabal Nafusah and comprises an old lava series (OLS), young lava series (YLS), volcanic cones, phonolite dome – shaped intrusions and pyroclastic rocks. The OLS are the most voluminous and form a fairly continuous plateau in the central part of the region. In contrast to the older flows, the YLS is mostly restricted to the periphery of the OLS plateau, as is clearly shown on satellite images. In addition, parts of the YLS occupy an ancient buried wadi system. Both the OLS and YLS are petrographically similar, although field evidence revealed a number of separate eruptive events. The suggestion that the OLS may represent the first phase of igneous activity in the area is debatable because of suspect dating.*

The phonolites are exposed at only a few localties. Field evidence and K-Ar Age dating suggest that they are much older than the late volcanic centres (LVC). These centres, erupted from central volcanoes and dykes, are represented by very small volume of the eruptive products throughout and outside the lava field.

Black, massive, poorly-sorted deposits made of fragmented products of explosive eruptions and matrix-supported blocks are encountered in the area. These deposites are considered to have been formed initially by vent opening phreatic – phreatomagnetic explosions and part of which were later reworked. Based on field criteria they have been classified into vent facies, near – vent facies and distal facies.

*Department of Geology, University of Al Fateh, P.O. Box 13258, Tripoli, G.S.P.L.A.J..

**Department of Earth Sciences, The University, Manchester M. 13 9PL, England.

INTRODUCTION

The rocks of the Gharyan Volcanic Province (GVP) are mostly contained within a quadrilateral area of some 7000 Km^2 between the towns of Gharyan, Tarhunah, Bani Walid and Mizdah (Fig. 1). The volcanic rocks themselves cover an area of approximately 3000 Km^2 and form a generally continuous sheet in the central part of the region, with some peripheral outlier and a number of more scattered intrusions, believed to be part of the same volcanic field originally.

A summary of the work undertaken up to 1970 has been given by Busrewil (1974). The chemistry of the main groups of the GVP has been briefly established by Almond *et al.*, (1974). Later work by Busrewil and Wadsworth (1980) discussed in more detail the genesis of the basanitic suite of rocks. Geologic maps of the area at a scale 1:250.000 with explanatory booklets were published by the Industrial Research Centre (Antonovic, 1977, El Hinnawy and Cheshitev, 1975; Mann, 1975; Zivanovic, 1976).

Several K: Ar data have been previously published on the volcanic rocks from the GVP (Piccoli, 1970; Ade-Hall, *et al.*, 1975). Some determinations from the YLS are contradictory and others are inconsistent with field relations.

In this paper we present 6 K: Ar whole rock ages from rock units of the GVP. These data are considered to provide valid estimates of the ages of each of the units measured. Based on more recent field work and petrography we reiterate some of earlier conclusions (Almond *et al.*, 1970, Busrewil and Wadsworth, 1980) but incorporate the results of the subsequent investigations. A discussion of the petrogenetic relationships within the GVP will be presented elsewhere (Busrewil and Wadsworth, in Prep.).

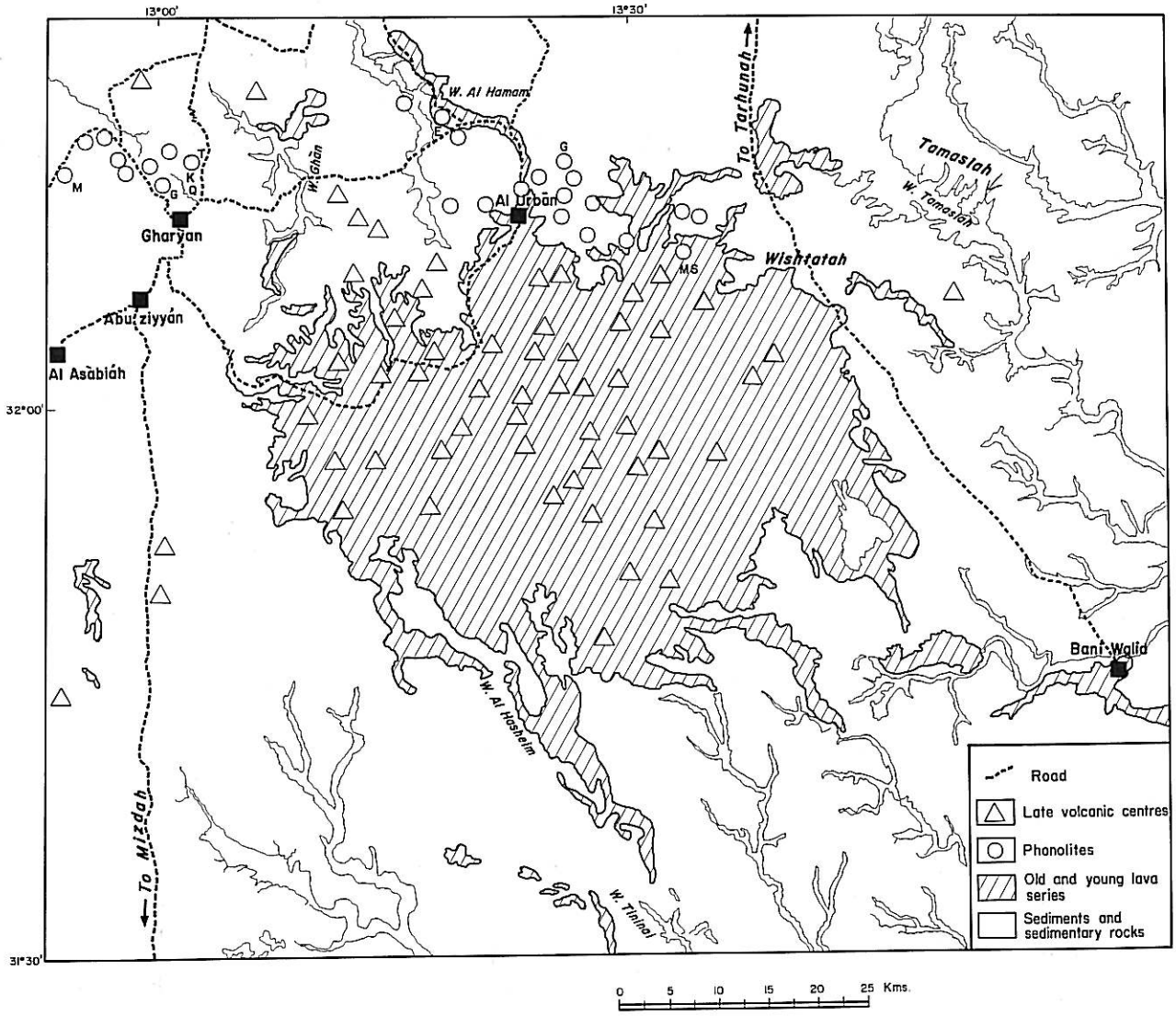


Fig. 1. Geologic map showing the distribution of the Gharyan Volcanic Province, E = Ras Umm al Ezz; G = Ras aj Jammah; K = Wadi Qurdu; M = Kaf Mantrus; Q = Wadi Qabil; RM = Ras al Massan; T = Kaf Tekut.

MODES OF OCCURRENCE

The igneous activity has four principal manifestations which can be easily recognized in the field. Firstly, there is the old lava series (OLS) with its subordinate young lava series (YLS) which cover most of the region (Fig. 1); secondly, there are the phonolitic intrusions which tend to occur as individual domes or clusters of domes just north of the Gharyan town along the northern limit of the escarpment; thirdly, there are the late volcanic centres (LVC), resting locally on top of the OLS, or represented by chemically similar minor intrusions outside the OLS area; fourthly, an episode of explosive volcanism, however, developed possibly during Quaternary time. The latter activity resulted in the emplacement of tuff cones and intrusive and reworked pyroclastics. This morphological grouping is supported by both field observation (Christie, 1955; Busrewil, 1974) and available radiometric ages (Table 1).

Table 1. K/Ar age determination of rock types in the GVP.

Locality	Age (Ma)	Classified here as
32°10′40″N 13°22′30″E*	1.3 ± 0.5	LVC
32°03′00 N 13°31′10″E*	2.9 ± 1.1	(basanitic suite)
32°12′00 N 13°13′45″E*	5.1 ± 1.5	
31°51′00 N 12°58′45″E*	7.7 ± 1.5	
32°12′30 N 12°23′00″E*	2.3 ± 0.3	YLS
32°12′30″N 13°08′30″E*	2.6 ± 0.8	(basaltic andesites)
32°05′45″N 13°19′45″E***	4.8 ± 0.4	
32°08′00″N 13°13′00″E***	5.05 ± 0.8	
32°15′05″N 13°14′31″E***	6.02 ± 1.3	
Kaf Tekut**	37.7	Phonolites
Kaf Mantrus**	39.7	
Kaf Abu Ghannush**	40.7	
Qulayb al Anz (32°23′36″N) (13°23′36″E)***	40.7 ± 1.2	
32°15′40″N 15°18′30″E***	41.4 ± 2	
Umm al Ezz***	47 ± 1.2	

* Analysed by Mobil Research Department, Dallas, Texas, 1967.
** Piccoli, 1970.
*** Carried out by the Isotope Geology Unit, British Geological Survey.

As far as the principal rock types are concerned, the OLS and YLS are composed of basaltic andesites and the LVC are generally basanitic (with related differentiates), while the domes are all phonolitic (Fig. 2).

FIELD RELATION OF THE GHARYAN VOLCANIC PROVINCE

Old Lava Series

This lava sequence rarely comprises more than four or five individual flows, reaching a maximum total

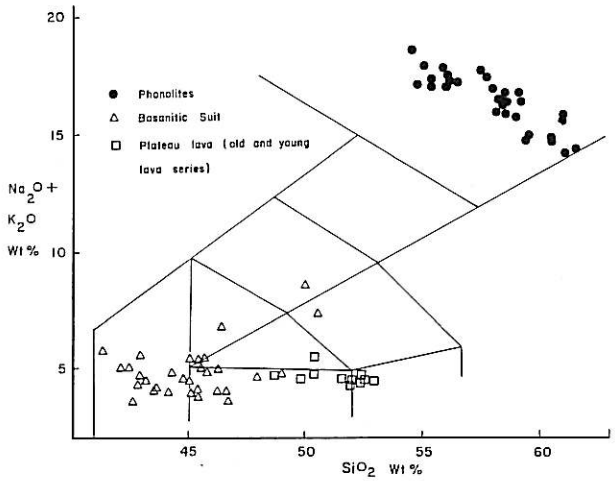


Fig. 2. Tatal alkali *vs* silica diagram for Gharyan volcanics. The style of notation is the same in the succeeding plots.

thickness of approximately 40 m. In the more peripheral parts of the lava field, only one or two flows are present, but they are nevertheless surprisingly persistent and dominate wide areas of the plateau coutry. In many places the base of the lavas is not exposed but elsewhere they are seen to rest unconformably on the sedimentary rocks (Upper Cretaceous age), particularly along the wadis.

Erosion has dissected parts of the volcanic terrain into wadis and ridges with a relief in excess of 60 m. Sets of columnar joints, are sometimes exposed and accentuated vertical developmet of landslides.

Young Lava Series

In contrast to the older flows, the younger lavas are almost barren of soil and vegetation covers. This unit produces distinctly dark colour on false colour landsat imagery. Field observation revealed that the initial invasion of the OLS was followed by a long period of erosion of unknown duration and down cutting to form new wadis which at a much later time were partly infilled by the YLS. The wadi filling lava form a thin resistant mass while the Mesozoic country rocks, on either sides, are much more rapidly removed. The original wadi segments are expressed today, either as a coherent basalt mass or as a particulate mass flow.

The existence of prominet wadi system before the eruption of the YLS is very well exhibited on satellite thematic mapper image. It is indicated by the long sinuous outcrops extending from the main volcanic region, particularly toward Beni Walid (Wadi Tininai, Wadi Ghubbeen), Wishtatah and northwards in the vicinity of the present drainage system of Wadi Ghan where Christie (1955) reported the existence of basalt on the crust of hard pan and caliche that had formed previously in the wadi bed. He believed that

the basalts postdated the topographic features and must be very young, possibly of early Quaternary or late Pliocene age. Piccoli (1970) distinguished these as "valley basalts" in contrast to the OLS (flood basalts). Along Wadi al Hamam (32° 15′ 36″N, 13° 19′ 55″E), the writers have observed the existene of basalt on top of a soil-supported conglomerate. The lava flow itself shows pronounced exfoliation and attains a maximum thickness in excess of one metre. At higher levels old wadi terraces consisting of loose conglomerate, composed of rounded limestones, sandstone and basalts approximately 4–12 cm in diameter, are cemented by clay matrix. Still at higher levels, an older lava flow approximately 10 m thick is exposed along the wadi banks and pre-dates the last period of wadi incision.

North of station 520, basalt lavas were observed underlying Quaternary sediments at near-surface section of Wadi Tamasillah where the pipe line route of the Great Man-Made River Project is constructed. The basalt was found to be very fresh and shows vesicular and columnar jointing structures. Preliminary chemical data of selected samples from this locality suggest that the lavas belong to the subalkaline magma type (Busrewil and Wadsworth, in prep.). The Quaternary sediments lie unconformably on the lava and in places where the basalt is either missing or not reached, its thickness exceed the depth of the pipe line trench (7 m). The wadi deposits show a well developed fining up sequence and are characterized by interbedded sand and pebbly layers with occasional ocurrence of alluvial soils. Cobbles and boulders with a fine sand/silt matrix approximately 50 cm thick were observed in the middle level of the trench. The occurrence of such a high energy discharge in wadi section is inferred and interpreted to indicate humid phase environments. The field observations from widyan Al Hamam, Ghan and Tamasillah suggest that a Quaternary period of volcanism poured out small quantities of basalt on the surface.

PHONOLITES

General Introduction

The phonolites occur in an approximately east-west belt along the northern edge of the plateau lava field (Fig. 1) where they form prominent conical hills. Occurrences of trachytes, phonolites and alkali trachytes between Mizdah and Gharyan were reported by Lipparini (1940). Further reconnaissance of this region revealed no traces of such exposures.

The phonolites form islated dome-shaped intrusions amid the broad expanses of Mesozoic sediments. In some cases they are clearly intrusive laccoliths with the overlying sediments strongly arched over the dome-shaped intrusion, while the underlying

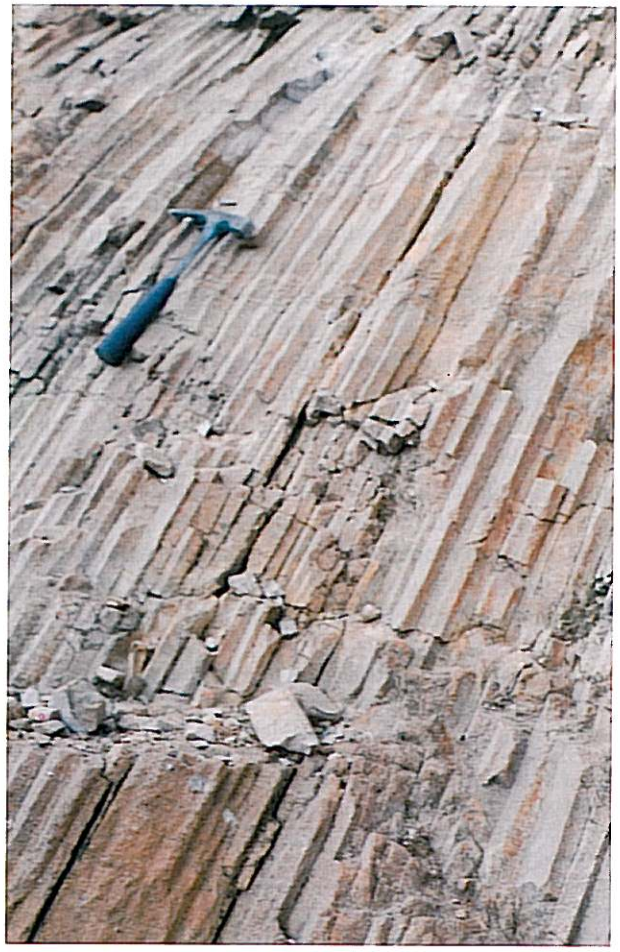


Fig. 3. Close view of columinar jointing in Abu Shaybah Formation (ss), about 1 km west of Kaf Tekut, Photo by Osama A. Joha of the Geology Department, Al Fateh University.

sediments are relatively undisturbed. In other examples, the phonolites are strikingly discordant with generally steep contacts against almost horizontal sediments, and with sill-like apophyses locally. The overall impression is of masses of viscous phonolitic magma rising diapirically through the sediments, with varying degrees of success; some appear to solidify at depth in transgressive mode, while others form domes beneath their roof of country rocks. It is believed that at few points near the top of the upheaval, the magma broke through the surface or was emplaced close to it. This is supported by the observation of vesicular phonolites at a small hill approximately 1 km NW of Kaf Abu Ghannush and horizontal jointing of the sandstone close to the contact between the Abu Shaybah Formation and the roof of an intrusive dike along the road cut about 1 km west of Kaf Tekut (Fig. 3). A brief description of few selected intrusions is summarised below:

Kaf Tekut: This is apparently the most straightforward phonolitic intrusion, as the country rock is

generally domed all around it. The intrusion, now has the appearance of a crater, breached on its east side and it is not entirely regular in shape, as the phonolites bulge out beneath a skin of sediments, when it reaches lower levels on the south and south-west side. Near this bulge occur the patchy outcrops of basaltic breccia (Wadi Qurdu).

The outer part of the dome is apparently a thick skin of porphyritic phonolite (approximately 30 m. thick), showing a progressive chilling of the groundmass towards the margin, and exhibitng a very prominent columnar jointing perpendicular to the margin. At the 'breached' entrance to the central crater of Kaf Tekut, this jointing is horizontal, while at higher levels it becomes progressively steeper as the skin turns over to form the domical roof.

Inside this jointed skin is a zone of smooth rounded outcrops of coarser (groundmass) phonolites, but equally porphyritic, and inside this is inferred to be the heavily altered zone responsible for the eroded (crater like) cores of the intrusive. It seems highly likely that the highest and most central part of the original dome-shaped plug would be the most susceptible to hydrothermal modifications, because the late stage fluids would all tend to concentrate here, beneath the viscous impervious skin. Indeed this may have helped the body rise diapirically through the sediments.

The presence of altered phonolites in the centre of the mass (G 128, Table 2) and Triassic sediments (Azizia Formation) on top of the SW part of the igneous body (Gray, 1971) suggest that the Kaf Tekut is best named as a shallow intrusive domal igneous body with an appearance of a physiographic ring structure today.

Table 2. Average of selected major chemical analyses of Charyan volcanics.

	1	2	3	4	5	G96	G127	G128
SiO_2	51.34	45.54	46.52	50.33	57.85	43.55	43.12	57.36
TiO_2	1.78	2.33	2.74	2.48	0.25	2.96	3.37	0.73
Al_2O_3	15.20	13.41	13.66	15.84	20.39	9.96	11.25	20.48
Fe_2O_3	2.25	4.02	3.72	4.41	2.32	6.43	10.34	3.17
FeO	7.88	7.05	7.52	5.09	0.91	3.87	3.52	0.55
MnO	0.15	0.18	0.18	0.21	0.20	0.22	0.22	0.11
MgO	7.07	12.23	9.36	4.94	0.20	13.99	11.85	0.94
CaO	9.28	10.40	10.29	7.92	0.70	14.98	10.55	3.49
Na_2O	3.77	3.03	3.74	5.40	9.92	2.03	2.79	2.79
K_2O	0.86	1.17	1.45	2.51	7.17	1.23	2.17	7.18
P_2O_5	O.42	0.64	0.85	0.87	0.09	0.77	0.82	0.20

1. Average of 11 YLS and OLS; 2. average of 5 alkali olivine basalts; 3. average of 7 hawaiites; 4. average of 2 mugearites; 5. average of 10 phonolites; G96 a clast of olivine basalt from the pyroclastics of Wadi Qurdu; G127 a clast of olivine basalt from the pyroclastics of Wadi Qabil; G128 phonolite from the central part of the Kaf Tekut igneous body.

Kaf Abu Ghannush: The Kaf Abu Ghannush phonolite is a discordant mass of irregular shape, displaying a variety of contact relationships. The mass itself is cut approximately in the centre by two phonolite sheets of dykes and at least one dyke-like mass at a lower level of the igneous body. The setting of the mass is best explained as a stock or laccolith with locally sill-like apophyses. Remnants of the country rock can be clearly seen in the centre. The relationship between this phonolitic mass and the country rocks is not very clear at the present level of erosion. However, the presence of a smal fault in the eastern part of the intrusion with marked dip of the sediments away from the igneous body suggests that the mass may have caused the tilting and faulting.

Kaf Mantrus: Another prominent hill with an impression of more resistant marginal facies (giving summit peaks) with steep jointing, this is also probably an intrusive dome.

It is very difficult to assess the field relationships between the phonolitic mass (Kaf Mantrus) and the country rock, as the sedimentary rocks are weathered all round, particularly north and north west of the phonolitic mass where the Jefarah lowland emerges. Piccoli (1970) interpreted the morphological setting of Kaf Mantrus as a doming protrusion or plug of highly viscous lavas similar to those known parts of the central Saharan zone of Atakor (Girod, 1964) and Tibesti (Vincent, 1970). Further reconnaissance of Kaf Mantrus and similarly formed phonolites (e.g. Ras Umm al Ezz, Ras al Jammah) suggests that they are best interpreted as shallow intrusive "phonolitic domes" rather than extrusive bodies.

LATE VOLCANIC CENTRES

These form prominent features scattered on and around the main plateau lava field. They almost always occur as distinct hills or clusters of hills rising above the general level of the plateau and usualy seen from a considerable distance in the field. Scoria cones are locally present at a few centres, suggesting that they are fairly young (Busrewil and Wadsworth, 1980). In some areas, only intrusive rocks are found, in the form of dykes, pipes, plugs and small dome-shaped masses that probably did not reach the surface in the liquid state, but have been exposed by erosion. The intrusive "centres" occur in different parts of the area, particularly north of Mizdah and the northern jabal escarpment where dykes of very limited length (a few tens of metres) indicate rather localized upwelling of magma, probably connected to a volcanic vent. Field description of the most prominent and accessible centres has already been given (Busrewil and Wadswoth, 1980) and details need not be repeated here.

PYROCLASTIC ROCKS

Initial Statement

The occurrence of numerous localities of fragmentary volcanic rocks in the GVP raised the problem as to the primary or secondary origin of these materials (Gray, 1971). Some may have flowed down wadis (Hey, 1962). Others are associated with dykes having a NW strike (Gray, 1971). Tuff cones composed of abundant thin beds made up of fragmentary materials with accretionary lapilli, presumably resulted from large eruptive pulses, characteristic of hydrovolcanic eruption, were encountered SE of Al Urban village. In addition, numerous occurrences of diatremes with occasional presence of herzolites are partially exposed along new road cuts. Furthermore, a well bedded pyroclastic materials appear to be sandwiched between lava flows of the YLS were also observed at Wadi Mugaitilah (32° 02′10″ N, 13° 12′20″E). Based on position relative to source, these rocks are divided into vent facies, near-souce facies and distal or fluvial facies as was recognized elsewhere by many writers (R. Walker, 1984; Fisher and Schmincke, 1984; Cas and Wright, 1988). The characteristics which gave clues to the mode of deposition or environmental condition, or both, at the time of emplacement, are emphasized. These are described in descending order of frequency of occurrence and also in descending order of aggregate volume of preserved deposits as follows.

Vent Facies

Numerous occurrences are partially exposed along wadi systems or new road cuts. At Kabdet al Jamel locality, there is a distinct area of pyroclastic rocks which are separated from Kaf Tekut phonolite by Wadi Qurdu and is entirely surrounded by Abu Ghaylan Formation (Middle Jurassic). These rocks are predominantly consolidated assemblages of pyroclasts. They are black, massive, poorly sorted deposits, consisted of a mixture of volcanic fragments (>90% of lapilli tuff) and sedimentary materials (approximately 5 cm in diameter). Matrix-supported blocks (up to 80 cm in diameter) of the underlying sediments and volcanics are common.

In several other localities including Wadi Qurdu and Wadi Qabil there are breccias which are restricted to outcrops within existing wadi systems. These deposits are uniformly massive, dull grey. Subangular to subrounded fragmens 5 cm. in diameter are common. Matrix-supported blocks of basic volcanics occur locally, as do a few Mesozoic sedimentary rock fragments. Dense and unvesiculated clasts of 10–15 cm. diameter showing impressive ball – milling were found associated with the pyroclastics of Wadi Qurdu and Wadi Qabil. A whole rock chemical analysis of two clasts show their alkaline character (Table 2). Volcanic dykes, which cut through the pyroclastics, range in width from 2 m. to 15 m. and can be followed over a distance in excess of 100 m.

Abundant ultramafic xenoliths, thought to be derived from the upper mantle, were found in the vent facies and their associated dykes as well (al Urban area, 200 m east of Ras al Masid). The latter are known for their abundance of ultramafic nodules (Busrewil and Wadsworth, 1980). This may suggest that magma composition and pyroclastic eruption appear to be related. Mineralogically, they comprise variable proportion of highly magnesian olivine, orthopyroxene and clinopyroxene, commonly together with spinel (Busrewil and Wadsworth, in prep.). The presence of associated ultramafic xenoliths and accidental pieces of the underlying sediments as well as the products of ball-milling and the overall stratigraphic position demonstrate that these fragmentary materials are obviously volcanic vents. The ascending magma may have intruded through reactivated faults and the deposits may have been formed initialy by vent opening phreatomagmatic activity. Renewal of volcanism in the form of localized dykes cutting in the middle part of the vent facies deposits may be related to lack or decrease in the efficiency of water/melt interaction as all observed fractures are filled with secondary minerals (mostly calcite).

Proximal Facies

This facies represent the northern part of Wadi Ghan pyroclastic deposits. The pyroclastics itself are approximately 15 m thick and consists of small fragments cemented together in a calcareous matrix. These fragments are all subangular (up to 3 cm in diameter) and apparently 80% basic rocks and 20% sediments. The lower part of the exposed facies show trough cross-bedding while the upper part is massive. Compared with the distal facies it is darker in colour and show very little or no systematic lateral and vertical variation in clast content, size and composition. It is suggested that the near-source facies, partialy exposed at this locality, may have been formed initially by vent opening phreatic-phreatomagmatic explosion. Unlike the vent facies it appears to have been remobilized shortly after deposition within possibly an old valley or a vent flank or a cut-off channel.

Distal Facies

These pyroclastics are best displayed in the walls of Wadi Ghan area for over 1 km stretch. The deposits were first described by Hey (1962) as a "mud flow" with uncertain climatic or volcanic origin. They are unconformably underlain by the Ain Tobi Member of

Cenomanian age and overlain sharply by Qasr al Haj Formation of Pleistocene age. At its head, this facies appears as massive water-laid volcanic breccias. It is dark grey in colour, approximately 6 m thick and consists of small fragments (basalt & sediments) cemented together in a calcareous matrix. The clasts, 1–4 cm, are subangular to subrounded and poorly sorted.

The massive unit passes down-flow within some 300 m to cross-bedded subfacies. Halfway along the direction of transport, a vent facies cutting this distal facies can be observed. Both of which were intruded by a basanitic dyke. The source of the reworked pyroclastics is thought to have resulted initially from localized explosive volcanism at or near the catchmet area of Wadi Ghan. The products of which were later transported with local sediments to its present day position. The presence of few tuff cones in the area of study may reinforce this conclusion. From the previous examples, it seems clear that the three types of pyroclastic rocks have much in common in terms of lithologies, nonetheless, they are distinct in both appearance and mode of emplacement.

RADIOMETRIC DATING

Piccoli (1970) made preliminary measurements of rocks from the Gharyan Volcanic Province which has provided K-Ar results around 52, 35.5 Ma for the old lava series, 37.9, 39.7, 40.7 Ma for the isolated phonolite masses, 29.5, 5.7, 3.5 Ma for the young lava series from Wadi Ghan and Bani Walid areas. He also reported ages of 11.5 and 8.5 Ma for two isolated shield volcanoes (Rus Al Moher and Tebrah). Further age determination by Ade-Hall *et al.*, (1975) yielded a young ages of 2–6 Ma from sites in the northern part of the main lava field. From Ade-Hall *et al.*, (1975) description of the localities, these samples appear to have been collected from the YLS. They have considered that the ages of the plateau lavas (OLS) are much younger than indicated by Piccoli (1970) and attributed this discrepancy to excess argon.

The present work presented six new whole rock K-Ar age data (Table 1). This is supplemented by unpublished data by Mobil. Based on age data and field observation the following suggestions are made.

1. Piccoli (1970) suggested that the OLS was extruded from fissure sources during Early Eocene (52 Ma). It is asssumed, until further age data are obtained, that such ages must remain conjectural, as no new data are available to substantiate such igneous activity.
2. The whole-rock ages for the phonolites, obtained from three different laboratories do cluster heavily around 40 Ma (Piccoli, 1970; Table 1). This suggests that the data are of value and supports an Eocene age for the early emplacement of the phonolites. It also suggestive of relatively long emplacement history spanning an interval of approximately 10 Ma. After long period of quiescence another phase of igneous activity led to the emplacement of the LVC and the YLS.
3. The 29 Ma age dating of a basalt sample from Wadi Ghan (Piccoli, 1970) should be considered suspect as a much younger age was obtained by Mobil from the same locality (2.6 Ma). The latter age is consistent with field observations and lies within the age range of the YLS. Two discrete episodes of the YLS are present and can best be seen in Wadi al Hamam area. The youngest of these may be of Holocene age.
4. Renewal of volcanism in the form of localized explosive volcanism is developed and resulted in the emplacement of tuff cones and intrusive as well as reworked pyroclastics. Field evidence suggests that this phase of igneous activity must be geologically very young (Pleistocene – Holocene) and could be contemporaneous with the emplacement of volcanic dykes and the extrusion of the last episode of the YLS.

PETROGRAPHY

The Lava Series (OLS and YLS)

These rocks are coarse grained compared with the basanitic suite. The phenocrysts consist exclusively of olivine and pyroxene but they are rarely abundant. Olivine phenocrysts are rounded to subhedral in shape and are partly iddingsitized, particularly in the peripheral zones. Clinopyroxene phenocrysts are usualy pale brown augite and exhibit slight zoning. The groundmass consists of plagioclase, pale brown augite, granular olivine and opaque oxides (Table 3). Plagioclase forms the dominant phase in all sections

Table 3. Microprobe analysis of selected minerals from GVP*

Rock Type	Pheonolite			Basaltic andesites		
Rock No	G66[1]	G66[2]	G66[3]	G116[4]	G19[5]	G19[6]
SiO_2	44.81	66.25	39.21	51.68	55.08	36.40
TiO_2		–	6.61	0.95	–	–
Al_2O_3	32.83	19.66	13.78	4.18	29.35	–
FeO	0.63	0.18	9.54	6.91	0.45	33.99
MgO	–	–	13.69	15.71	–	29.70
CaO	–	0.13	11.86	20.23	11.59	0.33
Na_2O	17.42	5.31	2.65	–	4.98	–
K_2O	3.96	9.43	1.18	–	0.17	–
MnO	–	–	0.09	0.15	0.07	0.50
Total	99.65	100.96	98.43	99.81	101.69	100.92

1 = Nepheline; 2 = K. Feldspar; 3 = Kaersutite; 4 = Augite; 5 = Plagioclase (An_{57}); 6 = Olivine (Fo_{61}). * = for Gharyan basanitic suite see Busrewil and Wadsworth (1980).

studied, exhibits slight normal zoning and occurs as tabular crystals. Albite twinning is common but combined carlsbad-albite twinning is often developed. The titaniferous oxides are abundant in the rocks and seem to belong to magnetite – ilmenite assemblages. Apatite needles are sparsely disseminated throughout the rocks.

Phonolites

Many of the phonolites are virtually aphyric but some of them are porphyritic. The phenocrysts include, in order of decreasing abundance, alkali feldspar, nepheline, amphibole, iron-titanium oxides and sphene. The alkali feldspar is represented by sparsely scattered phenocrysts of sanidine and to less extent of anorthoclase. Both types of alkali feldspar are locally zoned, have a patchy extinction and exhibit a small degree of late stage hydrothermal alteration in which the feldspar is altered to sericite. Small euthedral nephelines also occur as rectangular phenocrysts and are most abundant in the more sodic phonolites (Fig. 4). Phenocrysts of clinopyroxene are pale green to pale brown, weakly pleochroic sodic augite and occasionally a deep brown resorbed variety is

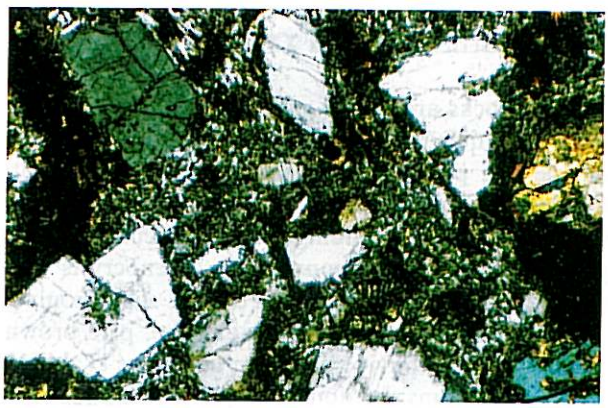


Fig. 4. Phenocrysts of anorthoclase, nepheline (top left) and augite set in a fine-grained groundness; X 35; X PL.

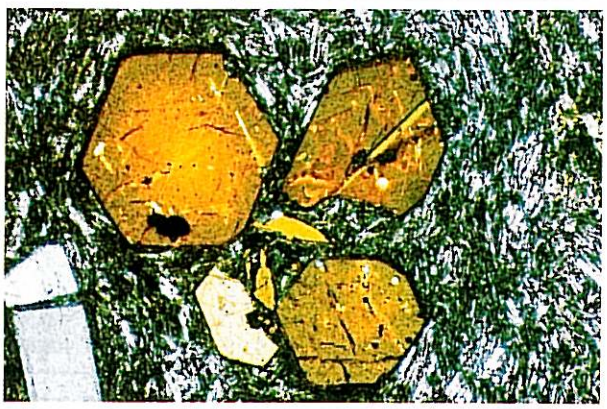


Fig. 5. Phenocrysts of sodic amphibole set in a very fine-grained groundmass; X 35; X PL.

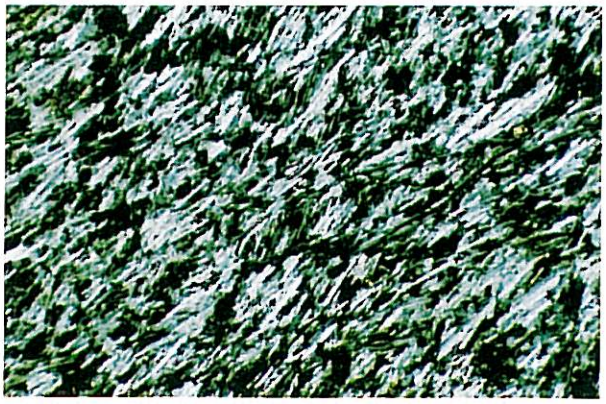


Fig. 6. Typical fine-grained phonolite. Alkali feldspar and aegirine form the bulk of the crystalline phases together with opaque oxides; X35, X PL.

locally recognised in some sections (Table 3). Phenocrysts of sodic amphiboles occur sporadically (Fig. 5). Dark brown kaersutite phenocrysts are mantled by granular clinopyroxene and opaque oxides. Similar aggregates without kaersutite cores are interpreted as completely resorbed amphibole crystals. Equant grains of iron ores are present as microphenocrysts whereas sphene occurs as euhedral grains. The groundmass is fine (trachytic texture) and consists of alkali feldspar laths (and maybe feldspathoid), laths are extremely ill-defined with marked patchy extinction (Fig. 6). The aegirine is found as minute grains which are strongly pleochroic with marked greenish colour. The iron ore is liberally scattered as interstitial patches throughout the groundmass. Apatite forms needle-shaped inclusions while the analcime makes up cloudy patches replacing the former groundmass. Deformation fabrics within the phonolites are lacking and this clearly indicates that the intrusions occurred prior to any significant crystallization of magma as this is typical of high-level forceful intrusions.

Basanitic Suite

Almost all the olivine basalts are characterised by the absence of plagioclase phenocrysts and by abundance of clinopyroxene and olivine phenocrysts. The clinopyroxene phenocrysts often occur in small clusters and individual crystals frequently display hourglass zoning. They are rarely pleochroic, though very occasionally they have mauve pleochroic rims, probably enriched in Ti. The olivine phenocrysts are often colourless, generally unzoned, unhedral or subhedral in shape and are commonly idingsitized. Large olivines (but less abundant anhedral variety) are now more magnesium-rich (Fo_{90}) and show evidence of deformation. These are interpreted as xenocrysts derived by fragmentation of the lherzolites. The compostion of resorbed olivine xenocrysts are similar to

those of olivines from the ultramafic xenoliths (Busrewil and Wadsworth, 1980). Orthopyroxene grains also occur locally and probably also resulted from distintegration of ultrabasic inclusions. The groundmass of the olivine basalt is on the whole very fine grained and glassy patches are not unusual. In addition it contains a high percentage of ore minerals and randomly oriented laths of plagioclase, olivine and titanaugite. Nepheline and/or analcime, although they may be present, have not been identified under the microscope. The aphyric types are identical texturally to the groundmass of the porphyritic types.

Many hawaiites are texturally indistinguishable from the olivine basalts, although olivine and augite are almost always coexisting phases (where they are present). Their only difference being the bulk chemistry. The groundmass of typical hawaiites tends to be less mafic than the basalts. It comprises very fine grained plagioclase laths associated with iron-oxides, clinpyroxene and olivine groundmass. Apatite and iron oxides are common accessores.

The mugearites are pedominantly aphyric. The groundmass is nearly the same colour as the hawaiites except in the reduction of olivine and to lesser extent clinopyroxenes. The plagioclase consists almost entirely of very fine grained laths. Larger microphenocrysts of pale green pyroxene and colourless olivine are encountered.

CHEMISTRY

Average chemical composition of the several groups from the GVP are listed in Table 2 and pertinent features of the alkalies are plotted on TAS variation diagram (Fig. 2). Although the petrology of these rocks will be the subject of a further contribution, the variation of selected major and trace elements against S.I. is deliberately presented to support the three fold divisions of th GVP (Figs. 7–8). The phonolite analyses are conspicuous features and obviously form a discrete group with very clear separation from other groups. The plateau lava (OLS + YLS) has a narrow compositional range and attains a differentiation index (D.I.) between 35–40 (Almond *et al.*, 1974; Busrewil, 1974). This suggests that they are not primary magma, but rather fractionated melts derived from a primary magma. In

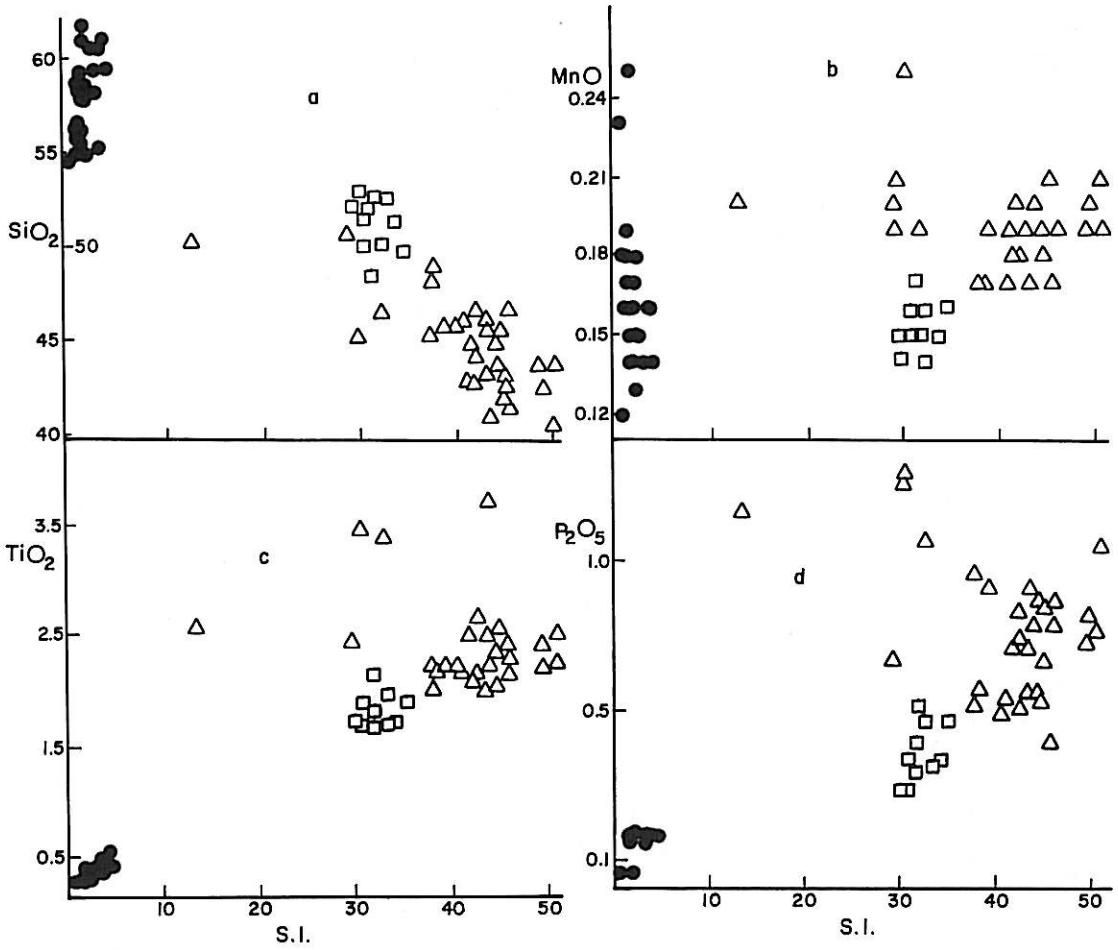


Fig. 7. SiO_2, MnO, TiO_2 and P_2O_5 *vs* Solidification Index (S.I.) for Gharyan volcanics.

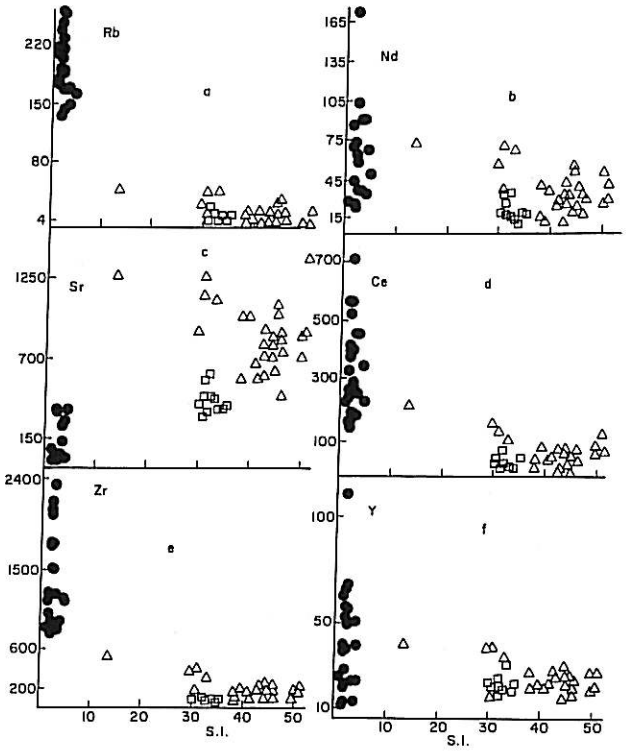


Fig. 8. Rb, Nd, Sr, Ce, Zr and Y *vs* Solidification Index (S.I.) for Gharyan volcanics.

addition most of the analysed rocks contain normative hypersthene and were thus named transitional hawaiites by Busrewil, (1974). Utilizing the parameters Total Alkali-Silica diagram for the chemical classification of volcanic rocks (Le Bas *et al.*, 1986, 92) they lie in the basalt andesite field (Fig. 2). The basanitic suit as a whole is strongly sodic with Na_2O/K_2O ratio exceeding 2:1 (Table 2). Compared with the OLS and YLS, they cover a much wider range (Basalt-hawaiite-mugearite) of composition. They also contain less SiO_2, Al_2O_3 and exhibit a more pronounced enrichment of the minor elements (TiO_2, P_2O_5, MnO, K_2O, Na_2O) and most of the trace elements (Figs. 7–8) compared with the lava series of similar S.I. values. This difference emphasises the individuality of the basanitic rocks when compared with the old and young lavas series and may be related to higher pressure fractionation or lower degrees of partial melting of upper mantle materials (Busrewil and Wadsworth, 1980).

The volcanic materials of the vent facies, although, altered, are mafic, very poor in silica and high in MgO (Table 2) suggesting little or no fractionation since equilibration of magma with mantle materials.

DISCUSSION

In Tertiary time the Gharyan area has been the site of extensive alkaline volcanism that has continued (but with interruption) to recent times and resulted in the emplacement of three suites of alkalic rocks. The products of the OLS and YLS were mildly basaltic andesites. These subalkaline rocks are by far the dominant rock type exposed on east Jabal Nafusah. They show no evidence of wide spread differentiation and form the lava plateau field. Similar subalkaline rocks were described from central Libya (Busrewil and Suwesi, 1993) and Ethiopia (Mohr and Zanettin, 1988). The phonolites form prominent isolated dome-shaped intrusions and display a variety of contact relationships with the associated Mesozoic sediments. In a few places the phonolites were intruded by the basanitic dykes (e.g. Kabdat al Jamal area) but nowhere show contact with the plateau lava. They are much older than the associated basanitic rocks and were thus interpreted as an ultimate residue of fractionation from an undersaturated basic parental melt at depth (Almond *et al.*, 1974). Similar suggestion was envisaged for the evolution of Harrat Kishb phonolites of Saudi Arabia (Camp *et al.*, 1992).

The LVC are, for the most part, extrusive (volcanic cones, shield volcanoes). However, there is a possibility that in some instances the dykes had an intact roof, and the magma never reached to the surface. The rocks themselves display a particularly rather wide variety of rock types (olivine basalt – hawaiite – mugearite). The more evolved varieties are exposed at only few localites and appear to constitute a very small volume of eruptive products (less than 2% in areal extent). The parental melts are thought to have been moved rapidly from depth to higher levels, where most of the chemical variation is produced by low pressure crystal fractionation (Busrewil and Wadsworth, 1980).

The pyroclastic rocks are predominantly consolidated assemblages of volcanic fragments. Based on field criteria, these rocks are divided into source or vent facis, near-source facies and distal facies. The source facies are thought to be related to pyroclastic dykes and tuff cones and their origin seems to be due to interaction between magma and subsurface water. The abundance of ultramafic nodules in this facies is a clear testimony to their rapid flow rate through the crust. The souce of the reworked pyroclastic rocks (near-source and distal facies) is probably related to these localised explosive volcanism. The products of which were later transported by wadi system to their present localities.

Radiometric dating of the GVP has been confined to limited number of K-Ar whole rock. Despite their inherent flaws (inherited Ar and/or Ar loss) existing K-Ar ages for the GVP do cluster heavily in two discrete episodes (around 40 Ma for the phonolites and 10-1 Ma for the LVC and YLS. There is thus an agreement that the two periods witnessed the emplacement of phonolites, the extrusion of volcanic

cones and pyroclastic rocks as well as the outpouring of the YLS. The age of the OLS has been much debated (Ade-Hall *et al.*, 1975) and the existing data emphasize the need for better understanding of relative age distribution within the GVP.

REFERENCES

Ade-Hall, J.M., Gerstein, R.E., Reynolds, R.H., Dagley, P., Mussett, A.E. and Hubbard, T.P., 1975. Geophysical studies of North African Cenozoic volcanic areas: III, Garian, Libya. *Can. J. Earth Sci.*, **12**, 1264–1271.

Almond, D.C., Busrewil, M.T. and Wadsworth, W.J., 1974. The Gharian Tertiary volcanic province of Tripolitania, Libya. *Geol. J.*, **9**, 17–28.

Antonovic, A., 1977. Geological map of Libya, 1:250.000. Sheet:Mizdah (NH 33-1) Explanatory Booklet. *Ind. Res. Cent.* Tripoli, 68 P.

Busrewil, M.T., 1974. *The Petrology and Geochemistry of Tertiary Volcanic Rocks from Ghirian Area, Tripolitania, Libya.* Ph.D. thesis, Victoria University of Manchester, 152 P.

Busrewil, M.T. and Suwesi, K.S., 1993. Geological map of Libya, 1:250.000. Sheet: Al Haruj al Aswad (NG-33-4). Explanatory Booklet. *Ind. Res. Cent.*, Tripoli, 95 P.

Busrewil, M.T. and Wadsworth, W.J., 1980. The basanitic volcanoes of the Gharyan area, NW Libya. In: Salem, M.J. and Busrewil, M.T. (eds.) *The Geology of Libya.* London: Academic Press, III, 1095–1105.

Camp, V.E., Roobol, M.J. and Hooper, P.R., 1992. The Arabian continental alkali basalt province: Part III. Evolution of Harrat Kishb, Kingdom of Saudi Arabia. *Bull. geol. Soc. Am.*, **104**, 379–396.

Cas, R.A.F. and Wright, J.V., 1988. *Volcanic Successions, Modern and Ancient.* London: Chapman & Hall, 528 P.

Christie, A.M. 1955. Geology of the Garian area, Tripolitania, Libya. U.N. Tech. Assistance Program Rept. TAA/LIB/2, 60 P.

El Hinnawy, M. and Cheshitev, G., 1975. Geological map of Libya, 1:250.000. Sheet: Tarabulus (NI 33-13). Explanatory Booklet. *Ind. Res. Cent.*, Tripoli, 65 P.

Fisher, R.V. and Schmincke, H.U., 1984. *Pyroclastic Rocks*, Berlin: Springer-Verlag, 472 P.

Girod, M., 1964. Mode de mise en place de protrusions de l'Atakor (Hoggar). *Bull Soc. Geol. Fr.*, **6**, 64–68.

Gray, C., 1971. Structure and origin of the Gharian dome. In: Gray, C. (ed.) *Symposium on the Geology of Libya.* Fac. Sci. Univ. Libya, Tripoli, 307–319.

Hey, R.W., 1962. The Quaternary and Paleolithic of northern Libya. *Quaternaria*, **6**, 435–449.

Le Bas, M.J., Le Maitre, R.W., Streckeisen, A. and Zanettin, B., 1986. A chemical classification of volcanic rocks based on the total alkali – silica diagram. *J. Petrology*, **27**, 745–750.

Le Bas, M.J., Le Maitre, R.W. and Woolley, A.R., 1992. The construction of the total alkali-silica chemical classification of volcanic rocks. *Mineral. Petrol.*, **46**, 1–22.

Lipparini, T., 1940. Tettonica e geomorfologia della Tripolitania, *Bull. Soc. Geol. Ital.* **59**, 222–301.

Mann, K., 1975. Geological map of Libya 1:250.000. Sheet: Al Khums (NI 33–14). Explanatory Booklet. *Ind. Res. Cent.*, Tripoli, 88 P.

Mohr, P. and Zanettin, B., 1988. The Ethipian flood basalt province. In: Macdougall, J.D. (ed.) *Continental Flood Basalts.* Dordrecht: Kluwer Academic Publishers, 63–110.

Piccoli, C., 1970. Outlines of volcanism in northern Tripolitania (Libya). *Boll. Soc. Geol. Ital.*, **89**, 449–461.

Vincent, P.M., 1970. The evolution of Tibesti volcanic province, eastern Sahara. In: Clifford, T.N. and Gass, I.G. (eds.) *African Magmatism and Tectonics.* Edinburgh: Oliver and Boyd, 301–319.

Walker, R.G. (ed.), 1984. Facies Models 2nd edn. *Geol. Assoc. Can.*, Geosci. Can. Repr. Ser.1.

Zivanovic, M., 1976. Geological map of Libya, 1:250.000. Sheet: Bani Walid (NH 33-2). Explanatory Booklet. *Ind. Res. Cent.*, Tripoli, 71 P.

PRJ, Vol. 8 (January 1996); P. 25–48, 3 FIGS, 9 PLATES

Foraminiferal Study of the Miocene From Well D2-NC41, Northwestern Offshore, Libya

Ahmed K. Abusrewil*

دراسة منخربات عصر الميوسين من البئر D2-NC41، شمال غربي الجرف القاري، ليبيا

أحمد أبو سريويل

من خلال المحتوى الأحافي للمنخربات لعدد 20 عينة فتاتية من المقطع تحت السطح للبئر D2-NC41 بمنطقة الجرف القاري لشمال غربي ليبيا والتي تغطي تكوينات المايا (جزء)، تبتة، مرسى زواغة، وجزء من السبابيل العائدة لعصور المايوسين الأوسط وحتى أسفل البلايوسين السفلي، قد تم التعرف على عدد 38 نوع من المنخربات الطافية و 85 نوع من المنخربات القاعية.

المنخربات الطافية في الجزء السفلي من المقطع تدل على النطاق ن8 للعالم بلو (1969، 1979) والدالة على عمر اللأنغيان (نطاق البري أوربيولينا كلوميروسا كلوميروسا). أما الأنطقة الحياتية ن8—ن18 والدالة على عمر السيرافاليان — أسفل البلايوسين السفلي فانه لم يكن بالإمكان تحديدهما بدقة نظراً لندرة المنخربات الطافية في هذا الجزء من المقطع.

الجزء السفلي من المقطع نسبياً غني بالمنخربات الطافية «25 نوع» وهذا يشير إلى بيئة ترسيبية ذات مياه عميقة، وباتجاه إلى أعلى المقطع نلاحظ نقص أو غياب المنخربات الطافية، وزيادة أو بداية ظهور بعض أنواع المنخربات القاعية مثل الالفيديوم والبينوروبليس، البوريليس ميلو وكوينكويلوكولينا تشير إلى أن تكاوين المايا العلوي (سيرافاليان)، وتبتة (تورتونيان) ومرسى زواغة (ميسينيان) كلها قد ترسبت تحت بيئة ترسيبية ضحلة، أما تكوين سبابيل (بلايوسين) فقد إبتدأ الترسيب عند بيئة بحرية أكثر عمقاً وهذا مشار إليه بواسطة ظهور منخربات طافية جديدة.

Abstract. *Analysis of the foraminiferal contents of twenty cutting samples from the subsurface section of well D2-NC41, offshore NW Libya, covering the Middle Miocene-lowermost Pliocene Al Mayah (part) Tubtah, Marsa Zouaghah, and Sbabil (part) Formations, has resulted in the recognition of 38 planktonic and 85 benthonic foraminiferal species.*

Planktonic Foraminifera at the lower part of the section indicate Zone N8 of Blow (1969, 1979) of Langhian age (=Praeorbulina glomerosa glomerosa Zone). Zones N9-N18 indicating Serravallian – lowermost Lower Pliocene are not precisely determined due to the lack of planktonic Foraminifera.

The lower part of the section is relatively rich in planktonic Foraminifera (25 species) indicating deep water paleoenvironment. Upward the section a noticeable decrease and/or absence of planktonic Foraminifera, and the increase and/or first appearance of benthonic foraminiferal species Elphidium spp., *Peneroplis* spp., *Borelis melo, and Quinqueloculina* spp. *would indicate continuous shallowing during the deposition of the upper Al Mayah Formation (Serravallian), the Tubtah Formation (Tortonian), and the Marsa Zouaghah Formation (Messinian). The Sbabil Formation (Pliocene) deposition commenced with more deep marine environment indicated by the new appearance of planktonic Foraminifera.*

INTRODUCTION

This study is part of a large micropalaeontological project of the Oligiocene–Pliocene of the Tarabulus Basin, Pelagian Platform, offshore northwestern Libya which is being carried out by the Petroleum Research Centre, Tripoli, to re-evaluate its foraminiferal contents, biostratigraphy, palaeoecology, stratigraphy and correlation with neighbouring areas.

* Petroleum Research Centre, P.O. Box 6431, Tripoli, G.S.P.L.A.J.

More than 50 exploratory wells have been drilled in this area. Many other biostratigraphical investigations have been published (Van Hinte *et al.*, 1980; Hammuda *et al.*, 1985; Eliagoubi, 1986, Hammuda *et al.*, 1991). On onshore areas of NW Libya Salem and Spreng (1980), and Sherif (1991) published more detailed studies on Miocene biostratigraphy of Al Khums Formation.

Well D2-NC41 which is situated in the centre of the Tarabulus Basin, (Fig. 1) was drilled in 1977. It penetrated a sedimentary sequence of 12377 ft (3772.5m) ranging in age from Cenomanian to Pliocene. The sea bed was encountered at 545 ft (166 m) and the first recovery at 805 ft (245 m) within the Sbabil Formation.

Twenty cutting samples were processed using standard micropalaeontological techniques. The Foraminifera were picked and partly identified at the Geology Department, Glasgow University, United Kingdom. The benthonic Foraminifera were photographed using scanning-electron microscope and 9 plates were prepared. The planktonic Foraminifera and other additional benthonic Foraminifera from the same samples were indentified at the Petroleum Research Centre, Tripoli, Libya. The nomenclature of Foraminifera is mainly based on those by Loeblich and Tappan (1964, 1988).

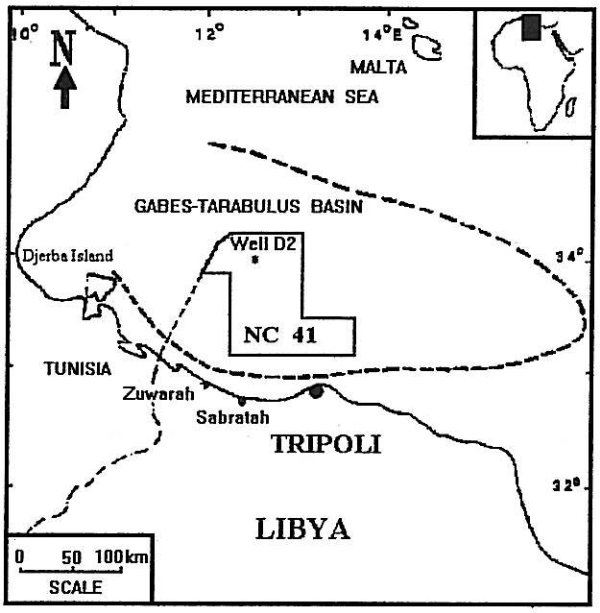


Fig. 1. Location map of the study area.

STRATIGRAPHY

The studied sequence in well D2-NC41 consists of four rock units, these are in ascending order:

Al Mayah Formation

Al Mayah Formation in well D2-NC41 consists of 2945 ft (depth 4990 ft–2045 ft) sequence of silty and sandy clays and shales with levels of sand. Originally the name "Mahmoud Formation" was given to the lower 1378 ft and the name "Beglia Formation" to the 1567 ft by Costa and Fandi (1977), however, the whole sequence is attributed to Al Mayah Formation (Hammuda *et al.*, 1985, pp. 25–32, 129–133).

Tubtah Formation

The Tubtah Formation in well D2-NC41 consists of 815 ft (depth 2045 ft–1230 ft) sequence of limestone (wackestone/packestone), grey green clay with levels of wackestone, and limestone (wackestone, locally boundstone), sometimes oolitic. Originally, Costa and Fandi (1977) considered this interval to belong to the upper part of the "Beglia Formation".

Marsa Zouaghah Formation

The Marsa Zouaghah Formation in well D2-NC41 consists of 360 ft (depth 870 ft–1230 ft) sequence of crystalline gypsum with levels of white, fossiliferous, slighty dolomitic limestone (wackestone/packestone). Costa and Fandi (1977) considered this interval as the "Saouaf Formation" which is unconformably overlain by "Raf Raf Formation" (=Sbabil Formation of Hammuda *et al.*, 1985).

Sbabil Formation

Only the lower 65 ft (depth 870 ft–805 ft) of this formation had been recovered from this well, however, the sea bed is at 545 ft giving possible thickness of 325 ft. The Sbabil Formation at this location consists of a sequence of mudstone and wackestone with interbeds of clay beds unconformably overlying the Marsa Zouaghah Formation.

BIOSTRATIGRAPHY

Planktonic Foraminifera

Thirty four planktonic forminiferal species have been identified (Fig. 2), they are: *Globigerina* cf. *apertura* CUSHMAN, *G. brazieri* JENKINS, *G. connecta* JENKINS, *G. eximia* TODD, *G.* cf. *falconensis* BLOW, *G.* cf. *globularis* ROEMER, *G. venezuelana* HEDBERG; *Globigerinita glutinata* (EGGER), *Gt. uvula* (EHRENBERG); *Globigerinoides apertasuturalis* JENKINS, *Gn. bisphericus* TODD, *Gn.* cf. *bollii* BLOW, *Gn. bullatus* CHANG, *Gn. dinapolii* OGNIBEN, *Gn. extremus* BOLLI, *Gn. immaturus* LEROY, *Gn. muratai* ASSANO, *Gn. obliquus* BOLLI, *Gn. quadrilobatus* (D'ORBIGNY), *Gn. parawoodi* KELLER, *Gn. sacculifer* (BRADY), *Gn. subsacculifer* CITA, PRIMOLI SILVA and ROSSI, *Gn. trilobus* (REUSS); *Globigerinopsoides algeriana* CITA and MAZZOLA; *Globoquadrina dehiscens* (CUSHMAN, PARR and

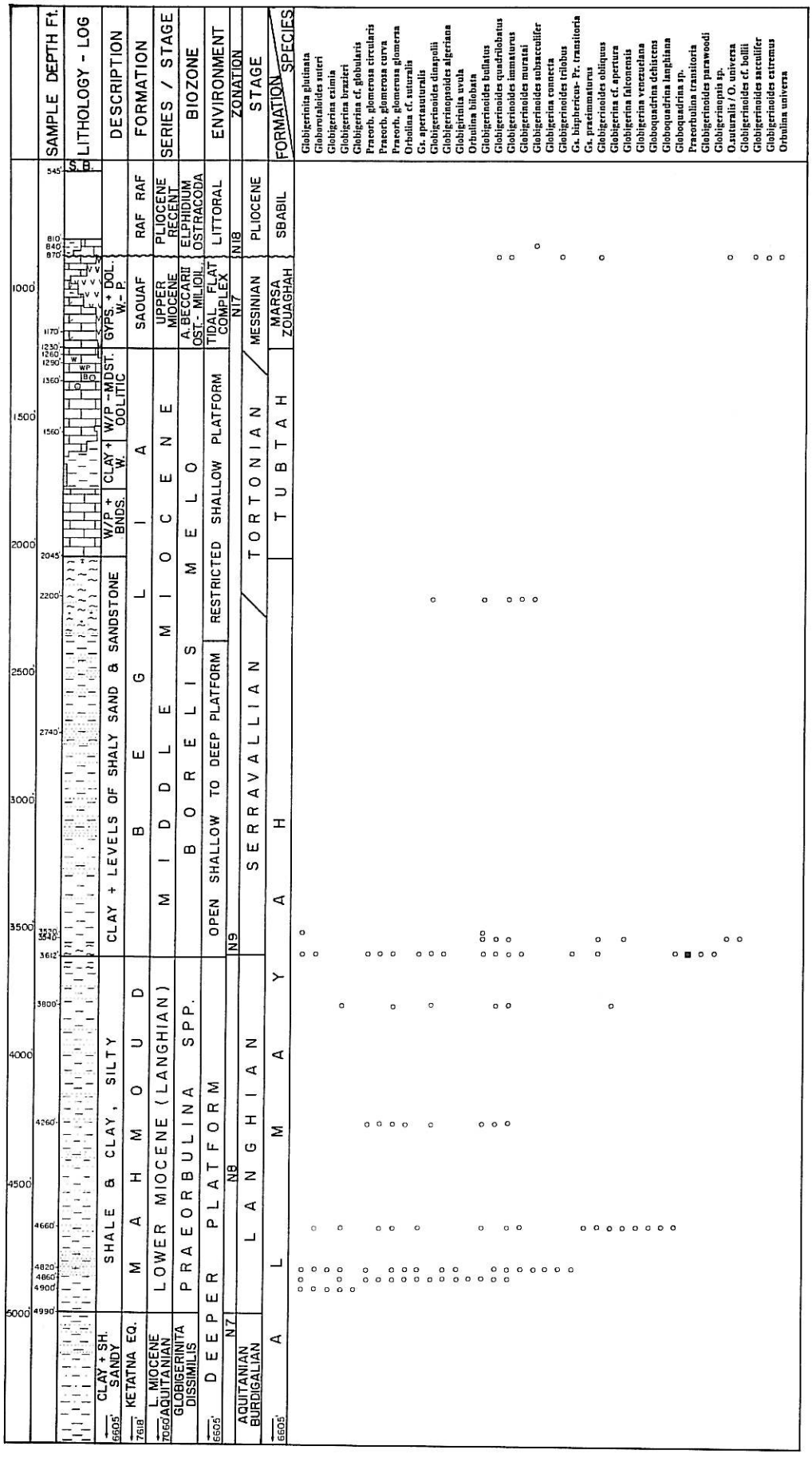


Fig. 2. Distribution of planktonic Foraminifera in the Miocene-Lowermost Pliocene of well D2-NC41, offshore, NW Libya.

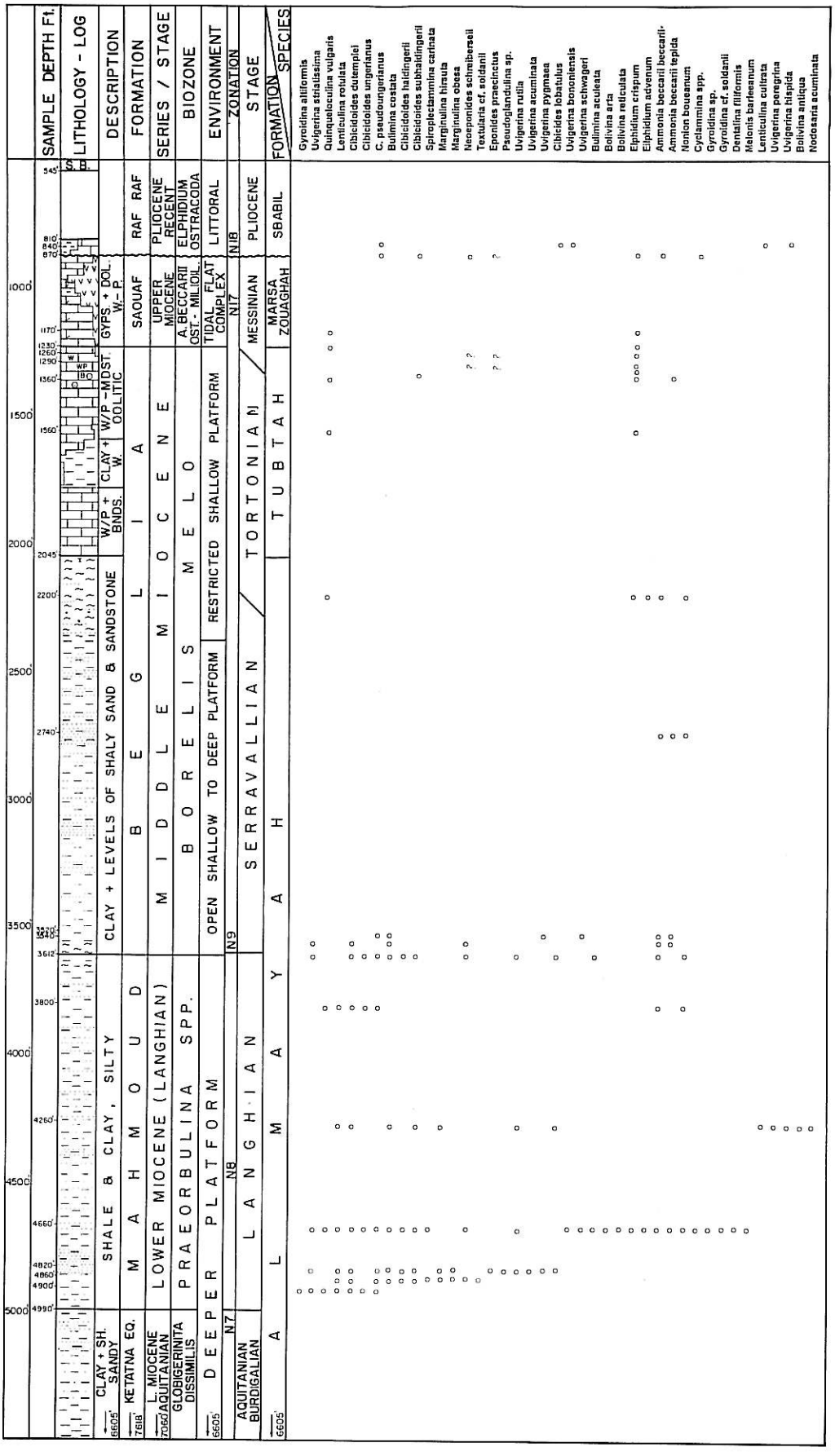


Fig. 3. Distribution of benthonic Foraminifera in the Miocene-Lowermost Pliocene of well D2-NC41, offshore, NW Libya.

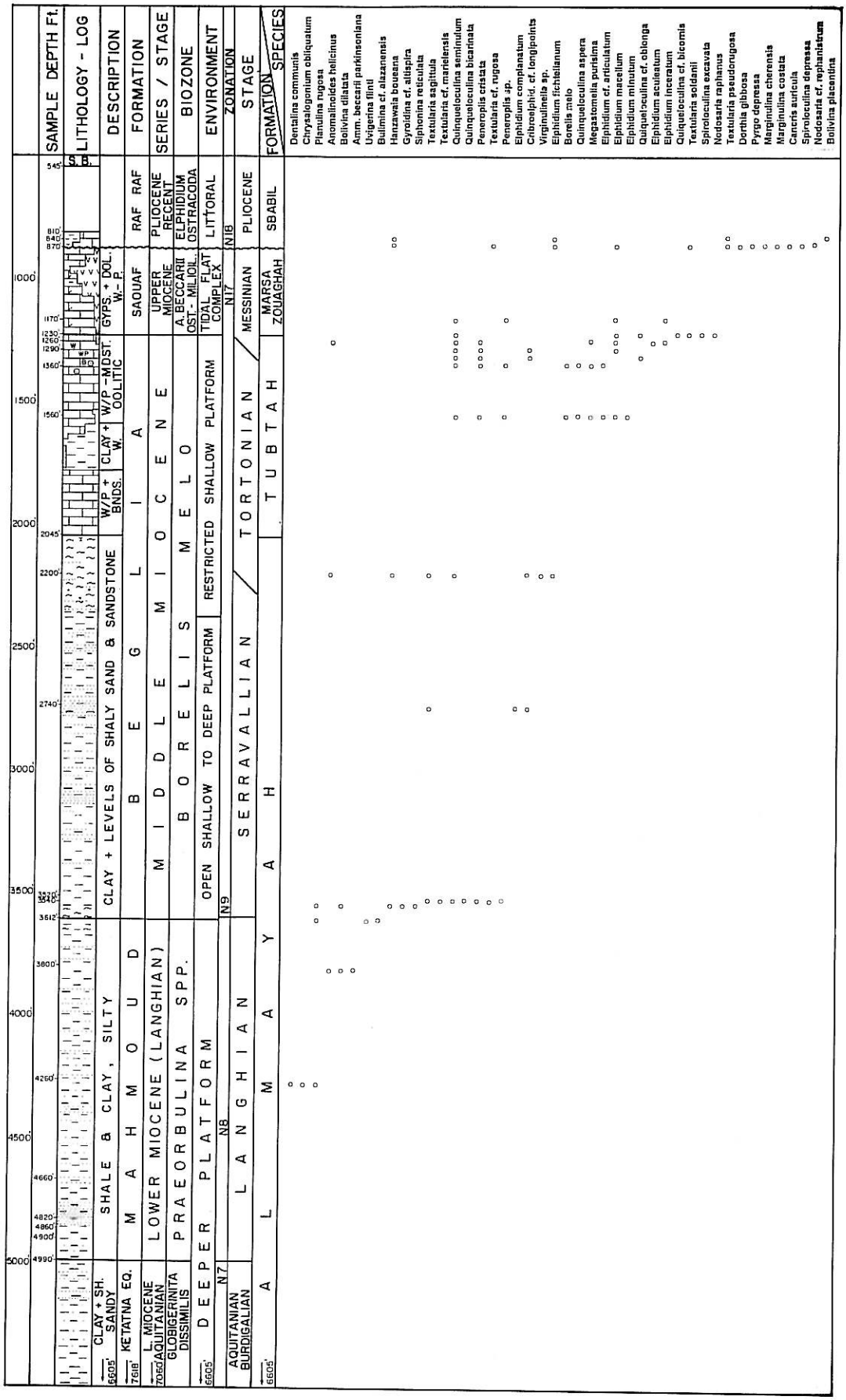


Fig. 3. Continuation.

COLLINS), *Gq. langhiana* CITA and GELATI; *Globorotaloides suteri* BOLLI; *Orbulina bilobata* (D'ORBIGNY), *O.* cf. *suturalis* BRONNIMANN, *O. universa* D'ORBIGNY; *Praeorbulina glomerosa circularis* (BLOW), *Pr. glomerosa curva* (BLOW), Pr. *glomerosa glomerosa* (BLOW) and *Pr. tranistoria* (BLOW).

Benthonic Foraminifera

Eighty five benthonic foraminiferal species have been identified (Fig. 3). They are: *A. Anomalinoides helicinus* (COSTA); *Ammonia beccarii beccarii* (LINNE'), *A. beccarii parkinsoniana* (D'ORBIGNY), *A. beccarrii tepida* (CUSHMAN); *Bolivina* cf. *antiqua* D'ORBIGNY, *B. arta* MACFADYEN, *B. dilatata* REUSS, *B. placentina* ZANMATTI, *B. reticulata* VON HANTKEN; *Borelis melo* (FICHTEL *and* MOLL); *Bulimina aculetata* D'ORBIGNY, *B.* cf. *alazanensis* CUSHMAN, *B. costata* D'ORBIGNY; *Cancris auricula* (FICHTEL and MOLL); *Chrysalogonium obliquatum* (BATSCH); *Cibicides lobatulus* (WALKER and JACOB); *Cibicidoides dutemplei* (D'ORBIGNY), *C. haidingerii* (BRADY), *C. pseudoungerianus* (CUSHMAN), *C. subhaidingerii* (PARR), *C. ungerianus* (D'ORBIGNY); *Cribroelphidium* cf. *longipointis* (SHCHEDRINA); *Cyclammina* sp.; *Dentalina communis* (D'ORBIGNY), *D. filiformis* (D'ORBIGNY); *Dorothia gibbosa* (D'ORBIGNY); *Elphidium aculeatum* (D'ORBIGNY), *E.* advenum (CUSHMAN), *E.* cf. *articulatum* (D'ORBIGNY), *E. complanatum* (D'ORBIGNY), *E. crispum* (LINNE'), *E. fichtelianum* (D'ORBIGNY), *E. incertum* (WILLIAMSON), *E. macellum* (FICHTEL and MOLL), *E. minutum* (REUSS); *Eponides praecinctus* KARRER; *Gyroidina altiformis* (CUSHMAN), *G. altispira* CUSHMAN and STAINFORTH, *G.* cf. *soldanii* (D'ORBIGNY), *G.* sp.; *Hanzawaia boueana* (D'ORBIGNY); *Lenticulina cultrata* (D'E'MONTFORT), *L. rotulata* (LAMARCK); *Marginulina cherensis* TEDESCHI and ZANMATTI, *M. costa* (BATSCH), *M. hirsuta* D'ORBIGNY, *M. obesa* CUSHMAN; *Megastomella purisima* (BRAMLETTE); *Meloniis barleeanum* (WILLIAMSON); *Neoeponides schreiberseii* (D'ORBIGNY), *Nodosaria acuminata* HANTKEN, *N.* cf. *raphanistrum* (LINNE'), *N. raphanus* (LINNE'); *Nonion boueanum* (D'ORBIGNY); *Peneroplis carinata* SILVESTRI, *P. cristata* SILVESTRI, *P.* sp., *Planulina rugosa* (PHLEGER and PARKER); *Pseudoglandulina sp.*; *Pyrgo depress* (D'ORBIGNY); *Quinqueloculina aspera* D'ORBIGNY, *Q. bicarinata* D'ORBIGNY, *Q.* cf. *bicornis* (WALKER and JACOB), *Q. oblonga* (MONTAGU), *Q. seminulum* (LINNE'), *Q. vulgaris* D'ORBIGNY; *Siphonina reticulata* (CZJEK); *Spiroloculina depressa* D'ORBIGNY, *S. excavata* D'ORBIGNY; *Textularia* cf. *marielensis* LALICKER and BERMUDEZ, *T. pseudorugosa* LACROIX, *T.* cf. *rugosa* COSTA, *T. sagittula* DEFRANCE, *T.* cf. *soldanii* FORNASINI, *T. soldanii* FORNASINI; *Uvigerina acuminata* HOSIUS, *U. bononiensis* FORNASINI, *U. flinti* CUSHMAN, *U. hispida* SCHWAGER, *U. peregrina* CUSHMAN, *U. pygmaea* D'ORBIGNY, *U. rutila* CUSHMAN and TODD, *U. schwageri* BRADY, *U. striatissima* PERCONIG; and *Virginulinella sp.*

AGE DETERMINATION AND ZONATION

Planktonic Foraminifera

Miocene

1. Aquitanian: In the Mediterranean area the Early Miocene boundary is taken at the base of the Aquitanian at the first appearance of *Globoqadrina dehiscens* (Iaccarino, 1985). The *Globoquadrina dehiscens dehiscens* Subzone (=Zone N4 and lower part of Zone N5 of Blow 1969, 1979) of the *Globoquadrina dehiscens dehiscens – Catapsydrax dissimilis* Zone was correlated with the Aquitanian stage (Iaccarino, *op. cit.*, p. 285), the upper boundary was taken at the first appearance of *Globigerinoides altiaperturus* which is in coincidence with the interval from the first appearance of *Globiquadrina dehiscens dehiscens* to the first appearance of *Globigerinoides altiaperturus.* In well D2/NC41 the Aquitanian has not been encountered in the studied samples.

2. Burdigalian: Iaccarino (1985, pp. 285–286) followed Demmarcq *et al.* (1974, *fide* Iaccarino, *op. cit.*) in their proposal of the second stratotype of the Burdigalian, they recognized Zones N5 (part), N6, and N7 of Blow (1969, 1979) to which Iaccarino (*op. cit.*, p. 285) correlated the *Globigerinoides altiaperturus – Catapsydrax dissimilis* Subzone of the *Globoquadrina dehiscens dehiscens* Zone and the *Globigerinoides-trilobus* Zone coinciding with the Burdigalian stage. The lower boundary of the Burdigalian was taken at the first occurrence of *Globigerinoides altiaperturus* and the upper boundary at the lower boundary of the Langhian coincident with the first occurrence of *Praerorbulina* spp. and *Globoquadrina langhiana* corresponding to the base of Zone N8 of Blow (1969, 1979). In well D2/NC41 the Burdigalian has not been encountered in the studied samples. However, Costa and Fandi (1977) drawn the base of the Langhian 90 ft below sample 4900 (i.e. at depth 4990 ft in well D2/NC41).

3. Langhian: Iaccarino (1985), Berggren and Miller (1989), and Miller and Katz (1987, part) considered the first appearance of *Praerorbulina glomerosa* marking the lower boundary of Zone N8 of Blow (1969, 1979) equivalent to the base of the *Praeorbulina glomerosa* Zone. Iaccarino (1985, p. 286) drawn the upper boundary of the *Praerorbulina glomerosa* Zone (=Zone N8) within the Langhian at the first appearance of *Orbulina saturalis* marking the lower boundary of the *Orbulina suturalis* Subzone of the *O. suturalis – Globorotalia peripheroronda* Zone corresponding to the base of Zone N9. The upper boundary of the Langhian corresponds to the first appearance of *Orbulina universa* marking the lower

boundary of the *Orbulina universa* Subzone of the *O. suturalis-Grt. peripheroronda* Zone, an event which is in coincidence with the last appearance of *Praeorbulina glomerosa* and thus identify the Langhian–Serravallian boundary (Iaccarino, *op. cit.*, p. 286, however, text-figure 4, p. 298 shows shorter range of *Pr. glomerosa*). Berggren and Miller (1989, p. 310) also considered the first appearance of *Orbulina saturalis* limiting the upper boudary of Zone N8 in the Lower Miocene.

However, studies by Blow (1969, 1979), Stainforth *et al.* (1975), Kennett and Srinivasan (1983), Bolli and Saunders (1985), Jenkins (1985), Belanger and Berggren (1986) and McLaughlin (1989) considered the *Praeorbulina glomerosa* Zone (=Zone N8 of Blow 1969, 1979) within the late Lower Miocene and the upper boundary of the Zone limiting the lower Middle Miocene boundary corresponding to the first appearance of *Orbulina suturalis*. Blow (1969, 1979) considered the Langhian equivalent to his Zones N9 – lower N15 corresponding to the whole Middle Miocene. Thus, based on the correlation with Iaccarino (1985), Miller and Katz (1987), and Berggren and Miller (1989) the Langhian is equivalent to Zones N8 and lower N9 of Blow (1969, 1979) and equivalent Zones corresponding to the interval from the first appearance of *Praeorbulina* spp. to the first appearance of *Orbulina universa* including the planktonic foraminiferal zones, the *Praeorbulina glomerosa* Zone and *Orbulina suturalis* Zone. In Well D2/NC41 this stage (i.e. the Langhian) is represented by 1390 ft (depth 3600–4990 ft) sequence in the lower part of the studied Al Mayah Formation in accordance with the total range of *Praeorbulina* spp. The first appearance of *Orbulina* spp. close to *O. universa* marking the top of the *Praeorbulina glomerosa* Zone (=Zone N8).

4. Serravallian: The first appearance of *Orbulina universa* marks the lower boundary of the Serravallian within the Middle Miocene of the Mediterranean area (Agip Mineraria, 1957, 1980; and Iaccarino, 1985). Similarly, the first appearance of *Orbulina* spp. was taken as the Middle Miocene lower boundary by Stainforth *et al.* (1975) and Kennett and Srinivasan (1983). Blow (1969, 1979) considered the Langhian representing the Middle Miocene and drawn its upper boundary (i.e. the Middle/Upper Miocene boundary) approximately at the middle of his Zone N15, slightly below the *Canadiana* Datum and the *Globorotalia acostaensis* Datum. Similarly Agip Mineraria (1957, 1980); Van Hinte *et al.* (1980), Belanger and Berggren (1986), and Berggren and Miller (1989) drawn the Middle Miocene upper boundary slightly below the first occurrence of *Neogloboquandrina acostaensis* which appeared very early in the Late Miocene limiting the lower boundary of Zone N16. Iaccarino (1985, pp. 285, 290, text-figures 1–4) also considered the upper boundary of the Middle Miocene corresponding to the upper boundary of the Serravallian slightly below the lower boundary of the *Globorotalia acostaensis* Zone within the uppermost Zone N15 (=*Globorotalia menardii* Zone) corresponding to the Middle/Upper Miocene boundary in the Mediterranean area. Stainforth *et al.* (1975), Kennett and Srinivasan (1983), Bolli and Saunders (1985), Miller and Katz (1987) and Mclaughlin (1989) took the upper boundary of the Middle Miocene with the first appearance of *Globorotalia acostaensis*, corresponding to the upper boundary of the *Globorotalia menardii* Zone (Stainforth *et al.*, 1975; Bolli and Saunders, 1985). In well D2/NC41 the lower boundary of the Serravallian is taken at the last appearance of *Praeorbulina* spp. This boundary is taken as the lower boundary of Zone N9 in accordance with Agip Mineraria (1957, 1980), Stainforth *et al.*, (1975), Kennett and Srinivasan (1983) and Iaccarino (1985). The upper boundary of the Serravallian is not exactly determined due to the lack of planktonic Foraminifera from the upper part of Al Mayah Formation in this well.

5. Tortonian: The lower boundary of the Tortonian (i.e. the Serravallian/Tortonian boundary) was drawn at the first occurrence of *Sphaeroidinellopsis seminulina*, *Globigerinoides sacculifer*, and *Globigerinita glutinata* slightly above the first occurrence of *Globorotalia menardii* and below the first occurrence of *Globorotalia acostaensis* (Agip Mineraria, 1957, 1980). Van Hinte *et al.* (1980, p. 214) placed the Tortonian lower boundary within the "*Globorotalia menardii*" Zone slighty below the first occurrence of sinistrally coiled *Globorotalia acostaensis*. Iaccarino (1985) following Cita and Blow (1969) (*Fide* Iaccarino, *op. cit.*) considered the lower boundary of the type Tortonian falls within the uppermost part of Zone N15 slightly below the first occurrence of *Globorotalia acostaensis*. Blow (1969) considered the Middle Miocene (lower part of Zone N15)/Late Miocene (upper part of Zone N15) boundary corresponding to the Langhian/Tortonian–Messinian boundary at the Middle of Zone N15 (*Globorotalia* (*Turborotalia*) *continuosa* Zone). Belanger and Berggren (1986, pp. 326–329) and Berggren and Miller (1989, pp. 310, 312) also considered the Middle Miocene/Late Miocene boundary slightly below the first occurrence of *Neogloboquadrina acostaensis*. Studies by Stainforth *et al.* (1975), Kennett and Srinivasan (1983), Bolli and Saunders (1985), and McLaughlin (1989) took the first appearance of *Globorotalia acostaensis* corresponding to the lower boundary of Zone N16 (=*Globorotalia acostaensis* Zone) in coincidence with Middle/Upper Miocene boundary. Based on the lack of planktonic Foraminifera above the base of the Serravallian in well D2/NC41, the exact boundary of the Tortonian is not determined, however, in accordance with pre-

vious studies, it is possible that the lower boundary could be drawn within the *Borelis melo* Zone (Costa and Fandi, 1977; Hammuda *et al.*, 1991). The upper boundary of the Tortonian is taken at the first appearance of *Globorotalia conomiozea* at the lower limit of Zone N17 (*Globorotalia conomiozea* Zone) (Van Hinte *et al.*, 1980; Iaccarino, 1985). Bolli and Saunders (1985) and McLaughlin (1989) placed the upper boundary of the Tortonian corresponding to the first appearance of *Globorotalia humerosa, Globigerinoides obliquus extremus, Turborotalia humerosa*, and *Sphaeroidinellopsis seminulina*. Agip Mineraria (1957, 1980) placed the upper boundary of the Tortonian at the first introduction of saline deposits, lacking in most sections the normal foraminiferal fauna of the Messinian. Similar procedure was adopted in well D2/NC41 by Costa and Fandi (1977) and the present work. However, further studies may prove that the top of the Tortonian (i.e. the Tortonian/Messinian boundary) may be below the present interpretation.

6. Messinian: The first occurrence of *Globorotalia conomiozea* was taken to limit the lower boundary of the Messinian in the Mediterranean area by Van Hinte *et al.* (1980, pp. 214–216), and Iaccarino (1985, p. 285, 293–299). The same criteria for limiting the lower boundary of the Messinian was also used by Kennett and Srinivasan (1983, p. 9, Temperate Zonation), Jenkins (1985, p. 266, 268), and Belanger and Berggren (1986, pp. 326–329), the later authors correlated the uppermost late Miocene with Zone N17 (the *Globorotalia conomiozea* Zone) above the *Neogloboquadrina acostaensis* Zone. Agip Mineraria (1957, 1980) considered the Messinain corresponding to the *Globorotalia humerosa* Zone in coincidence with the last appearance of most planktonic Foraminifera in the Mediterranean area in response to the Messinian Salinity. Bolli and Saunders (1985, pp. 159, 167—176) and McLaughlin (1989) considered the uppermost Miocene (Zone N17 = *Globorotalia humerosa* Zone) start at the first occurrence of *Globorotalia humerosa*. Blow (1969, p. 250–252, 289, 1979, pp. 52–56, 91) considered the Messinian corresponding to Zone N17 (*Globorotalia* (*G.*) *tumida plesiotumida* Zone) in coincidence with the first evolutionary appearance of *Globorotalia* (*G.*) *tumida plesiotumida*. Kennett and Srinivasan (1983, p. 8) considered Zone N18 representing the uppermost Miocene corresponding to the first appearance of *Globorotalia tumida tumida* in the tropical zonation. While Berggren and Miller (1989, pp. 310, 312) considered Zone N17 corresponding to the late Upper Miocene. The upper boundary of the Messinian in the Mediterranean area (i.e. the Miocene/Pliocene boundary) is taken at the first open marine conditions after the late Miocene salinity crisis in the area corresponding to the first appearance of *Sphaeroidinellopsis* spp., *Orobulina* spp., and other planktonic foraminiferal species (Agip Mineraria 1957, 1980) and to the first appearance of *Sphaeroidinellopsis, Globorotalia humerosa, Globigerinoides elongatus and Globigerinoides ruber* (Iaccarino, 1985, pp. 285, 287, 290). The first appearance of *Globorotalia margaritae* was taken as the upper boundary of the Miocene corresponding to the lower limit of the *Globorotalia margaritae* Zone (Stainforth *et al.*, 1975, p. 15, 88, 90–96). Van Hinte *et al.* (1980, pp. 214–216), Bolli and Saunders (1985, pp. 159, 167–176) and McLaughlin (1989) also considered the first appearance of *Globorotalia margaritae* as the upper boundary of the Miocene. In well D2/NC41 the Messinian is determined in correlation with lithostratigraphic equivalents in the Gabes–Tarabulus Basin (Costa and Fandi 1977; Van Hinte *et al.*, 1980; Hammuda *et al.*, 1991, Kassab *et al.*, 1995).

The Miocene/Pliocene Boundary

The Miocene/Pliocene boundary in the Mediterranean region is taken at the end of the salinity crisis corresponding questionably to the N17–N18 boundary coinciding with appearance of open marine fauna characterized by the first occurrence of *Sphaeroidinellopsis sphaeroides, Globorotalia humerosa, Globigerinoides elongatus* represented by the *Sphaeroidinellopsis seminulina* Zone below the *Globorotalia margaritae* Zone (Iaccarino, 1985, pp. 285, 287, 294–299). Similarly Agip Mineraria (1957, 1980) took the Miocene/Pliocene boundary slightly below the first appearance of *Globorotalia margaritae* corresponding to appearance of planktonic Foraminifera above the Messinian due to the salinity crisis in the Mediterranean area. Elsewhere, the Miocene/Pliocene boundary is taken at the first appearance of *Globorotalia margaritae* (Stainforth *et al.*, 1975; Bolli and Saunders, 1985; McLaughin, 1989), first appearance of *Globorotalia puncticulata* (Kennet and Srinivasan, 1983, p. 9; Jenkins, 1985; Belanger and Berggren, 1986), first appearance of *Globorotalia tumida* (Berggren and Miller (1989), and the first appearance of *Sphaeroidinella dehiscens* in the tropical areas (Kennett and Srinivasan, 1983, p. 8). In well D2/NC41 the Miocene/Pliocene boundary is taken at the first appearance of planktonic Foraminifera at the Messinian/Zanclean boundary characterized by *Orbulina universa, Globigerinoides extremus, Gn. sacculifer, Gn. trilobus, Gn. quadrilobatus*, and *Gn. immaturus*.

Benthonic Foraminifera

Most of the benthonic foraminiferal species recorded in this study from the Miocene to lowermost Pliocene have been recorded elsewhere in the Mediterranean

region and other areas ranging throughout the Miocene and some cross the Miocene to the Pliocene–Pleistocene (Agip Mineraria, 1957, 1980, Mediterranean area; Souaya, 1963, 1967, Miocene of Egypt; Eliagoubi, 1972, NE Libya; Mazzola, 1976, Miocene of Sirt Basin, Libya; Hageman, 1979, Pliocene–Pleistocene of Greece; Salem and Spreng, 1980, Sherif 1991, Middle Miocene of NW Libya; Boltovsky, 1980, DSDP, S. Pacific and Indian Ocean; Van der Zwaan, 1982; Late Miocene of the Mediterranean, Van der Zwaan *et al.*, 1986, Miocene–Pleistocene of the Mediterranean; Morkhoven *et al.*, 1986, Miocene–Recent, Borsetti *et al.*, 1986, Miocene–Pleistocene of the Mediterranean; and Brun *et al.*, 1984, Middle–Upper Miocene of Nigeria). However, some of the benthonic foraminiferal species encountered in the studied section of well D2/NC41 have been reported elsewhere in a restricted occurrence. Species that were reported to first occur in strata as old as Middle Miocene (Langhian) and may range to younger strata (Eliagoubi, 1972; Mazzola, 1976; Salem and Spreng, 1980; Van der Zwaan, 1982; Brun *et al.*, 1984; Borsetti *et al.*, 1986; and Van der Zwaan *et al.*, 1986) and occur in the Langhian of well D2/NC41 are: *Cibicides lobatulus*, *Bolivina antiqua*, *Elphidium advenum*, *Uvigerina bononiensis*, *U. rutila*, *U. schwageri*, *U. striatissima*, *Cibicidoides haidingerii*, *and Eponides praecinctus*. The last five species are restricted to the Langhian in well D2/NC41.

Species reported elsewhere to first occur in the Serravallian and younger strata (Maazola, 1976; Van Hinte *et al.*, 1980; Van der Zwaan, 1982; Borsetti *et al.*, 1986) and first occur in the Serravallian of well D2/NC41 are: *Uvigerina flinti and Elphidium complanatum. Elphidium aculeatum* has been recorded from the Tortonian to Pliocene (Agip Mineraria, 1957, 1980; Hageman, 1979, Pliocene to Pleistocene; Van der Zwaan, 1982, Late Miocene). In well D2/NC41 it is also first observed in the Tortonian. *Textularia pseudorugosa*, *Spriloculina depressa*, and *Dorothia gibbosa* made thier first appearance within the Pliocene to Pleistocene of the Mediterranean (Agip Mineraria, 1957, 1980) also first appeared in the lower part of the Pliocene Sbabil Formation of well D2/NC41 (Fig. 3). The nature of the studied material (sandstones, siltstones, silty shales, evaporites and limestones) and the interval of sampling and the crystallization of many species specimens resulted in a not well defined distribution of species, thus out of the 85 benthonic species recorded in this study 25 species are identified from one samply only, and 15 species are recognized in 2 samples only (Fig. 3). Twenty two species are identified from one sample each in the Langhian, two species from the Serravallian, one species from the Tortonian and three species from the Messinian. Most of these species may occur in older and/or younger strata elsewhere in the Mediterranean and other parts of the world. However, some of them have facies controlled stratigraphic intervals (Agip Mineraria, 1957, 1980; Eliagoubi, 1972; Salem and Spreng, 1980, Van Hinte *et al.*, 1980, Van der Zwaan, 1982; Brun *et al.*, 1984; Borsetti *et al.*, 1986; Belanger and Berggren, 1986; Morkhoven *et al.*, 1986; Van der Zwaan *et al.*, 1986; Miller and Katz, 1987; Sherif 1991).

PALAEOECOLOGY

AL MAYAH FORMATION: The lower part of the studied Al Mayah section (depth 4900 ft–4660 ft., 4 samples) consists of silty shales and silty clays. It is relatively rich in planktonic (30 species) and benthonic (36 species) Foraminifera. The increase in percentage of planktonic Foraminifera indicates deep open marine environment (Smith, 1955; Bandy, 1964; and Boltovsky, 1969). Benthonic Foraminifera identified from this interval characterized by

1. *Cibicidoides* spp.: *C. dutemplei*, water depth 100 m–600 m; *C. haidingerii*, W.D. 100–600 m; *C. pseudoungerianus*, W.D. 35 m–1000 m; *C. subhaidingerii*, W.D. 100 m–2000 m; and *C. ungerianus*, 500 m. These species are found in muddy substrate, normal open marine, outer neritic to lower bathyal (W.D. 100 m–2000 m) (Brolsma, 1978; Hageman, 1979; Haynes, 1981, Van der Zwaan, 1982; Morkhoven *et al.*, 1986).

2. *Uvigerina* spp: *U. striatissima*, rich; *U. rutila*, common, *U. acuminata*, *U. pygmaea*, *U. bononiensis*, and *U. schawageri* rare. *Uvigerina* spp. are found most abundant at outer shelf and upper continental slope, outer neritic (100 m)–u. bathyal (1600 ml) (Haynes, 1981). Borsetti *et al.* (1986) found *Uvigerina bononiensis* in the outer neritic and less than 300 meters water depth.

3. *Ammonia* spp. (rare). The rare occurrence of *Ammonia* spp. may indicate water depth of open normal marine environment deeper than middle neritic (more than 90 m) (Hageman, 1979; Walton and Sloan, 1990).

The second interval of Al Mayah Formation (drilling depth 4260 ft–3520 ft., 5 samples) also contains a relatively rich planktonic Foraminifera (24 species) indicating open marine environment (Smith, 1955; Bandy, 1964; Boltovsky, 1969). Forty one benthonic species are identified from this interval characterized by

1. *Ammonia beccarii beccarii* (rich). Shallow, warm, normal marine, inner-middle neritic (Hageman, 1979).

2. *Bolivina spp.: B. dilatata and B. antiqua.* Outer neritic to middle bathyal (100 m–1000 m) muddy substrate, normal open marine (Brolsma, 1978, Van Hinte *et al.*, 1980; Haynes, 1981; Van der Zwaan, 1982, Brun *et al.*, 1984; Sherif, 1991).

3. Bulimina spp.: *B. costata* and *B. acuteata.* Open

normal marine, water depth 100 m–3000 m, outer neritic–abyssal, prefered depths 100 m, 400 m, 600 m, 800 m (Brolsma, 1978, Van Hinte *et al.*, 1980; Van der Zwaan 1982; Morkhoven *et al.*, 1986).

4. *Cibicidoides* spp.: *C. dutemplei* (W.D. 100 m–600 m); *C. pseudoungerianus* (W.D. 35 m–1000 m); *C. ungerianus* (W.D. to 500 m). *C. subhaidingerii* (W.D. 100 m–2000 m), *and C. haidingerii* (W.D. 100–600 m) (Hageman, 1979; Van der Zwaan, 1982; Morkhoven *et al.*, 1986).

5. *Lenticulina rotulata: Lenticulina* spp. prefer outer neritic – upper bathyal (100 m–400 m), also found at 100 m–1000 m (Brolsma, 1978).

6. *Peneroplis* spp. (rare): Inner to middle neritic (W.D. 0-152 meters) (Souaya, 1963).

7. *Quinqueloculina seminulina* (rare): Restricted shallow to shallow open marine, inner to middle neritic (25 m–35 m) (Haynes, 1981).

8. *Uvigerina* spp.: *U. striatissima*, *U. rutila*, *U. hispida*, *U. peregrina*, *U. pygmaea*, and *U. schwageri. Uvigerina* species are found most abundant at water depth 100 m–600 m (Haynes, 1981). *Uvigerina hispida* inhibits upper bathyal to lower bathyal, 200–2000 m, (Morkhoven *et al.*, 1986). Brun *et al.* (1984) estimated 500 m water depth. *Uvigerina peregrina* inhibits normal marine of wide water depth range, 100 m–1600 m (Brolsma, 1978; Sejrup *et al.*, 1981; Haynes, 1981; Van der Zwaan, 1982; Belanger and Berggren, 1986; Cassell and Sen Gupta, 1989), however, Brolsma (1978), Sejrup *et al.* (1981), and Cassell and Sen Gupta (1989) referred to 100 m–600 m water depth preference for *U. peregrina.*

9. *Nonion boueanum*: The rare occurrence of *Florilus boueanum* would indicate water depths less than upper bathyal (Van Hinte *et al.*, 1980). Hageman (1979) refers to open normal marine environment. Sherif (1991) quoted open shallow marine.

The uppermost Al Mayah Foramtion consists of 1475 ft. (drilling depth 3520 ft.–2045 ft.) of clays, shaly sands and sandstones. More shallow environment prevailed during the deposition of this part of Al Maya Formation indicated by the low diversity of both planktonic (5) and benthonic (13) species. The increase in *Ammonia*, *Textularia* and *Elphidium* would indicate inner to middle neritic (Souaya, 1963; Hageman, 1979; Haynes, 1981; Van der Zwaan, 1982; Sherif, 1991). The presence of panktonic Foraminifera in low diversity would indicate open marine connections (Smith, 1955; Bandy, 1964; Boltovsky, 1969).

TUBTAH FORMATION AND LOWERMOST MARSA ZOUAGHAH FORMATION: Drilling depth interval 2045 ft.–1170 ft. This interval consists of limestones (wackestone, packestone) with interbeds of clay and is oolitic in the upper part of the Tubtah Formation. It is relatively rich in *Borelis melo*, *Elphidium* spp., *Peneroplis*, and *Quinqueloclina* spp. and very poor in planktonic Foraminifera.

1. *Elphidium aculealtum* prefers sandy, vegetated substrate of normal salinity (Hageman, 1979).

2. *E. macellum* is found in innershelf, 0–5 m (Sherif, 1991), *E. crispum* inhibits open normal marine inner neritic to middle neritic (0–90 m) environment (Souaya, 1963; Eliagoubi, 1972; and Sherif, 1991).

3. *Quinqueloculina seminulum* may flourish in open shallow marine with vegetated substrate, it is slightly tolerant to hyposaline, water depth 25–35 meters, inner neritic (Hageman, 1979; Haynes, 1981).

4. *Peneroplis* spp.: Vegetated carbonate substrate, inner to middle neritic (0–152 m), rich from 0–18 m (Souaya, 1963).

5. *Borelis melo*: Large milolids inhibit shallow, warm, clear hypersaline environments (Haynes 1981; Walton and Sloan, 1990). *Borelis melo* inhibits shallow, warm, clear, marine waters of the inner neritic, 0–33 m on sandy and oolites substrate (Haynes, 1981; Sherif, 1991). This interval reflects shallow, warm, normal marine vegetated inner neritic platform with slight restrictions upward.

MARSA ZOUAGHAH FORMATION: Drilling depth interval 1170 ft–870 ft. This part of the Marsa Zouaghah Formation consists of wackestone-packestones, gypsum and dolomitic wackestone–packestone. No Foraminifera have been found. The presence of evaporites is interpreted as Sabkha deposits (0–10 m) in the Messinian of well NC35A, offshore NW Libya (Van Hinte *et al.*, 1980).

SBABIL FORMATION: Drilling depth interval 870 ft.–840 ft. The Sbabil Formation, at this locality, is made of clay, wackestone, and mudstone–sequence. Twenty one benthonic species and nine planktonic species are identified. The benthonic assemblage is characterized by:

1. *Elphidium* spp. (*E. fichtelianum*, vegetated substrate, Hageman, 1979; *E. crispum*, inner neritic – upper bathyal, Souaya, 1963; *E. macellum.* inner shelf, Sherif, 1991).

2. Miliolids: *Spiroloculina depressa, and Pyrgo depressa.* Smal miliolids inhibit warm, clear, shallow marine waters (Haynes, 1981) and shallow, warm clear, shallow marine waters (Haynes, 1981) and shallow, warm clear, hypersaline waters (Walton and Sloan, 1990).

3. *Bolivina antiqua:* Brun *et al.* (1984) refer to waters deeper than 150 m and abundant in bathyal depths.

4. Nodosarids: *Nodosaria* cf. *rephanus* inhibits outer neritic – middle bathyal, 100 m–1000 m (Haynes, 1981).

5. *Uvigerina peregrina*: Hageman (1979) referred to open marine waters of 0–1600 m depth. Van Hinte *et al.* (1980) concluded a water depth of 610 m for a benthonic association contains *Uvigerina peregrina* in

the Sbabil Formation of well NC35A, offshore, NW Libya.

6. *Cibicidoides pseudoungerianus* has been found at water depth range 0–1800 m (Brolsma, 1978).

7. *Cibicidoides subhaidingerii* water depth range 100–2000 m (Morkhoven, 1986).

Thus, it is possible that this faunal association of planktonic and benthonic Foraminifera indicates open normal marine middle neritic to upper bathyal (100 m – less than 600 m water depth).

CONCLUSIONS

Twenty samples from well D2-NC41, offshore, NW, Libya, drilling depth interval 4900 ft–840 ft have been studied for their foraminiferal contents in aim to re-evaluate the biostratigraphy and palaeoecology of the studied section. This resulted in:

1. Eighty five benthonic and 38 planktonic foraminiferal species are recognized.

2. Based on the planktonic foraminiferal species the N8 Zone of Blow (1969, 1979) (=*Praeorbulina glomerosa glomerosa* Zone), the boundary of Zones N8/N9, and Zone N17/N18 are determined.

3. The lack of planktonic Foraminifera in some parts of the section did not permit precise zonation for those parts.

4. Four rock units are encountered, Al Mayah, Tubtaha, Marsa Zouaghah, and Sbabil Formations. Based on their foraminiferal contents and/or stratigraphic position, these rock units are considered of Middle Miocene to lowermost Pliocene as follows:

(a) Al Mayah Formation (part): Langhian – Serravallian (Middle Miocene).

(b) Tubtah Formation: Tortonian (low Upper Miocene).

(c) Marsa Zouaghah Formation: Messinian (high Upper Miocene)

(d) Sbabil Formation: Lower Pliocene

The boundary between the Serravallian and Tortonian is not determined.

5. The Langhian part of Al Mayah Formation was deposited in normal open marine, muddy to fine substrate platform with water depth that may range between outer neritic to upper bathyal (100 m–600 m). A decrease in depth is noticed upward the section towards the top of Al Mayah Formation to probably lesser than outer neritic open marine platform.

6. The Tubtah Formation and the lower part of the Marsa Zouaghah Formation contain benthonic Foraminifera indicative of deposition under warm, clear, shallow, normal marine environment in a vegetated inner neritic platform (less than 100 m W.D.) with slight restrictions upward.

7. The remaining interval of the Marsa Zouaghah Formation (upper 300 ft) yielded no Foraminifera, the presence of evaporites suggests Sabkha deposits (0–10 m) in accordance with the Messinian salinity crisis.

8. The lowermost Sbabil Formation foraminiferal fauna indicates open marine middle neritic to upper bathyal (100 m – less than 600 m W.D.).

ACKNOWLEDGEMENTS

The author wishes to thank the management of the Petroleum Research Centre, Tripoli, Libya, for awarding the grant to carry out this research in the United Kingdom and permission to publish this work, Prof. M. Keen and Staff members of the Geology Department, Glasgow University, U.K., for various help during his stay in U.K., Mr. Peter for the scanning electron microscopy, Mr. Douglas for photography. Thanks are also extended to my colleagues and staff members of the Geology Department, Exploration Management at P.R.C. for their encouragement and support, for Mrs. Laila El-Aradi, for typing the manuscript.

Major part of this research has been carried out at P.R.C., Tripoli, under the supervision of Dr. I.I. M. Kassab to whom I am deeply indebted.

Plate 1

1. *Bolivina reticulata* (VON HANTKEN), × 100, S. 4660
2. *Bolivina arta* (MACFADYEN) × 87, S. 4660
3. *Bolivina* cf. *antiqua* (D'ORBIGNY), × 110, 9. 840
4. *Bolivina dilatata* (REUSS), × 175, S. 3540
5. *Bolivina dilatata* (REUSS), × 140, S. 3540
6. *Virgulinella* sp., × 130, S. 2200
7. *Virgulinella* sp., × 140, S. 2200
8. *Virgulinella sp.*, × 125, S. 2200
9. *Textularia* cf. *soldanii* (FORNASINI), × 40, S. 4860
10. *Textularia sagitttula* (DEFRANCE), × 82, S. 2200
11. *Textularia sagittula* (DEFRANCE), × 93, S. 2200
12. *Textularia soldanii* (FORNASINI), × 24, S. 870
13. *Textularia soldanii* (FORNASINI), × 18, S. 870
14. *Textularia soldanii* (FORNASINI), × 25, S. 1230
15. *Textularia pseudorugosa* (LACROIX), × 53, S. 840
16. *Textularia* cf. *rugosa* (COSTA), × 145, S. 3520
17. *Cyclammina* sp., × 40, S. 4660
18. *Spiroplectammina carinata* (D'ORBIGNY), × 66, S. 4660
19. *Spiroplectammina carinata* (D'ORBIGNY), × 54, S. 4860

Plate 2

1. *Elphidium crispum* (LINNE'), × 52, S. 1170
2. *Elphidium crispum* (LINNE'), × 60, S. 1260
3. *Elphidium crispum* (LINNE'), × 70, S. 1230
4. *Cribroelphidium* cf. *longipoints* (SHCHEDRINA), × 78, S. 1350
5. *Elphidium complanatum* (D'ORBIGNY), × 120, S. 2740
6. *Ephidium advenum* (CUSHMAN), × 112, S. 4660
7. *Cribroelphidium* cf. *longipoints* (SHCHEDRINA), × 56, S. 1290
8. *Peneroplis* sp., × 100, S. 3520
9. *Gyroidina* sp., × 190, S. 4660
10. *Cancris auricula* (FICHTEL and MOLL), × 122, S. 870
11. *Peneroplis carinata* (SILVESTRI), × 70, S. 1350
12. Peneroplis cristata (SILVESTRI), × 73, S. 3520

Plate 3

1. *Spiroloculina depressa* (D'ORBIGNY), × 25, S. 876
2. *Spiroloculina excavata* (D'ORBIGNY), × 62, S. 1230
3. *Quinqueloculina* cf. *bicornis* (WALKER and JACOB), × 66, S. 1230
4. *Quinqueloculina* cf. *oblonga* (MONTAGU), × 35, S. 1320
5. *Quinqueloculina* cf. *oblonga* (MONTAGU), × 91, S. 1230
6. *Quinqueloculina vulgaris* (D'ORBIGNY), × 67, S. 1230
7. *Quinqueloculina vulgaris* (D'ORBIGNY), × 58, S. 3800
8. *Quinqueloculina aspera* (D'ORBIGNY), × 65, S. 1350
9. *Quinqueloculina aspera* (D'ORBIGNY), × 45, S. 1560
10. *Quinqueloculina bicarinata* (D'ORBIGNY), × 95, S. 3520
11. *Borelis melo* (FICHTEL and MOLL), × 78, S. 1560
12. *Borelis melo* (FICHTEL and MOLL), × 71, S. 1560
13. *Borelis melo* (FICHTEL and MOLL), × 65, S. 1560
14. *Borelis melo* (FICHTEL and MOLL), × 57, S. 1560
15. *Borelis melo* (FICHTEL and MOLL), × 68, S. 1350

Plate 4

1. *Nonion boueanum* (D'ORBIGNY), × 119, S. 3600
2. *Nonion boueanum* (D'ORBIGNY), × 192, S. 4660
3. *Nonion boueanum* (D'ORBIGNY), × 158, S. 4660
4. *Nonion boueanum* (D'ORBIGNY), × 106, S. 2200
5. *Nonion boueanum* (D'ORBIGNY), × 100, S. 2200
6. *Nonion boueanum* (D'ORBIGNY), × 123, S. 3800
7. *Lenticulina cultrata* (DE MONTFORT), × 114, S. 4260
8. *Marginulina obesa* (CUSHMAN), × 38, S. 4860
9. *Lenticulina rotulata* (LAMARCK), 122, S. 4820
10. *Lenticulina rotulata* (LAMARCK), × 77, S. 4660
11. *Lenticulina cultrata* (DE MONTFORT), × 130, S. 4260
12. *?Dentalina filiformis* (D'ORBIGNY), × 55, S. 4660
13. *Dentalina communis* (D'ORBIGNY), × 41, S. 4260
14. *Lenticulina rotulata* (LAMARCK), × 104, S. 4260
15. *Marginulina obesa* (CUSHMAN), × 36, S. 4820
16. *Nodosaria* cf. *raphanistrum* (LINNE'), × 95, S. 840
17. *Chrysalogonium obliquatum* (BATSCH), × 20, S. 4260
18. *Nodosaria raphanus* (LINNE') × 26, S. 1230
19. *Marginulina hirsuta* (D'ORBIGNY), × 50, S. 4820

Plate 5

1. *Cibicidoides subhaidingerii* (PARR), × 91, S. 3600
2. *Cibicidoides subhaidingerii* (PARR), × 104, S. 3600
3. *Cibicidoides subhaidingerii* (PARR), × 112, S. 3540
4. *Cibicidoides subhaidingerii* (PARR), × 132, S. 3600
5. *Cibicidoides subhaidingerii* (PARR), × 95, S. 3600
6. *Cibicidoides subhaidingerii* (PARR), × 141, S. 3600
7. *Cibicidoides subhaidingerii* (PARR), × 125, S. 4660
8. *Hanzawaia boueana* (D'ORBIGNY), × 210, S. 840
9. *Cibicidoides pseudoungerianus* (CUSHMAN), × 163, S. 840
10. *Megastomella purisima* (BRAMLETTE), × 64, S. 1260
11. *Megastomella purisima* (BRAMLETTE), × 33, S. 1560
12. *Megastomella purisima* (BRAMLETTE), × 40, S. 1350
13. *Cibicidoides dutemplei* (D'ORBIGNY), × 90, S. 3540

Plate 6

1. *Cibicidoides dutemplei* (D'ORBIGNY), × 142, S. 4260
2. *Cibicidoides dutemplei* (D'ORBIGNY), × 84, S. 4860
3. *Cibicidoides dutemplei* (D'ORBIGNY), × 135, S. 3600
4. *Cibicidoides dutemplei* (D'ORBIGNY), × 105, S. 4820
5. *Cibicidoides dutemplei* (D'ORBIGNY), × 142, S. 4860
6. *Cibicidoides dutemplei* (D'ORBIGNY), × 142, S. 4660
7. *Cibicidoides dutemplei* (D'ORBIGNY), × 142, S. 3600
8. *Planulina rugosa* (PHLEGER and PARKER), × 186, S. 3540
9. *Planulina rugosa* (PHLEGER and PARKER), × 108, S. 4260
10. *Planulina rugosa* (PHLEGER and PARKER), × 110, S. 4260
11. *Cibicides lobatulus* (WALKER and JACOB), × 137, S. 4820
12. *Cibicidoides ungerianus* (D'ORBIGNY), × 80, S. 3600
13. *Cibicidoides ungerianus* (D'ORBIGNY), × 137, S. 3600

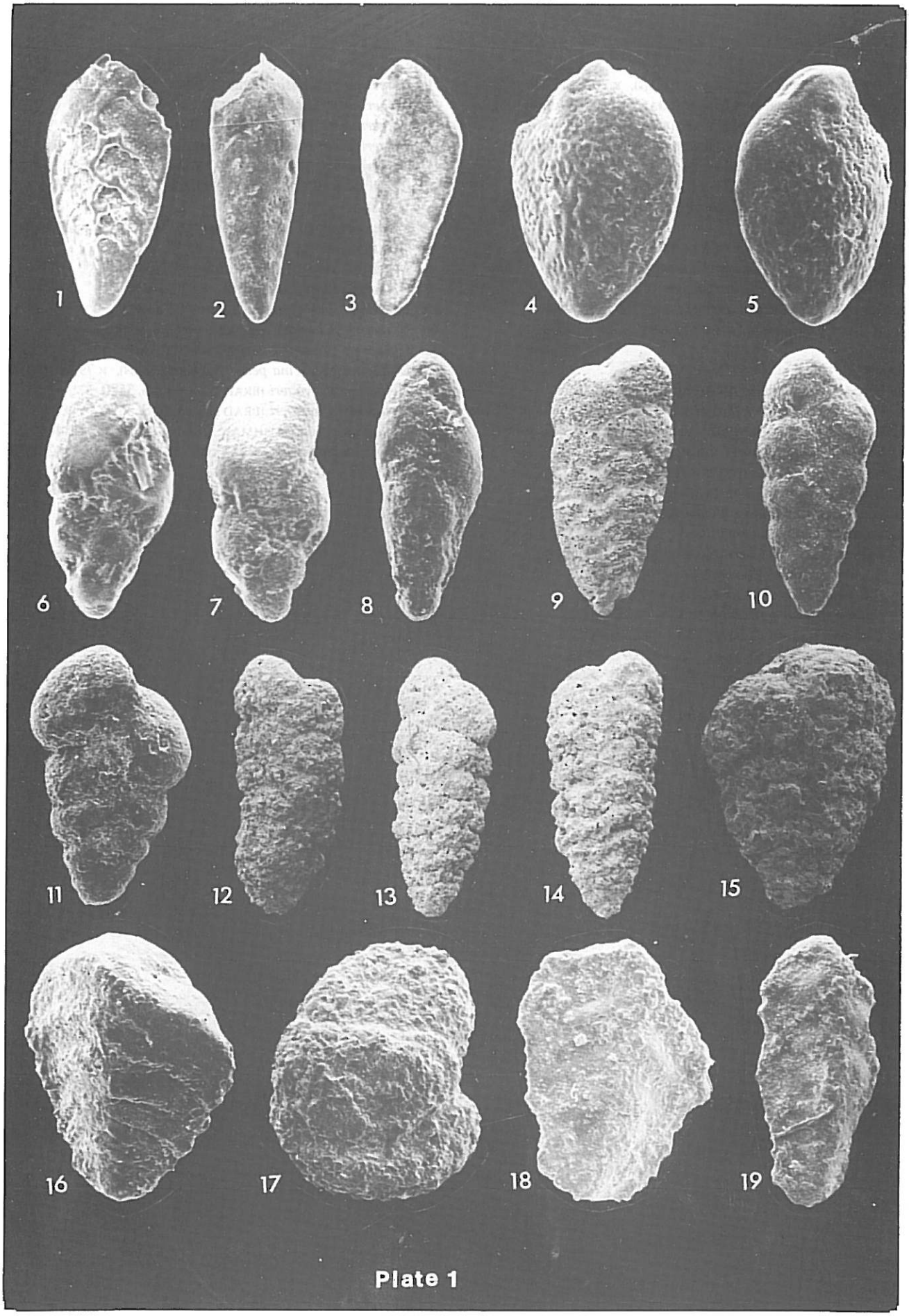


Plate 1

Plate 7

1. *Ammonia beccarii tepida* (CUSHMAN), × 202, S. 2740
2. *Ammonia beccarii tepida* (CUSHMAN), × 195, S. 3540
3. *Ammonia beccarii tepida* (CUSHMAN), × 208, S. 4660
4. *Ammonia beccarii tepida* (CUSHMAN), × 181, S. 4660
5. *Ammonia beccarii tepida* (CUSHMAN), × 75, S. 4260
6. *Ammonia beccarii tepida* (CUSHMAN), × 65, S. 1350
7. *Ammonia beccarii parkinsoniana* (D'ORBIGNY), × 166, S. 3800
8. *Ammonia beccarii tepida* (CUSHMAN), × 142, S. 3520
9. *Ammonia beccarii beccarii* (LINNE), × 56, S. 3800
10. *Gyroidina altiformis* (CUSHMAN), × 184, S. 4900
11. *Gyroidina* cf. *soldanii* (D'ORBIGNY), × 62, S. 4660
12. *Melonis barleeanum* (WILLIAMSON), × 70, S. 4660

Plate 8

1. *Uvigerina acuminata* (HOSIUS), × 82, S. 4820
2. *Uvigerina acuminata* (HOSIUS), × 91, S. 4820
3. *Uvigerina rutila* (CUSHMAN and TODD), × 113, S. 3600
4. *Uvigerina pygmaea* (D'ORBIGNY), × 120, S. 3520
5. *Uvigerina pygmaea* (D'ORBIGNY), × 108, S. 4820
6. *Uvigerina hispida* (SCHWAGER), × 108, S. 4260
7. *Uvigerina bononiensis* (FORNASINI), × 97, S. 840
8. *Bulimina aculeata* (D'ORBIGNY), × 133, S. 3600
9. *Bulimina aculeata* (D'ORBIGNY), × 183, S. 4660
10. *Bulimina costata* (D'ORBIGNY), × 108, S. 4820
11. *Bulimina costata* (D'ORBIGNY), × 88, S. 4660
12. *Bulimina costata* (D'ORBIGNY), × 88, S. 4860
13. *Bulimina costata* (D'ORBIGNY), × 128, S. 4660
14. *Bulimina costata* (D'ORBIGNY), × 100, S. 4260
15. *Bulimina costata* (D'ORBIGNY), × 100, S. 4660
16. *Bulimina costata* (D'ORBIGNY), × 110, S. 3540.
17. *Bulimina costata* (D'ORBIGNY), × 152, S. 3520

Plate 9

1. *Uvigerina striatissima* (PERCONIG), × 91, S. 3600.
2. *Uvigerina striatissima* (PERCONIG), × 91, S. 4660.
3. *Uvigerina striatissima* (PERCONIG), × 76, S. 3540.
4. *Uvigerina striatissima* (PERCONIG), × 99, S. 3600.
5. *Uvigerina bononiensis* (FORNASINI), × 116, S. 4660.
6. Detail of wall surface of specimen illustrated in fig. 2, × 483.
7. More detail of wall surface of the same specimen illustrated in fig. 2, × 950.
8. Apertural view of same specimen, × 200.
9. *Uvigerina flinti* (CUSHMAN), × 83, S. 3600.
10. *Uvigerina flinti* (CUSHMAN), × 97. S. 3600.
11. *Uvigerina schwageri* (BRADY), × 97, S. 4660.
12. *Uvigerina peregrina peregrina* (CUSHMAN), × 95, S. 840.
13. *Uvigerina peregrina peregrina* (CUSHMAN), × 79, S. 840.
14. *Uvigerina schwageri* (BRADY), × 162, S. 3520.
15. *Uvigerina schwageri* (BRADY), × 186, S. 3520.
16. *Uvigerina rutila* (CUSHMAN and TODD), × 108, S. 4660.
17. *Uvigerina rutila* (CUSHMAN and TODD), × 125, S. 4260.

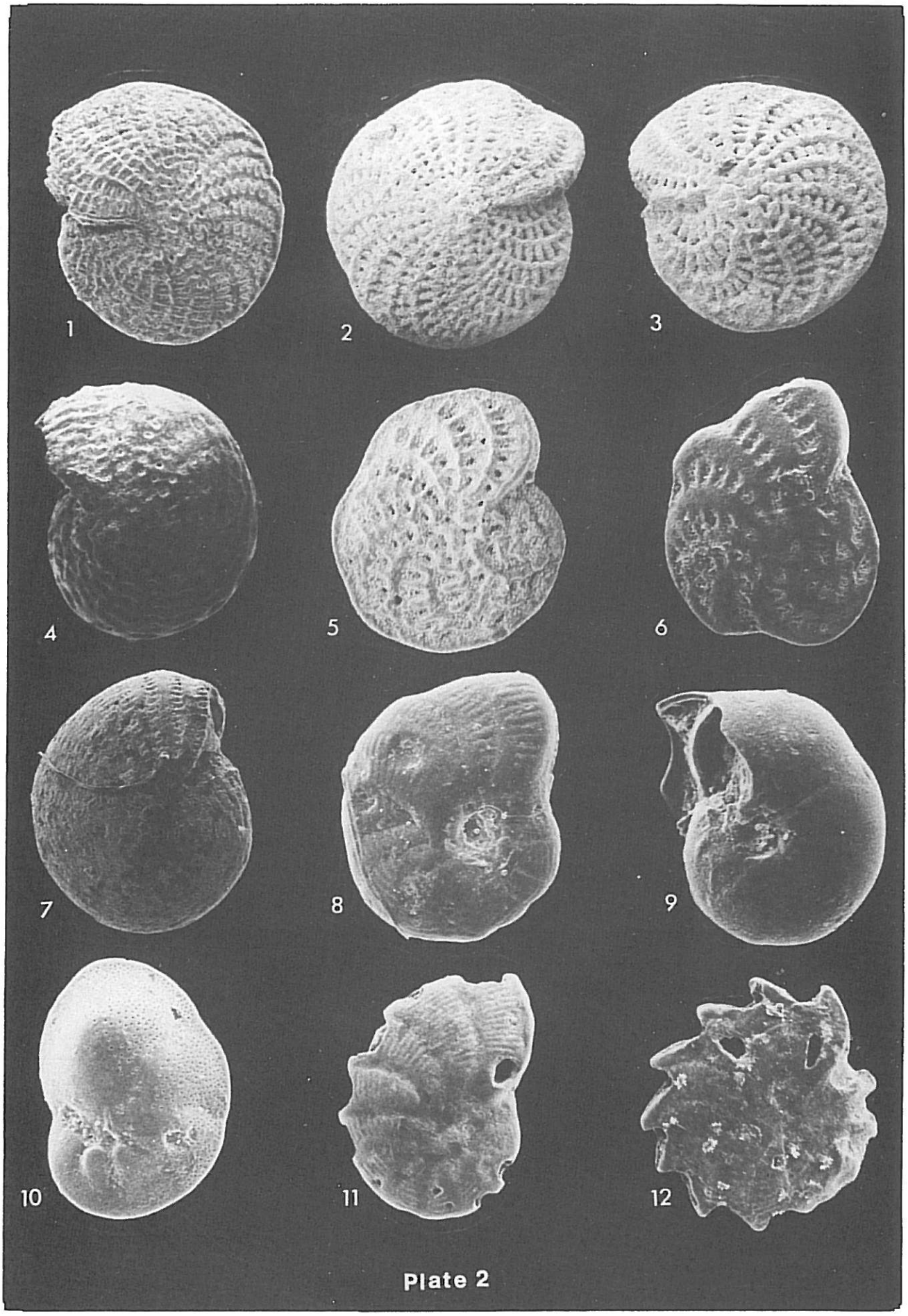


Plate 2

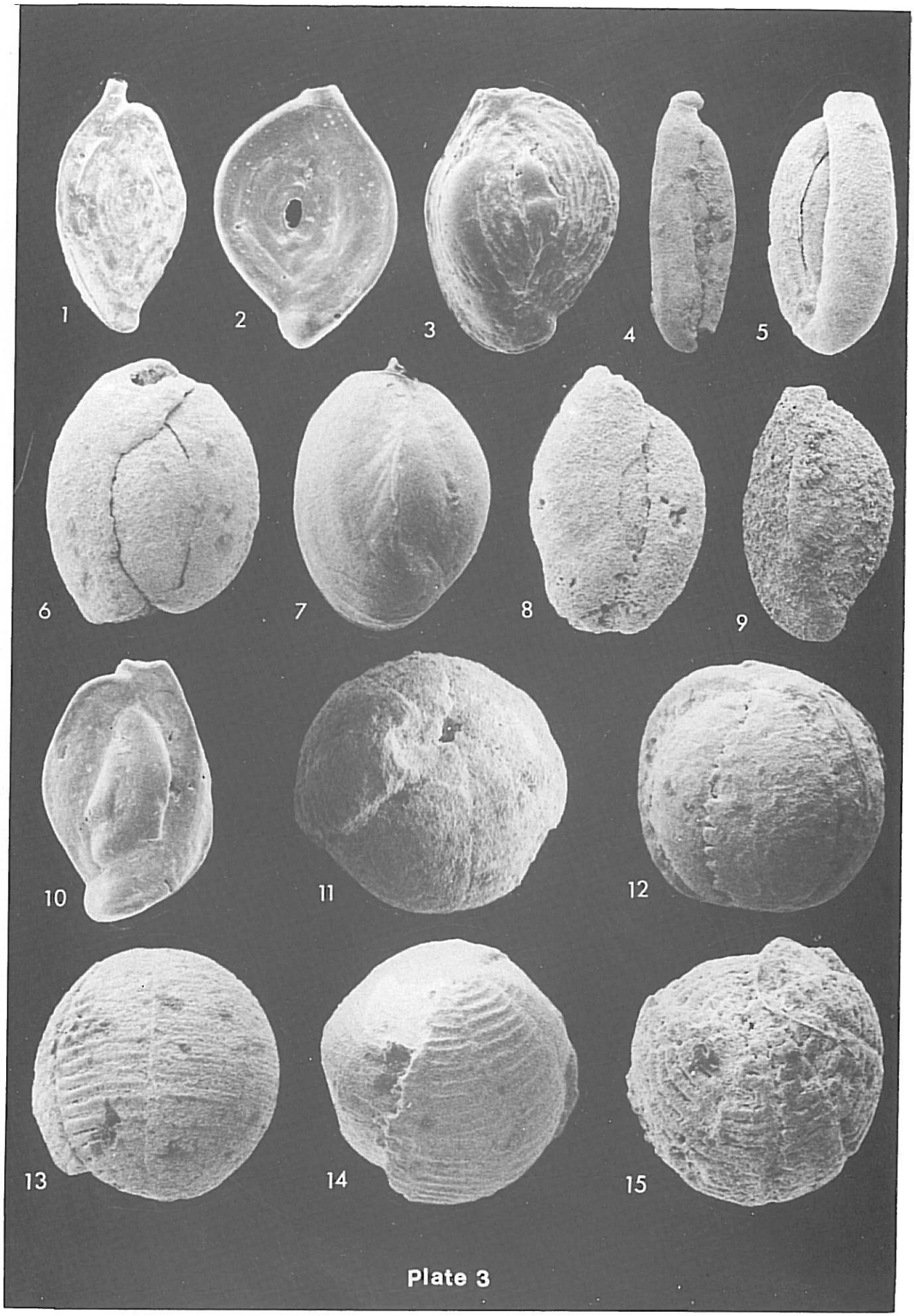


Plate 3

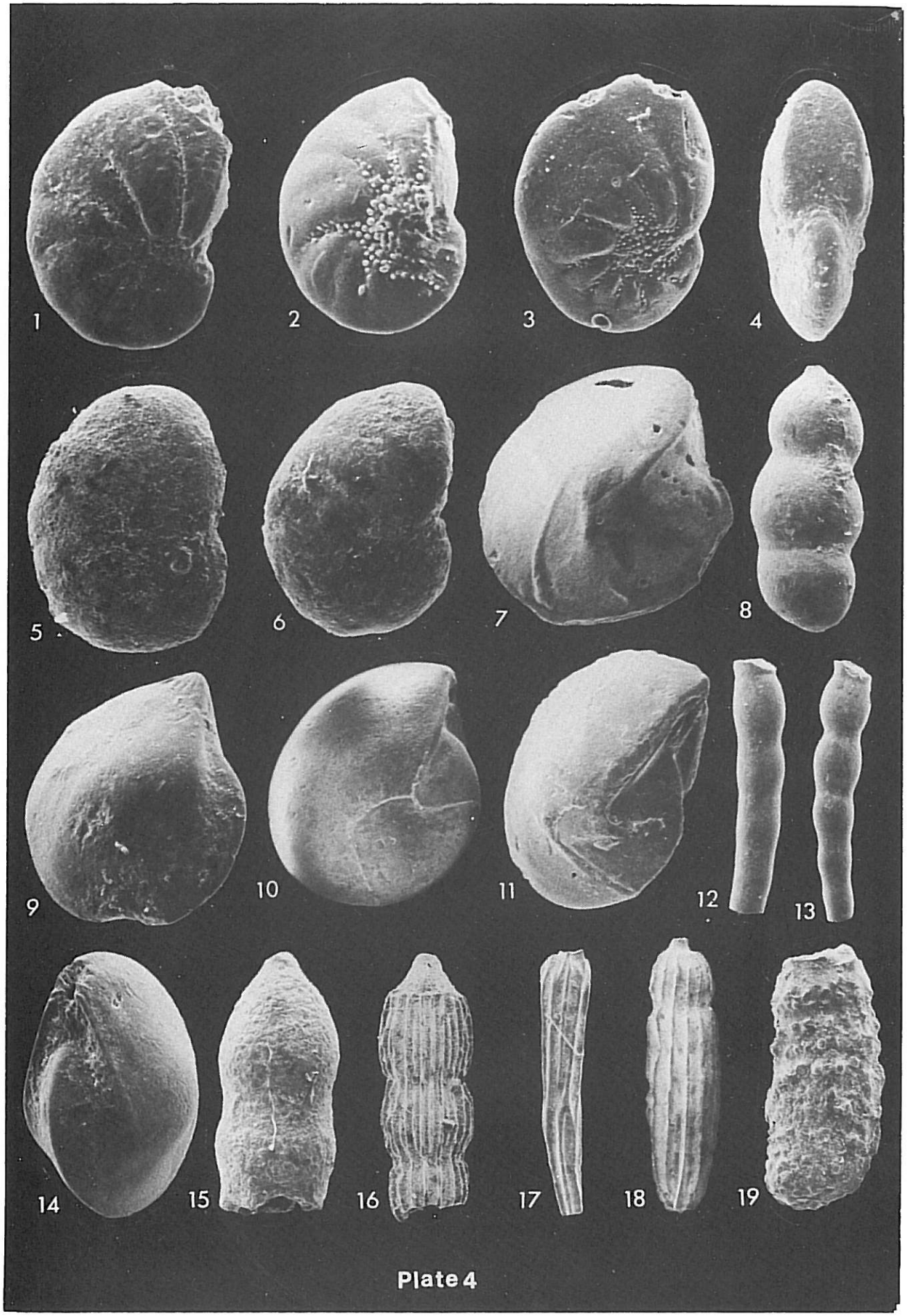


Plate 4

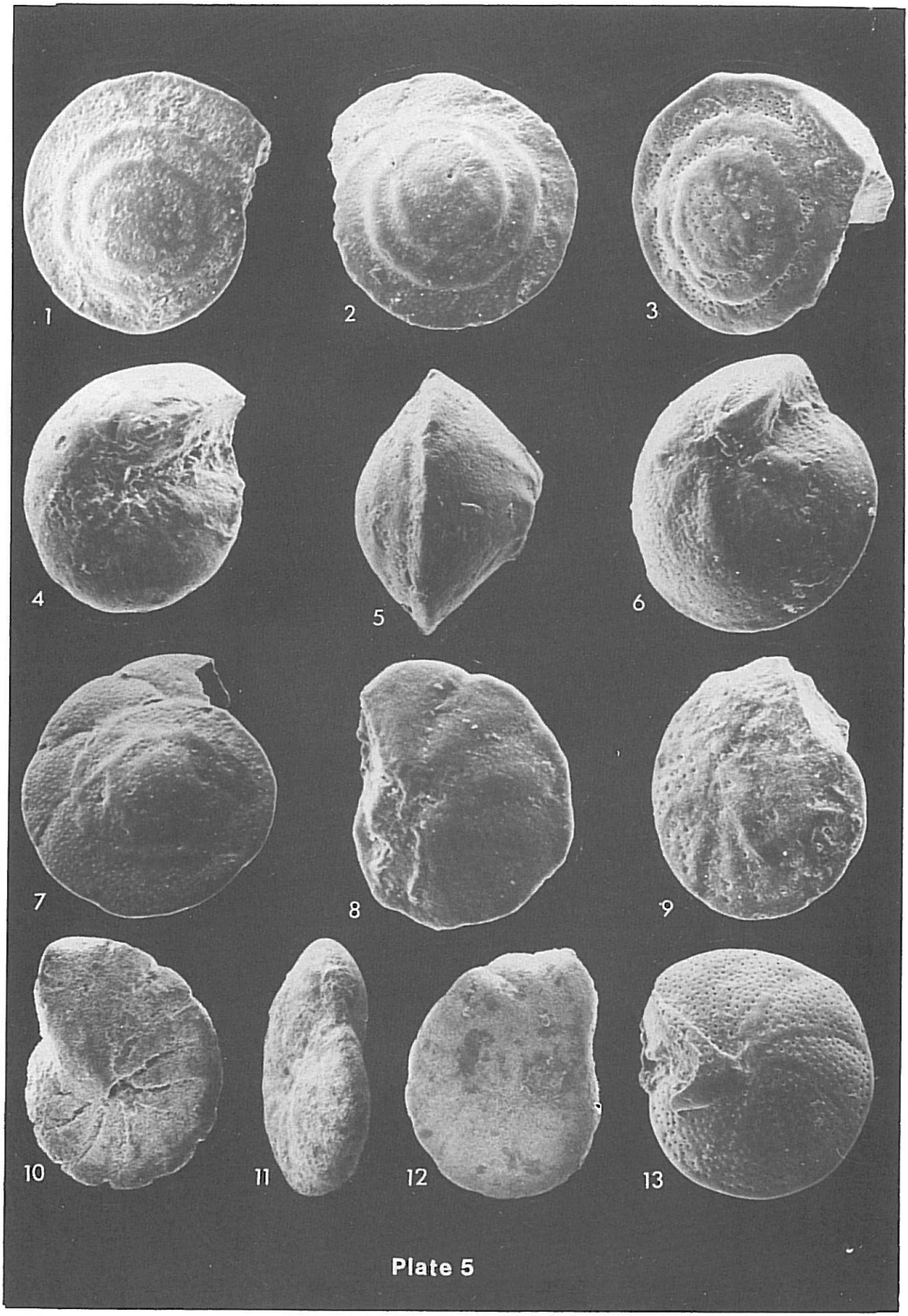


Plate 5

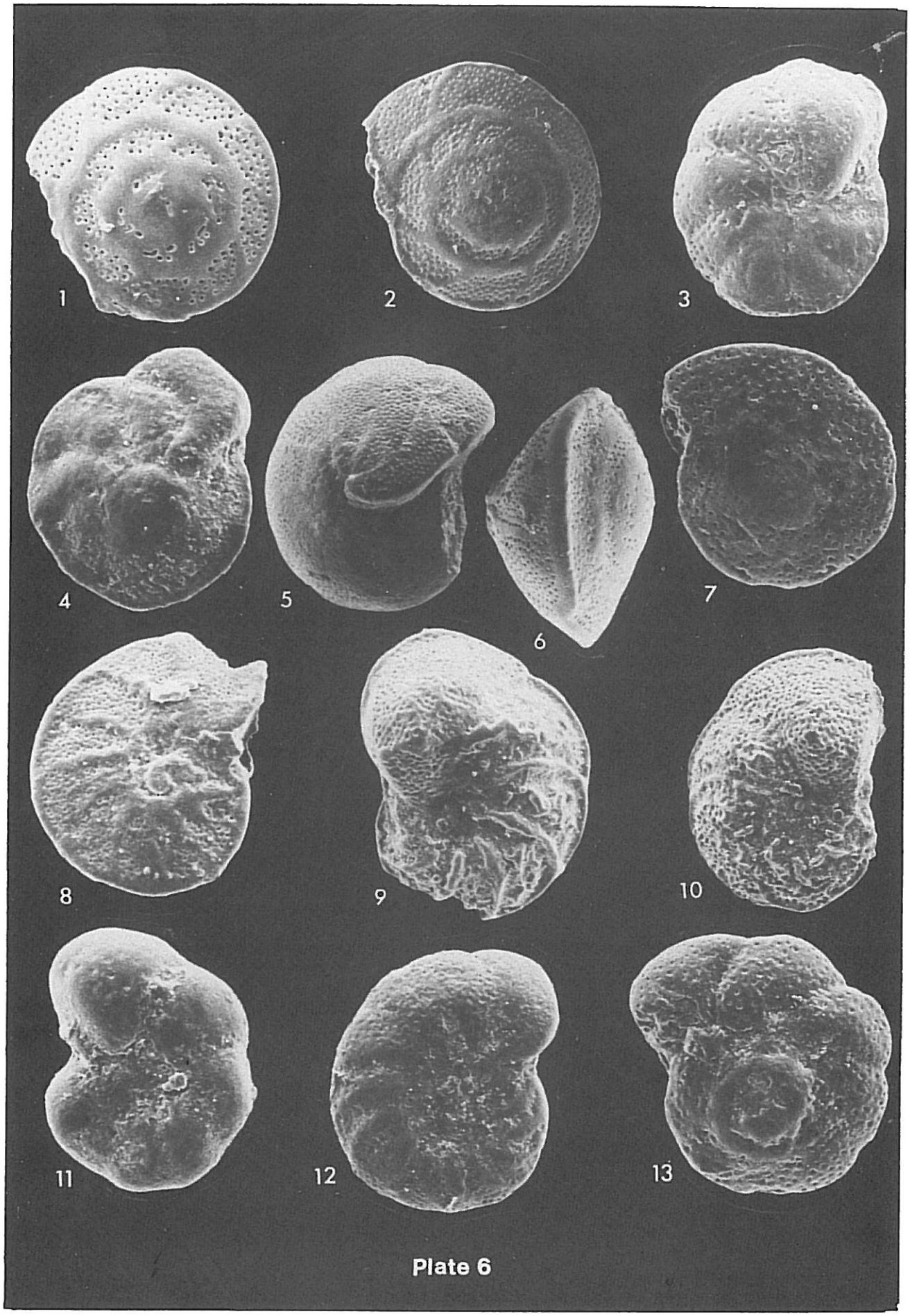


Plate 6

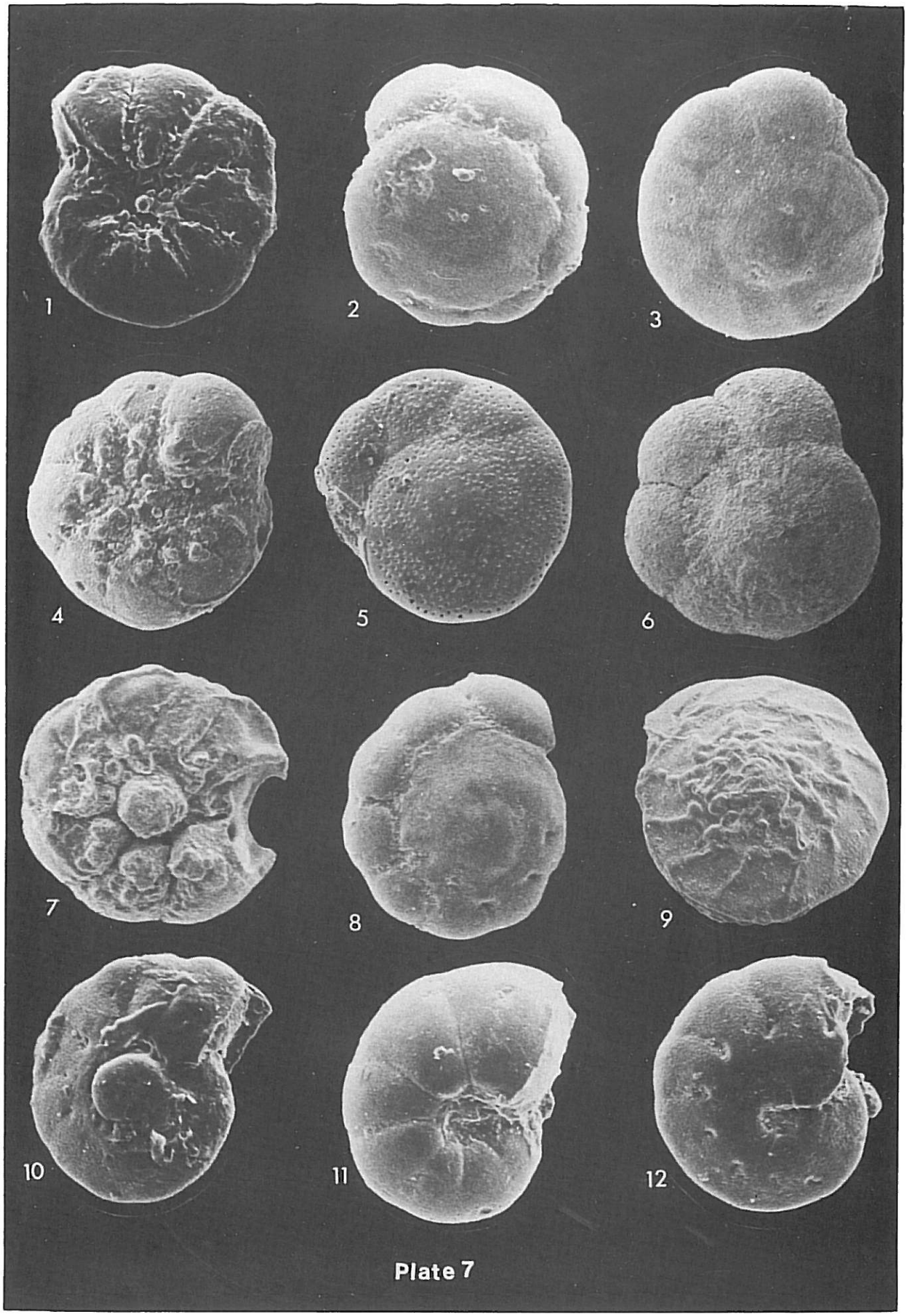


Plate 7

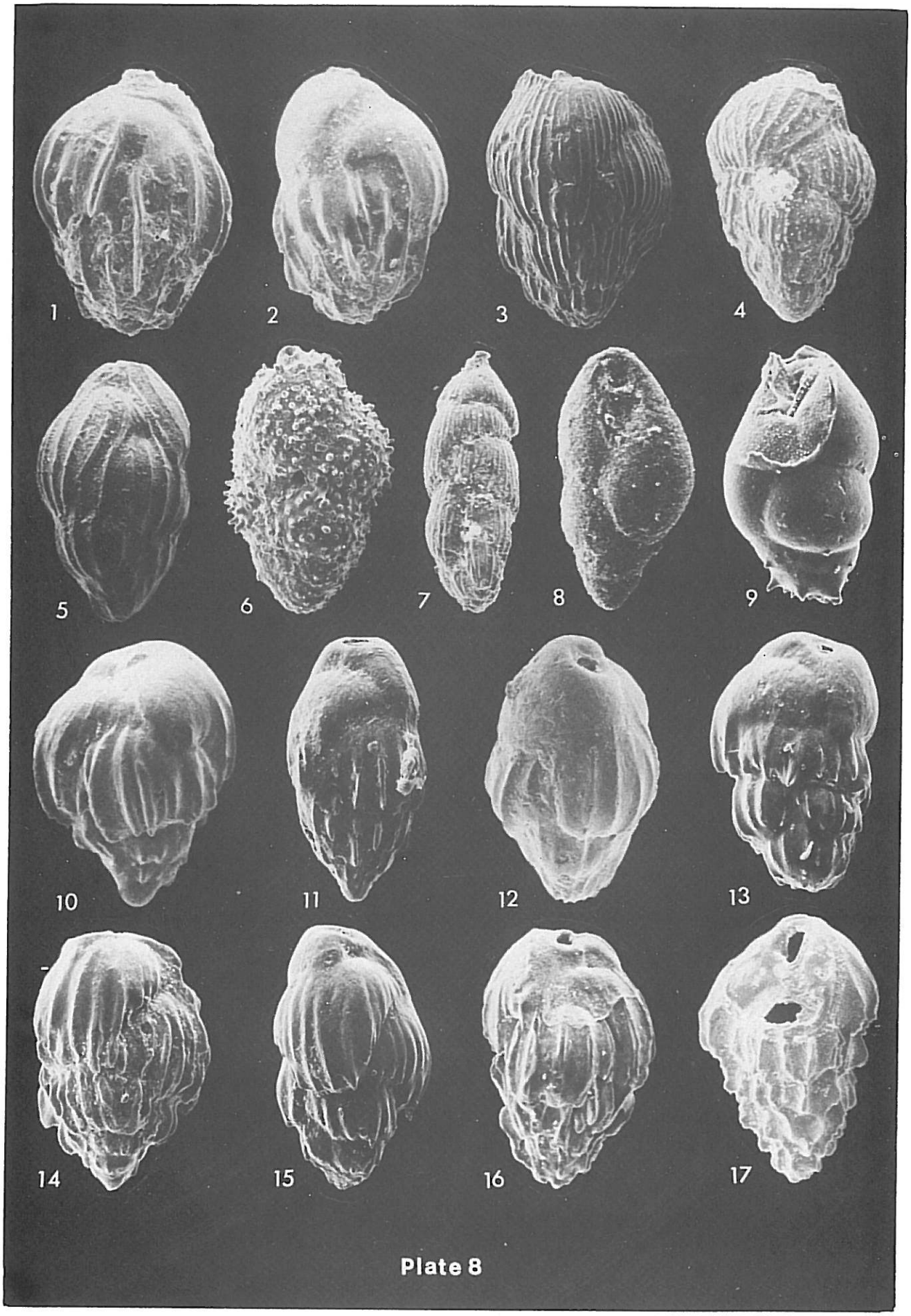


Plate 8

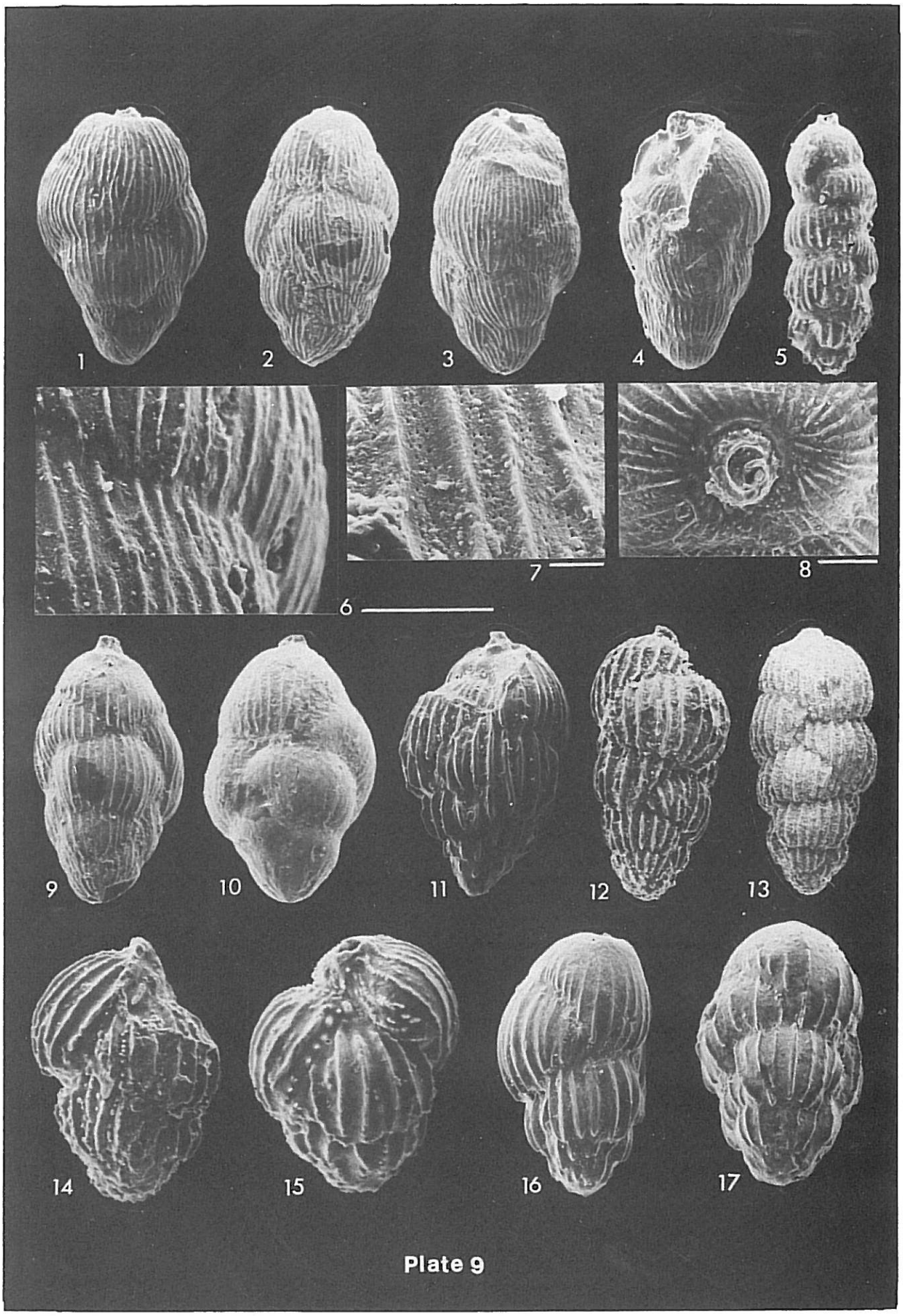


Plate 9

REFERENCES

Agib Mineraria, 1957, Foraminifera Padani (Terziario e Quaternario), Atlante 1 conografico e Distribuzione stratigrafica. *Agib Mineraria*, Milano 1957, 52 pls, 1st. Edition.

Agib Mineraria, 1980, Foraminifera Padani (Terziario e Quaternario), Atlante 1 congrafico e distribuzione stratigrafica. *IBID*, 68 pls, 2nd Edition.

Bandy, O.L., 1964, Cenezoic planktonic foraminiferal zonation. *Micropal.*, **10**, **1**, 1–17, 6 text-figs., 1 table.

Belanger, P.E. and Berggren, W.A., 1986, Neogene benthic Foraminifera of the Hatton – Rockall Basin. *Micropal.* **32**, **4**, 324–356, pls. 1–7, 6 text-figs, 3 append.

Blow, W.H., 1969, Late Middle Eocene to Recent planktonic foraminiferal biostratigraphy. In: P. Bronnimann and H.H. Renz (Eds.), *Proceed. Ist. Int. Conf. Plankt. Microfoss.*, Leiden: E.J. Brill, **I**, 199–422, 54 pls., 43 figs.

Blow, W.H., 1979, *The Cainozoic Globigerinida*. Leiden: E.J. Brill, 3 vols. 1413 p., 264 pls., 65 figs.

Bolli, H.M. and Saunders, J.B., 1985, Oligocene to Holocene low latitude planktonic Foraminifera. In: H.M. Bolli, J.B. Saunders and K. Perch-Nielson (Eds.) and K.E. Fancett (Assist.), *Plankton Stratigraphy, Planktonic Foraminifera, Calcareous Nannofossis and Calpionellids*. Cambridge Earth SC. Ser., Cambridge Univ. Press, Cambridge, U.K., **I**, 155–262, 46 figs.

Boltovsky, E., 1969, Living Planktonic Foraminifera at the 90° E miridian from the equator to the antarctic. *Micropal*, **15**, **2**, 237–255, pls. 1–3, 4 text-figures.

Boltovsky, E.,1980, On the benthonic bathyal-zone Foraminifera as stratigraphic guide fossils. *J. Foram. Res.* **101**, **3**, 163–172, pls. 1–4.

Borsetti, A.M., Iaccarino, S., Jorissen, F.J., Poignont, A., Sztrakos, K., Van der Zwann, G.J. and Verhallen, P.J.J., M., 1986, The Neogene development of *Uvigerina* in the Mediterranean. In: Atlantic–European Oligocene-Recent *Uvigerina*, taxonomy, paleoecology and paleobiogeographyy. *Utrecht Micropal.* Bull. **35**, 183–235, 19 pls, 1 figure.

Brolsma, M.J., 1978, Quantitative forminiferal analysis and environmental interpretation of the Pliocene and topmost Miocene on the south coast of Sicily. Int. Geol. Correl. Project No. 1. *Utrecht Micropal. Bull.* **18**, 159, 8 pls., 50 figs.

Brun, L., Chierici, M.A., Meijer, M. and Monteil, L., 1984, Stratigraphic and paleoecological distribution of some diagnostic species of Bolivinitidae (Foraminifera) from the Tertiary of the Gulf of Guinea. *Benthonics '83, 2nd International Symp. Benthic Foraminifera (Pau, Apri 1983)*, 91–104, 5 figs., 2 pls.

Cassell, D.T. and Sen Gupta, B.K., 1989, Foraminiferal stratigraphy and paleoenvironments of the Tertiary Uscari Formation, Limon Basin, Costa Rica. *J. Foram. Res.* **19**, **1**, 52–71, 7 text-figs., 1 table, 8 pls.

Costa, V. and Fandi, A., 1977, N.O.C. composite well log: D_2/NC41. *N.O.C.* Tripoli, Libya, Encl. no. 1.

Eliagoubi, B.A.H., 1972, *Vindobonian (Miocene) Foraminifera from the Faidia Formation, Umm Errzem region, northeastern* Libya. M. Sc. Thesis, University of Idaho Graduate School, April 1972, 107 pp., 2 pls., 9 figs., 3 tables.

Eliagoubi, B.A. H., 1986, Upper Cretaceous – Lower Tertiary planktonic Foraminifera from the northwestern Libyan offshore. *J. Afric. Earth Sc.* **5**, **4**, 423–440, 9 pls., 3 figs., (Pergamon).

Hageman, J., 1979, Benthonic foraminiferal assemblages from Plio-Pleistocene open bay to lagoonal sediments of the western Peloponnesus (Greece). *Utrecht Micropal.* Bull. **20**, 171 pp., 10 pls., 28 figs.

Hammuda, O.S.,, Sbeta, A.M., Mouzughi, A.J. and Eliagoubi, B.A., 1985, *Stratigraphic Nomenclature of the Northwestern Offshore of Libya*. Earth SC. Soc. Libya, Tarabulus, Libya 166 pp.

Hammuda, O.S., Van Hinte, J.E. and Nederbracht, S., 1991, Geohistory analysis mapping in central and southern Tarabulus Basin, northwestern offshore. In: M.J. Salem, O.S. Hammuda and B.A. Eliagoubi (Eds.), *The Geology of Libya*. Amsterdam, Elsevier, **IV**, pp. 1657–1680, 13 figs.

Haynes, J. R., 1981, *Foraminifera*. Macmillan Publishers Ltd. (G.B.). John Wiley and Sons, Ins. New York (Halsted Press), 433 p., 15 plates, 94 text-figs.

Iaccarino, S., 1985, Mediterranean Miocene and Pliocene Planktonic Foraminifera. In: H.M. Bolli, J.B. Saunders, and K. Perch-Nielsen (Eds.) and K.E. Fancett (Assist.) *Plankton Stratigraphy, Planktonic Foraminifera, Calcareous Nannofossils*. Cambridge Earth Sc. Ser. Cambr. Univ. Press, Cambridge, **I**, 283–314, 6 figs.

Jenkins, D.G., 1985, Southern mid-latitude Paleocene to Holocene Planktonic Foraminifera, In: H.M. Bolli, J.B. Saunders and K. Perch-Nielsen (Eds.) and E. Karin (Assist.), *Plankton Stratigraphy, Planktonic Foraminifera, Calcareous Nannofossils and Calpionellids*. Cambridge Earth Sc. Ser. Camb. Univ. Press, Cambridge, **I**, 263–282, 7 tex-figs.

Jongsma, D., Van Hinte, J.E. and Woodside, J.M., 1985, Geologic structure and neotectonics of the North African continental margin south of Sicily. *Marine Petrol. Geol.* **2**, 156–179, figs. 1–17.

Kassab, I.I.M.,Abusrewil, A.K. and Abuhmida, F.E., 1995, Biostratigraphy of the Oligocene-Miocene of subsurface offshore northwestern Libya typified by well H1/NC41. *Unpub. Rep. Pet. Res. Cent.* (N.O.C.), Tripoli, Libya.

Kennett, J.P. and Srinivasan, M.S., 1983, Neogene Planktonic Foraminifera, a Phylogenetic Atlas. Hutchinson Ross Pub. 256 p., 61 pls., 26 text-figures, 1 table.

Loeblich, A.R., Jr., and Tappan, H., 1964, Sarcodina chiefly "Thecamoebians" and Foraminiferida, in R.C. Moore (Ed.) *Treatise on Invertebrate Paleontology, Part C, Portista* **2**, Lawrence: *Geol. Soc. Am. and* Univ. Kan. Press, 900 p., 650 figs.

Loeblich, A.R., Jr., and Tappan, H., 1988, *Foraminiferal genera and their classification*. Van Nostrand Reinhold Pub. New York, U.S.A., **1**, 970 p., **2**, 212 p., 847 plates.

Mazzola, G., 1976, *Atlas of Tertiary Benthonic Microforaminifera from Sirte Basin (Libya)*. Agip NAME, Libyan Branch, Tripoli, 18 pls., 1 range chart.

McLaughlin, P.P., Jr., 1989, Neogene planktonic foraminiferal biostratigraphy of the southwestern Dominican Republic. *J. Foram. Res.* **19**, **4**, 294–310, pl. 1–3, 6 figures, 3 tables.

Miller, K.G. and Katz, M.E., 1987, Oligocene to Miocene benthic-foraminiferal and abyssal circulation changes in the North Atlantic. *Micropal.* **33**, **2**, 97–149, pls. 1–13.

Morkhoven, F.P.C.M. van, Berggren, W.A. and Edwards, A.S., 1986, Cenozoic cosmopolitan deep-water benthic Foraminifera. *Bull. Centres Rech. Explor. Prod. Elf-Aquitaine*, **11**, Pau. 4211 p., 126 pls, 8 text-figs.

Salem, M.J. and Spreng, A.C., 1980, Middle Miocene stratigraphy, Al Khums area, northwestern Libya. In: M.J. Salem and M.T. Busrewil (Eds.), *The Geology of Libya*, London, Academic Press, **I**, 97–116, 20 figs.

Sejrup, H.-P., Fiaeran, T., Hold, M., Beck, L., Hagn, J.M., Miljeteig, I., Morvik, I. and Norvik, O., 1981, Benthonic Foraminifera in surface sample from the Norwegian continental margin between 62° N and 62° N. *J. Foram. Res.* **11**, **4**, 277–295, pls. 1–2, 24 text-figs.

Sherif, Kh. A.T., 1991, Biostratigraphy in Al Khums area, northwestern Libya. In: M.J. Salem, O.S. Hammuda, and B.A. Eliagoubi (Eds.), *The Geology of Libya*, Elsevier, **IV** 1421–1456, pls. 1–7, 23 figs.

Smith, F.D., Jr., 1955, Planktonic Foraminifera as indicators of depositional environments. *Micropal.* **1**, **2**, 147–151, 2 text-figures.

Souaya, F.J., 1963, Micropaleontology of four sections south of Qoseir, Egypt. *Micropal.* **9**, **3**, 233–266, pls. 1–8, 3 test-figs.

Souaya, F.J., 1965, Miocene Foraminifera of the Gulf of Suez

region, U.A.R. part 1 – Systematics (Astrorhizoidea – Buliminoidea). *Micropal.* 11, no. 3, 301–334, pls. 1–3, 2 text-figs.

Stainforth, R.M., Lamb, J.L., Luterbacher, H., Beard, J.H. and Jeffords, R.M., 1975, Cenozoic planktonic foraminiferal zonation and characteristics of index forms. *Univ. Kansas Paleont. Contributions*, **Article 62**, *Lawrence, Kansas*, pp. 1–425, fig. 1–213, tables 1–9.

Thomas, E.,, 1980, Details of *Uvigerina* development in the Cretan Mio-Pliocene. Int. *Geol. Correl. Project no. 1. Utrecht Micropal. Bull.* **23**, 168 p., 5 pls., 65 figs.

Van der Zwaan, G.J., 1982, Paleoecology of Late Miocene Mediterranean Foraminifera. *Utrecht Micropal. Bull.* **25**, 202 pp., 15 pls., 65 figs.

Van der Zwaan, G.J., Jorissen, F.J., Verhallen, P.J.J.M. and Van Daniels, C.H., 1986, *Uvigerina* from the eastern Atlantic, North Sea Basin, Paratethys and Mediterranean. In: G.J. Van der Zwann, F.J. Jorissen, P.J.J.M. Verhallen and C.H. Van Daniels (Eds.), *Atlantic-European Oligiocene-Recent Uvigerina. Utrecht Micropal. Bull.* **35**, 1986, pp. 7–20, 5 text-figs.

Van Hinte, J.E. Colin, J.P. and Lehmann, R., 1980, Micropaleontologic record of the Messinain Event at Esso Libya Inc. Well B1-NC 35A on the Pelagian Platform. In: M.J. Salem and M.T. Busrewil (Eds), *The Geology of Libya.* London, Academic Press, I, 205–243, pls. 1–13, 8 figs.

Walton, W.R. and Sloan, B.J., 1990, The genus *Ammonia* BRUNNICH, 1772, Its geographic distribution and morphologic variability. *J. Foram. Res.* 1990, **20**, **2**, 128–156, pls. 1–4, 7 figs.

PRJ, Vol. 8 (January 1996); P. 49-60, 3 FIGS, 2 TABLES.

The pre-Cretaceous (Triassic) Sequence in the Subsurface of Maradah Trough, Eastern Sirt Basin, Libya

R.N. Sinha*, and H.B. Eland*

التتابع الطبقي لصخور ما قبل الحين الكريتاسي (الترياسي) تحت سطح منخفض مرادة ، شرقي حوض سرت — ليبيا

ر. ن. سنها و هـ. ب. ايلاند

يقع منخفض مرادة في الجهة الشرقية من حوض سرت بمحاذات الحافة الشرقية لمرتفع الركب الغني بالنفط كما تحده هضبة أمال من الجهة الشرقية. ومن خلال حفر الآبار ب1 وب2 وب3 وب4 بعقد الإمتياز 96 الواقع بنفس المنخفض تم اختراق تتابع صخري من الأحجار الرملية مع تراكمات بسيطة من صخور الطفلة اللتان يعتقد أنها قد ترسبا أوان ما قبل الحين الكريتاس العلوي.

قامت شركة وينترشل بتقسيم التتابع الطبقي لصخور هذا الحين إلى وحدتين صخريتين هما PUCأ وPUCب كما أعتبرت الشركة أن الوحدة أ أكثر حداثة من الوحدة ب من حيث العمر، حيث يربو سمك الوحدة ب عن 995 قدما وتتكون في مجملها من صخور الحجر الرملي مع تراكمات ضئيلة ونادرة من صخور الطين. أما صخور الوحدة أ فأنها تتكون من صخور من الحجر الرملي والطين ، وتغطي هذه الوحدة الصخرية الوحدة ب بسطح عدم توافق. يتراوح سمك الوحدة أ ما بين 510 قدما عند الشرق إلى 765 قدماً عند الناحية الغربية من منطقة الدراسة ويصل سمكها إلى 1450 قدماً في أقصى الغرب عند منطقة جخرة. وبناء على المحتوى الصخري وخواص السرود الجيوفزيائية فقد تم تقسيم صخور هذه الوحدة (أ) إلى أربع وحدات صخرية صغرى.

يتكون التتابع الصخرى للوحدتين أ و ب غالباً من صخور مرو الأرنيت ذات الخواص البتروغرافية المتشابهة إلا أنه بالإمكان فصل صخور هاتين الوحدتين عن بعضها باستعمال بتروغرافية مجمل المحتوى الصخري وتواجدات المعادن الثقيلة وخواص حبوب اللقاح النباتية ، حيث تشير الأخيرة (أي حبوب اللقاح) بالرغم من ندرتها أن صخور الوحدة ب كانت قد ترسبت عند أوان دهر الحياة القديمة المبكر (الكامبريان — أو ما قبله). كما تشير المعلومات المستوحاة من دراسة حبوب اللقاح لصخور الوحدة أ أنها تنتمي إلى ترسبات الحين الترياسي المتوسط. وقد يشير هذا ومعلومات أخرى إلى وجود سطح عدم توافق بين صخور الوحدتين أ و ب. ومن المحتمل وبناء على الخواص البتروغرافية والصفات الصخرية وتواجدات حبوب اللقاح ، أن صخور الوحدة ب كانت قد ترسبت في منخفض نشط تكتونيا وفي بيئة غير بحرية في وجود الأكسجين أبان ما قبل دهر الحياة القديمة ، حيث يبدو أن الصخور الفتاتية معادة الترسيب وأن المنطقة قد تعرضت لظاهرة الرفع والتجوية حتى بداية الحين الترياسي. كما يعتقد أن صخور الوحدة أ قد ترسبت في منخسف تحت ظروف غير بحرية وربما إنتقالية أحياناً تتراوح بين وفرة وندرة الأكسجين أثناء الحين الترياسي الأوسط (الأنيزيان واللأدينيان؟). هذا وقد مر المنخسف بفترة تكتونية هادئة أثناء أغلب مرحلة الأنيزيان نتج عنها رواسب من الطين الغير بحري مع صخور ثانوية من الحجر الرملي. كما إشتهرت هذه الفترة الزمنية الأخيرة بهبوط تخلله بعض التأثير من البحر.

تشير زيادة سمك الوحدة أ عند الغرب وازدياد محتواها الرملي أن منخفض مرادة كان غير متناسق وأن الصدوع التي تحدد الجهة الغربية منه كانت أكثر نشاطاً أثناء فترة الحين الترياسي الأوسط. كما يبدو أن الطقس كان أكثر برودا أثناء أوائل دهر الحياة القديمة عند تواجد صخور الوحدة ب ثم ما لبث أن تغير إلى طقس رطب أثناء تطور الجزء الأسفل من الوحدة أ وتبع ذلك أنواع من الطقس الرطب والجاف في وقت اللأدينيان أثناء ترسب الجزء العلوي من الوحدة أ. هذا وقد إشتقت الصخور الفتاتية للوحدتين أ و ب من تتابع صخري من الصخور المتحولة والصخور النارية الحمضية الفقيرة بمعدن الفلدسبار. وقد ترجع تواجدات العناصر المعاد ترسيبها بالوحدة أ إلى صخور قديمة قد تنتمي إلى تكوين القرقاف وربما صخور الوحدة ب أيضاً.

*Petroleum Research Centre P.O. Box 6431, Tripoli, G.S.P.L.A.J.

Abstract *A fairly thick sequence of sandstones with very subordinate shales, designated as Pre-Upper Cretaceous (PUC) by the operating company (Wintershall), are met at B1, B2, B3 and B4-96 in the subsurface of Maradah Trough, Sirt Basin. The Amal Platform defines its eastern limits. The operating company divided the PUC sequence into PUC 'B' (older) and PUC 'A' (younger) units. The PUC 'B' is 995+ feet thick and comprises mainly sandstones with very rare and thin levels of shales. The PUC 'A' unconformably overlies the PUC 'B' and consists of sandstones and shales. It is divisible into Units I–IV on basis of gross lithology and log characteristics. The thickness of PUC 'A' ranges from 510 feet in the east to 765 feet in the west. It thickens to 1450 feet further west towards Jakhira.*

PUC 'B' and PUC 'A' sequences comprise mostly quartz-arenites of fairly similar petrographic characters. It, however, is possible to resolve one from the other on basis of gross lithologic, and palynologic criteria.

The palynofossil assemblage, though scarce, suggests PUC 'B' to be ?Precambrian–Cambrian. The assemblage recovered from PUC 'A' is relatively very rich and referable to Middle Triassic (Anisian and ?Ladinian). These and other data suggest an unconformity between PUC 'B' and the overlying PUC 'A'.

Lithologic characters, petrographic attributes and palynofossil contents suggest that PUC 'B' was probably laid in a tectonically active graben under mainly non-marine oxic environments during ?Pre-Cambrian. The detritus appears to be partly recycled. Subsequently, the depositional area underwent uplift and erosion till the close of Early Triassic. The PUC 'A' appears to have been laid in a graben under fluctuating oxic-anoxic and non-marine to at times probable transitional environments during Middle Triassic (Anisian and ?Ladinian). Tectonically the graben was fairly subdued during most of the Anisian and promoted evolution of mainly non-marine shales with subordinate sandstones. The later period was marked by a relatively accelerated negative tectonism and interludes of marine influence. Westerly increments in thickness and overall increase in sandstone contents of PUC 'A' indicate that the Marada Trough was asymmetric and the faults defining its western fringes were tectonically more active during the Middle Triassic.

Relatively colder climates appear to have prevailed during ?Precambrian–Cambrian when the PUC 'B' sequence was developed. The palaeoclimates during the evolution of the lower part of PUC 'A' sequence, dated as Anisian, were mainly hygrophytic. These, however, switched over to mixed hygrophytic-xerophytic types during Ladinian when the upper part of the PUC 'A' sequence was laid.

INTRODUCTION

Sediments of Triassic age are usually considered to be absent in the Sirt Basin (Barr and Weegar, 1972). The geologic period extending from Carboniferous to ?Jurassic is opined to be denoted by non deposition possibly due to continued uplift and erosion of the Sirte anticlise (Massa and Delort, 1984). The adjoining Ghadamis Basin to the west and the Cyrenaica Platform to the east, being syneclises contain a fairly complete record of palaeozoic and Mesozoic sediments (Adloff *et al.*, 1986 Karr *et al.*, 1972; Bellini and Massa, 1980; Brugman *et al.*, 1985 and Brugman and Visscher, 1988).

The Pre-Palaeocene quartzose clastics met in the subsurface of Sirt Basin broadly belong to three ages. The Gargaf–Hofra quartzites and Amal Formation are considered to be of Cambrian–Ordovician age (Roberts, 1970; Barr and Weegar, 1972). The mostly non-marine Nubian-Sarir sandstones and other homotaxial deposits are generally assigned a ?Jurassic – Early Cretaceous age (Bannerjee, 1980). The shallow marine – marine sandstones and shales included into several other formations (e.g. Maragh, Bahi, Etel, Rachamat, Sirte etc.) are dated as Late Cretaceous XX (Barr and Weegar, 1972).

Brugman *et al.*, 1985, and Thusu *et al.*, 1988, reported the presence of Triassic palynomorphs from shale levels in subsurface sandstones met at Al-96 in the Maradah Trough, Eastern Sirt Basin, Libya (Fig. 1).

The present study deals with the occurrence of Triassic sediments in the subsurface from another

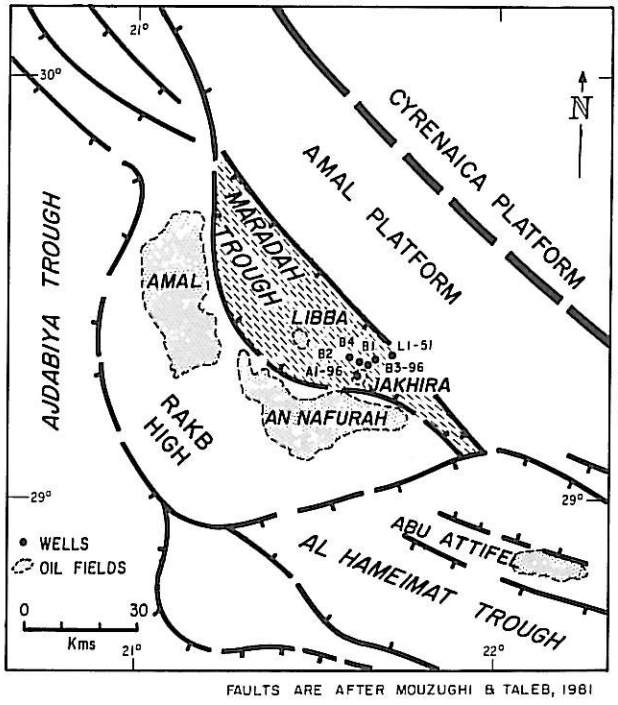


Fig. 1. Location map, Maradah Trough, Sirt Basin, Libya.

new locality (B1, B2, B3, and B4-96 wells) in the Maradah Trough and mainly discusses their evolution, age and environment sedimentation. The study is based on lithologic and petrographic investigations by the senior author and palynologic studies by the junior author.

GENERALISED STRATIGRAPHY

The pre-Late Cretaceous sequence met in the studied wells comprises sandstones and minor shales. The operating company (OPCO) divided these sandstones into Pre-Upper Cretaceous 'B' (older) and PUC 'A' (younger) sequences (Fig. 2). The PUC 'B' comprises mainly sandstones with rare-scarce thin levels of shale. The sandstones are whitish, light gray, grayish brown, moderately hard, sometimes cross-bedded, locally friable, partly quartzitic, medium to coarse grained, rarely fine grained, moderately sorted, at times pebbly (3–4 mm), scarcely argilaceous and micaceous. Graded bedding is common. Detrital grains are generally cemented by silica and at times by barite and comprise angular – subangular and at times subrounded quartz grains. Sub-vertical fractures filled by siliceous matter and barite are present. Shales are rare to scarce. They are present as streaks and thin to very thin beds. They are light grey to dark gray, grayish brown, reddish brown, varicoloured, mottled, subfissile – fissile, brittle, often laminated, silty-sandy and scarcely micaceous. Fissility is more pronounced due east whereas, the micaceous content increases towards the west (Table 1). Siltstones are fairly rare. They are medium gray, light beige, micaceous, argillaceous and display sub-vertical fractures. The thickest (995+ feet) drilled section of PUC 'B' is met at B1-96. Basement is not reached in any of the four wells (Table 1).

The PUC 'A' comprises sandstones, shales and minor siltstones. Sandstones are off-white, greenish gray, occasionally with reddish tint, brownish gray, yellowish brown, light brown, beige, dark gray occasionally variegated, moderately consolidated, fine to medium grained, at times coarse grained, and micromicaceous. Graded bedding and alternation of finer and coarser grained sandstones are fairly common. Subrounded, clear, white and moderately well sorted quartz grains are the most dominant constituent. Ferriginous matter, pyrite, plant remains and claystone clasts are present. Siliceous and carbonate

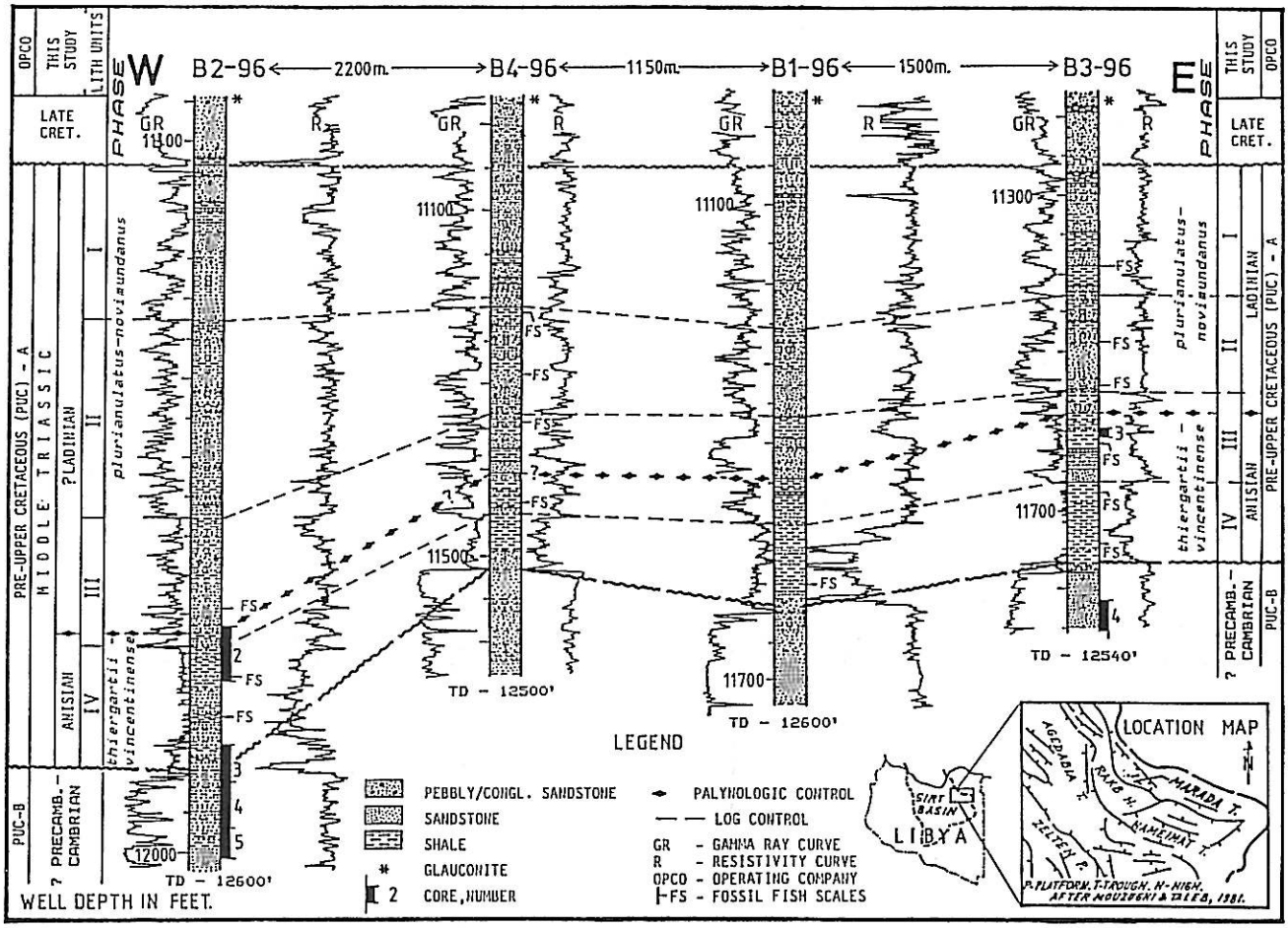


Fig. 2. Stratigraphic section through wells, Maradah Trough, Sirt Basin, Libya.

Table 1. Gross lithologic characteristics of Pre-Upper Cretaceous (PUC) 'B' and 'A' sequences, Maradah trough, Sirt Basin, Libya.

Units	B2-96	B4-96	B1-96	B3-96	Age
PRE-UPPER CRETACEOUS (PUC) 'A' — UNIT I	*Sandstone with thin shales* *SST.:* Wh., lt., gr., f. – cse., subang. – subrounded, pyr., fria., poor cement. congl. in upper part. *SHALE:* Med. lt. brn. gr., red. brn., grn. brn., hd., splintary, sli. silty, subfiss. THICKNESS =195 FEET.	*Sandstone with thin shale* *SST.:* Gr., med.-cse., loose, partly congl., sub-rounded, at times alternates with shale. *SHALE:* Brn. gr., beige, dk. brn., blk, silty, pyr., fiss. *SILTST.:* In traces, brn, arg. THICKNESS =160 FEET.	*Sandstone with thin shale* SST.: off wh., dk, red brn., fria., mod, hd., f, – cse., tr. arg., sh. alternations. SHALE: Dk. gr. – grn. gr., fiss., carb., coaly matter, sli. silty, lenses of silt. THICKNESS =250 FEET.	*Sandstone and shale* SST.: Variegated, orange, fria., mod. sorted, arg. SHALE: Variegated, gr. brn., red, ochre, sft., form, fissile, partly carb., pyr., silty, *fish scales.* THICKNESS =120 FEET.	MIDDLE TRIASSIC (ANISIAN-?LADINIAN)
UNIT II	*Alternating sandstone and shale* *SST.:* Wh., med. – cse., pebbly, congl., grn. org. matrix, loc. loose, sil cement. *SHALE:* Brn. gr., red. brn, hd., splintery, sh. silty, subfiss. *SILTST.:* Scarce, lt. gr. beige, fria., grad. to sst. THICKNESS =250 FEET.	*Alternating sandstone and shale* *SST.:* Wh., lt. gr., f. – med., siliceous, partly qtzitic. *SHALE.:* Gr. – dk. gr., beige, silty, pyr., v. fissile. *common fish scales.* *SILTST.:* Traces. THICKNESS =125 FEET.	*Alternating sandstone and shale* *SST.:* As above. SHALE: Gr. – dk. brn. gr., mod. hd., fiss., carb. – coaly matter, silty. *SILST.:* Gr. – dk. gr. sli. calc. THICKNESS =105 FEET.	*Alternating sandstone and shale* *SST.:* Variegated, gr. brn., red, ochre, f. – cse., mic. SHALE: Variegated, gr. brn., pale grn., red, sft., fiss., partly carb., mic., sandy, pyr., *fish scales.* sand interbeds. THICKNESS =120 FEET.	
UNIT III	*Sandstone with SILTST. & shale* *SST.:* variegated, partly red brn., f. – med. & cse., pyr., org., micromic., siliceous. *SHALE:* Variegated, dk. gr. – brn. gr. laminated, hd., subfiss., splintery, pyr. plant remains, *comm. fish scales,* silty. *SILTST.:* Scarce. Beige gr., fria., grades to f. sst. THICKNESS =165 FEET.	*Sandstone and shale* *SST.:* Wh., f. – med., sil., locally qtzitic. *SHALE:* Beige, lt. – dk. gr., brn. gr., silty., pyr., partly micromic., fiss., *rare fish scales.* THICKNESS =115 FEET.	*Sandstone with shale in lower & upper part* SST.: Off-wh., lt. brn., fria., loose med. – cse., subang. – subrounded, poorly cemented, sh. arg. SHALE: Gr. – dk. brn. gr. mod. hd., fiss., carb. – coaly matter, thin silst. THICKNESS =140 FEET.	*Shale with sandstone levels* SST.: Gr. – med. gr., gr. brn., dk. gr. – blk, f. – cse., firm – fria., arg., calc. – dolotic. SHALE: Dk. gr. – blk., grn, brn., ochre, thinly lamina., fiss., mic., carb., – pyr., silty, tr. coal., *common fish scales.* THICKNESS =110 FEET.	
UNIT IV	*Sandstone and shale* *SST.:* Brn. gr., red. brn., cse. – med., pyr. sil., fria. *SHALE.:* Variegated, brn. gr., laminated, med. hd., silty, f. sandy, v. fiss., splintery, *common fish scales,* pyr. plant remains, v. pyr., horiz. burrows, micromicaceous. *SILTST.:* Beige, med. hd., also fria., arg. THICKNESS =155 FEET.	*Shale with sandstone levels* *SST.:* Lt. brn., f. – cse., subang. – subrounded, *SHALE:* Beige, dk. med. gr., v. pyr., subfis., micromic., *rare fish scales.* *SILST.:* Rare, Brn. gr., bituminous. THICKNESS =65 FEET.	*Shale with scarce sandstone* SST.: As above. SHALE: Dk. gr. – blk. gr. firm, mod hd., fissile, splintery, silty, *scarce fish scales.* THICKNESS =105 FEET.	*Sandstone with thin shales at base* SST.: Wh., brn., f. – med., loose – fria., sil., dolotic, arg. SHALE: Med. dk. gr., v. dk. brn., blk., sft., fiss., partly lam., pyr., coaly carb., dolotic., *fish scales, plant remains.* THICKNESS =110 FEET.	
PUC 'B'	*Sandstone with a few shale levels* *SST.:* Wh., lt. brn., med-ese., fria., qtzitic, sili. cement, pyr., mic., ang. – subang., subvertical fractures filled by quartz. *SHALE:* Grn. gr. – beige, red, ochre, sli. pyr., hd., subfiss., plant remains. *SILTST.:* Streaks, grn. gr., v. mic. THICKNESS =700+ FEET.	*Sandstone with a few shale levels* *SST.:* Lt. – med. brn., poorly cemented, partly qtzitic, also fria., med. – cse., subang. – subrounded. *SHALE:* Trace; med.. gr., subfiss. THICKNESS =985+ FEET.	*Sandstone with a few shale levels* SST.: Beige, lt. brn., gr., mod. hd., – hd., locally fria., f. – cse., subrounded, sil. cement, qtzitic., mic., laminated. SHALE: Lt. gr., red. brn., subfiss., occ. v. hd., mic. THICKNESS =995+ FEET.	*Sandstone with a few shale levels* *SST.:* V. lt. gr., brn., pale grn., pale red, qtzitic, sil., fractures, med-cse., filled with barite and anhy. SHALE: Trace; beige, med. dk. gr., brn. gr., variegated, mottled, partly mic., brittle, fissile, silty. THICKNESS =775+ FEET.	?PRECAMB. – CAMB.

(dolomitic) cements are observed. Matrix, though low, is argillaceous. The Siltstones are gray to dark brownish gray, greenish gray, light brownish, micromicaceous, argillaceous, often grading to very fine sandstones and silty shales, at times sub-fissile, laminated and locally with abundant organic matter. Thin levels of brownish, fine-medium grained and well consolidated sandstones are present. The shales are gray, medium dark gray-dark brownish, locally greenish brown, reddish, variegated, microfaulted, medium hard, subfissile–fissile, laminated, splintery, often pyritic, silty-sandy and often grade to siltstones. Traces of carbonaceous, coaly matter, pyritised plant remains and streaks–stringers and interbeds of brownish gray, friable sandstones and siltstones with siliceous and dolomitic cements are present. In general, the micaceous content of sandstones and shales increases towards the west (Table 1). Shales are more fissile and paper thin due east. The thickness of PUC 'A' varies from 510 feet in the east to 765 feet in the west (Fig. 2). It rapidly increases to about 1450 feet in A4-96 located very close to A1-96 in another fault block approximately six kilometres south of B2-96 (Fig. 2).

Variations in gamma ray and resistivity curves together with changes in lithologic characters and organization enable classification of PUC 'A' into four units (Fig. 2, Table 1). It is unconformably overlain by pebbly to coarse grained and at times conglomeratic sandstones containing abundant glauconites and levels of greenish gray shales as well as carbonates. These are included into the Maragh Formation of Late Cretaceous age (Fig. 2). The glauconites reported in well cuttings from several levels within the PUC 'A' may be contaminations from the Maragh Formation.

Gross characters of the principal lithologies forming the PUC 'A' and PUC 'B' sequences are summarized in Table 2.

PETROGRAPHIC STUDY

The study follows the classification and nomenclature of sandstones proposed by Gilbert (1954). Abundance of various detrital components were determined visually using diagrams of Shvestov (Terry and Chillinger, 1955) and Bacelle and Bosellini (1965). Roundness was estimated after the chart of Krumbein (1941).

Sandstones form the bulk of PUC 'B' and PUC 'A' sequences. Compositionally, they are classed as quartz-arenites. Shales are very subordinate in PUC 'B' but relatively more abundant in PUC 'A'. Petrographic differences between the quartz-arenites and shales of PUC 'B' and PUC 'A' sequences are too subtle and they alone cannot be objectively used to identify one from the other. The general petrographic characters of quartz-arenites and shales are as given below.

Quartz-arenites

The arenites are constituted mainly by quartz and minor amounts of chert, rock fragments and traces of feldspars as well as ore minerals. In general, they are fairly deficient in matrix. A few levels, however, seem to contain up to 5% of clayey-chloritomicaceous-quartzose matrix. Most of the principal detrital fraction is of 200–350 μ size. A few grains larger than 500 μ also are present. Rounding in the 200–350 μ population ranges from 0.3 to 5. Coarser detrital grains are usually better rounded (0.5 to 0.7). Grains with roundness exceeding 0.7 are rare. Some of the detrital grains seem recycled.

Quartz forms nearly 80% of the essential detrital fraction. Various varieties are recognised. Slightly-strongly strained quartz with undulose extinction and inclusions are the most common. The inclusions are generally of rutile, zircon, micas and tourmaline. A few grains also display gaseous inclusions. Quartzitic aggregates, polycrystalline quartz and stretched metamorphic quartz also are present. Unstrained grains with uniform extinction are noticeable. Authigenic growths defined by dust rings and rims caused by dissolution and replacement by carbonates are frequently observed. A few quartz grains are very well rounded and seem recycled. Detrital chert forms 3–5% of the detrital fraction. They usually are fairly well rounded (0.5) and characterised by an aggregate of mutually interfering or interlocking minute silica grains exhibiting characteristic pin-head extinction. A few well rounded broken chert grains are noticeable. Some of the chert grains are ferruginous while a few others are recycled. Feldspars are present only in traces. In most cases they are untwinned and fairly fresh. Their identification could thus be possible only on basis of cleavage traces, at times feeble to very feeble alteration to ?sericite and if possible, the optic sign. Most of the feldspars are marked by small extinction angles suggestive of the albite-oligoclase range. Some of the feldspars exhibit straight extinction and may represent orthoclase. Rock fragments exclusive of chert are usually scarce and seem to form less than 3–5% of the detrital mass. The rounding ranges from 0.3 to 0.5 but a few are very well rounded and seem recycled. Metaquartzites are the most common and those of argillites, quartz-schist, orthoquartzites are very rare. Accessory detrital minerals include a host of heavy minerals and micas. Zircon, tourmaline, sphene and rutile are fairly common and most of these are recycled.

The non detrital constituents include cements. Silica is the most common cement. Clayey, carbonate

Table 2. Gross characters of arenites and shales of (PUC) 'B' and (PUC) 'A' sequences, Maradah trough, Sirt Basin, Libya.

	Characters etc.	*PUC 'B' (?Precamb.–Cambrian)*	*PUC 'A' (Middle Triassic)*
Arenite ↓	General	Whitish – lt. gr., hard, med – cse'. qtzitic, pebbly, well compacted, sub – vert, fractures, rarely fria. Grains subrounded, a few well rounded, mod. sorted, and with authegenic growths. Rarely micaceous. Non-calcareous.	Off white – gray, variegated, reddish, f. – med., rarely pebbly, compacted and locally friable. Grains are sub. ang. – subrounded, also very well rounded, with authegenic growths. Micaceous, often calc – dolomitic.
	Composition	Strained quartz, tr. fresh alkali feldspars. Chert and qtzitic rock frag. traceable. Strained micas, recycled quartz.	Strained quartz, tr. alkali feldspar, fairly common chert and metaqtzitic and other rock frag. Strained micas, and frequent recycled quartz.
	Matrix	Rare, patchy; usually silty; clay altering to micas.	Patchy; usually argill., altered to micas
	Diagenesis	Moderately compacted, indurated cemented by silica and ferru. matter. Some fractures filled by barite. Authegenic growths on quartz are common.	Well compacted, cemented by carbonates, silica and ferru. matter. Authegenic growths on quartz grains are less common.
	Heavy Mineral Suite	Generally impoverished, scarce to very scarce. Includes rounded zircon, tourmaline, rutile and sphene and a few zoisite, chtd, garnet. Ore minerals are abundant.	Relatively richer and abundant. Flooded by very well rounded zircon, tourmaline, sphene and rutile. Others include epidote, zoitite, chloritoid, staurolite, monazite, allanite and garnet etc. Ore minerals are less abundant.
	Glauconite	Absent	Absent
Shales ↑	General	Gray, very dark gray, black, hard, fissile, slickensided, non-calc., rarely silty, brittle, often laminated. Generally rare	Gray, very dark gray, black, med. soft, fissile, at times paper thin, slickensided, pyritiferous. Generally more common.
	Glauconite	Absent	Absent
	Plant Remains	Rare to scarce; often pyritized.	Often present, at times very common, usually pyritized.
	Coaly Matter	Absent	Present. Well structured.
	Organic Matter	Mainly amorphous, very dark gray to black, very mature to metamorphosed. TAI = 3+ to 5.	Mainly herbaceous, light brn – dk. brown, mature. TAI = 2 to 3+.
	Worm Burrows	Not present	Present. Horizontal more common than vertical.
	Palynofossils	Ornamentation is obliterated. Grains are corroded. *?Leiosphaeridia* spp.. and *?Kildinella ripheica* etc.	Well preserved. Several species are recorded. See text and Appendix I.
	Other Fossils	None recorded	*Branchiopods*, fragments of *Conularids*, fishscales and part of fish tooth.
	Age	?Precambrian – Cambrian on basis of palynofossils	Middle Triassic (Anisian and ?Ladinian) on basis of palynofossils.

and cherty cements are patchy and subordinate. Cementation by ferruginous and chloritomicaceous matter is also observed.

The petrographic characters of arenites forming the PUC 'B' and PUC 'A' sequences are fairly similar to one another. The differences are subtle and these alone cannot be employed to differentiate one from the other. Their principal characters are summarized in Table 2.

Shales

The shales are dark gray to black, fissile and usually hard. They comprise clay minerals and carbonaceous and bituminous matter. Silt is subordinate. The chloritomicaceous clay minerals occur generally as evenly oriented shred-like and moderately crystalline aggregates. Organic matter is often present. Ferruginous stains are common. Authigenic minerals, other than the micas, mainly include pyrites. These occur generally as anhedral – subhedral crystal grains throughout the shale fabric.

The shales of PUC 'B' and PUC 'A' are fairly similar to one another. They are, however, more abundant in PUC 'A'. Fissility is at times more pronounced and slickensiding is common in shales of PUC 'A'. These shales are fairly rich in comminuted organic remains. Anhedral pyrite is commonly present and evenly disseminated in the clay mineral fabric. It, however, also occurs as stringers, films and less frequently as euhedral crystal aggregates. Several fossils of Branchiopods and plants are pyritized. Diagenetic anhydrite is at times present along some of the shaly planes. The shales of PUC 'B' are hard, extremely low in organic content and fairly deficient in pyrites. Their micaceous content, however, exhibits better crystallinity and orientation.

DIAGENESIS

Compaction

Alternating sandstone–shale laminae display the best evidence of compaction megascopically. In quite a few cases (B3-96, core 2, 11593–11606 ft; B2-96, core 2, 11724–11784 ft) the two are squeezed into one another. The laminae exhibit thickness variations due to differential compaction. Compaction and packing, which are reflected by the nature of detrital grain contacts, control porosity (Gilbert, 1949; Taylor, 1950; Thompson, 1950 and Siever, 1959).

The grain contacts in the quartz-arenites are usually concavo-convex. Planar, line or tangential contacts are less common. Sutured contacts formed by interpenetration assisted by pressure solution are very rare. At times, relatively larger (exceeding 350 μ) quartz grains are penetrated by those of silt grade and their contacts seem to be marked by a thin film of ferruginous-argillaceous mass. Fused contacts are usually absent. In general, the arenites exhibit a moderate degree of pre-diagenetic compaction.

Cementation and Authigenesis

Silica is the most common cement. It occurs as thin films between detrital grains and in some cases, also as interfering authigenic growths. Films are more common in finer and medium grained arenites. Chert cement marked by typical pinhead extinction is also present. Authigenic growths are relatively more common over quartz grains exceeding 350–400 μ and at times form interlocking textures. The original detrital grain boundaries are defined by dust rings. In several cases, the dust rings of adjacent quartz grains are not in contact with one other. This indicates that diagenesis by silica occurred during early burial stage when the detrital mass was inadequately compacted. The quartz grains of arenites with clayey matter are generally devoid of authigenic growths. The presence of clayey matter probably inhibited authigenesis by silica.

Cementation by chloritomicaceous matter is more frequent in finer and medium grained arenites. It is brought about by diagenetic encroachment of clayey minerals into the peripheral regions of detrital quartz grains. Very fine clays fill part of the intergranular voids and act as cement when partially recrystallized.

Cementation by carbonates is very limited and usually patchy. Dolomite appears to be the principal constituent and whenever present, replaces the silica cement. Quartz–carbonate reaction rims surrounding some of the larger detrital quartz grains and displaying several stages of peripheral dissolution are noticeable. Quartz grains floating in poikilitic carbonate cement are observed though rarely.

Pyritization

Diagenetic pyrite is present in arenites and shales. It, however, is relatively more abundant in the dark grey organically rich fissile shales of PUC 'A' (B2-96, core 2, 11724–11784 ft, B3-96, core 3, 11593–11606 ft). It occurs as evenly distributed disseminations, individual euhedral–anhedral crystals and irregular stringers or films along the fissility planes. Mutually interfering microcrystalline aggregates and nodules are rare. Some of the fossilised plant remains, fish scales and Branchiopods are pyritized.

PALYNOLOGIC ASSEMBLAGE

Palynofossils were separated using standard techniques involving disintegration of samples, treatment with hydrochloric acid to remove carbonates and

ferruginous matters, dissolution of siliceous fractions in hydrofluoric acid (40%), thorough washing to remove the acid, sieving through 10 μ sieves and finally, separation using zinc bromide solution (Sp.Gr. = 2.00).

In general, the assemblage is usually scarce and relatively poor in PUC 'B' but richer in PUC 'A' where several species are recorded (Fig. 3, Appendix I).

PUC 'B'

The assemblage is very poor, fragmentary, and largely unidentifiable. The palynofossils are usually structureless, with obliterated ornamentation and their peripheral areas are substantially corroded possibly by bacteria. The rest of the organic matter is mostly amorphous, very dark gray to black and thermally over matured with TAI (Staplin, 1969; Geochem, 1980) ranging from 3+ to 5. The reddish brown partly oxidised shales in well B2-96 yielded a sphaeromorph similar to *Leiosphaeridia spp.* and *Kildinella ripheica.*

PUC 'A'

In general the organic residue is light brown to dark brown with TAI ranging from 2 to 3+. It is mostly herbaceous, algal and woody. Inertinitic matter are minor to subordinate. Palynofossils are more varied (Fig. 3, Appendix I), better preserved and well identifiable. Their ornamentation is fairly intact and largely unobliterated.

The palynologic assemblage includes several species. The more important of these include *Stellapollenites thiergartii, Alisporites* complex, *Platysaccus queenslandii, Lunatisporites*, sp., *Aratrisporites*, sp., *Stroterisporites* sp., *Triadispora crass, Cyadopites* sp., *Calamospora tener*, and *Alisporites magnus* besides several others (Appendix I). *Veryhachium* sp. and *Micrhystridium* sp., though rare and sporadic, are observed in the PUC 'A' met at B2 and B3-96.

FOSSIL FAUNAL ASSEMBLAGE

The sandstones and shales of PUC 'B' seem to be devoid of fossil fauna. The assemblage recorded in the PUC 'A' (B2-96, cores 2 and 3; B3-96, core 3) comprises numerous Branchiopods (*Lioestheria* sp.), *Conulariids*, fish spine, fish scales and part of fish tooth (M.C. Keen, personal communication, 1993).

DISCUSSION

Age

A reddish brown partly oxidised shale in PUC 'B' met in well B2-96 yielded sphaeromorphs similar to *Leiosphearidia* spp. and *Kildinella ripheica. Leiosphearidia* spp. is also reported from the Precambrian–Cambrian succession developed over the Cyrenaica Platform which adjoins the Maradah Trough (Boudet, 1988). The PUC 'B', hence, could be of Precambrian–Cambrian age.

The palynologic assemblage of PUC 'A' is referable to Middle Triassic and enable classification of this sequence into that of Anisian and ?Ladinian ages. The assemblage referable to Anisian is marked by low to fair diversity. It is noted from the intervals 11740–11900 ft in B2-96, ?11410–11515 ft in B4-96, 11440–11605 ft in B1-96 and 11575–11675 ft in B3-96. Diagnostic forms include *Stellapollenites thiergartii, Alisporites* complex, *Platysaccus queenslandii, Lunatisporites* sp., *Aratrisporites* sp., *Stroterisporites* sp., *Triadispora crassa, Cyadopites* sp., *Calamospora tener*, and *Alisporites magnus. Veryhachium* sp. and *Micrhystridium* sp., though rare and sporadic, are observed in the sequence met B3-96.

The assemblage indicative of ?Ladinian is recorded in the succession overlying that of Anisian age and underlying the unconformity separating PUC 'A' from the Maragh Formation (Fig. 2). Typical forms include *Cycadopites* sp., *Lunatisporites* sp., *Calamospora tener, Triadispora crassa, Alisporites magnus, Aratrisporites* sp. and *Partitisporites novimundanus* morphon besides several others (Fig. 3). *Veryhachium* sp. and *Micrhystridium* sp. though rare and sporadic, are observed in sequences met at B2 and B3-96. The assemblages are fairly comparable to those recovered from the Middle Triassic (Anisian and ?Ladinian) met in the subsurface of nearby areas (Brugman and Visscher, 1988 and Thusu *et al.*, 1988).

Palynological Phases

Evolution of a floral assemblage during a geologic time interval can be traced through several transitionary palynologic associations designated as "phases". The concept of phase, first propagated by Schurman (1977), is employed for inferring palaeoenvironments. According to Van der Zwan (1980), a phase is "any recognisable step in the (local, regional or inter-regional) gradual compositional development of successive (palynological) assemblages". The overall assemblages indicate gross ecology and age but when resolved into phases and sub phases, reflect changes in ecologic parameters during relatively shorter time slices. Qualitative and quantitative compositional characteristics of the palynologic assemblage are important aspects of the "phases" and these are employed for age dating and deducing palaeoenvironments. The concept of phase also helps in bringing out minor changes in palaeoenvironments. Brugman (1986, p. 34), however, opines that "the phases are primarily based on quantitative data concerning (land derived) spores and pollen grains. The phases

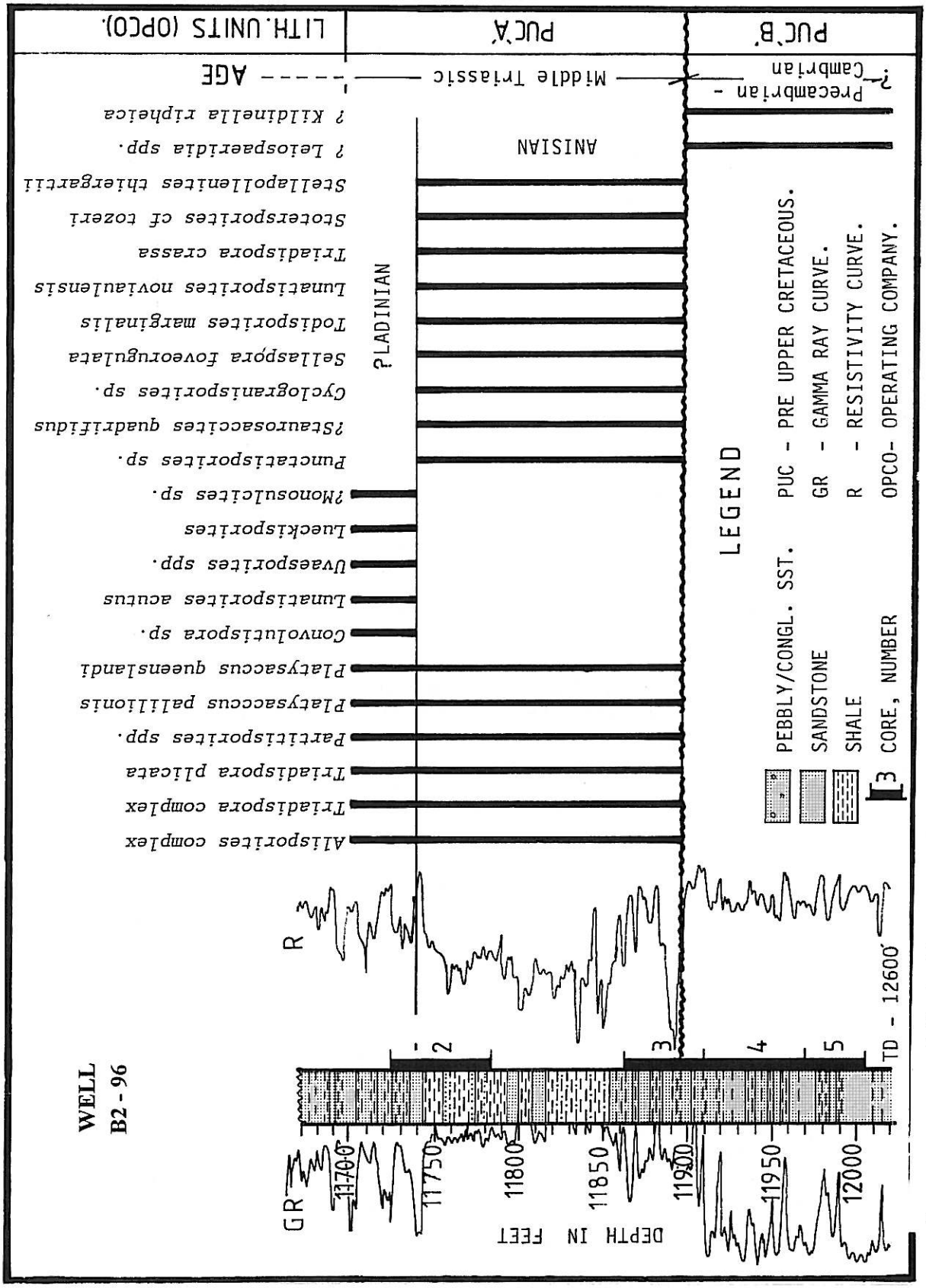


Fig. 3. Palynofossils in cores from Triassic & older sequence, Maradah Trough, Sirt Basin, Libya.

reflect the inter-regional floral development and are considered to be indepenent of local environmental gradients. Their characters, may in time, provide a basis for a regional scheme of differentially diagnosed palynological assemblage zones."

Regional changes in ecology are dependent upon tectonic, physicochemical and climatic conditions. All of these effect sedimentation. Variations in phases may be gradual or sudden. All the transitional ecologic regimes may be present or a few may be absent due to changes in geomorphotectonic attributes prevailing in the provenance and the depositional areas. Thus, it may be possible to relate the presence or otherwise or type of "phases" to local and regional tectonic and ecologic conditions attending evolution of the sedimentary pile. Visscher and Van der Zwan (1981) proposed fifteen categories of readily recognisable and environmentally sensitive groups of spores and pollen grains on basis of a study of coals and evaporites. Categories 'A' to 'G' are regarded hygrophytic whereas, 'K' to 'O' reflect xerophytic affinities. The status of categories 'H', 'I' and 'J' is either indifferent, indeterminate or unknown.

The assemblage of palynofossils from PUC 'B', dated as ?Pre-Cambrian–Cambrian is poor and scarce and inadequate for resolution into phases. The assemblage from PUC 'A', dated as Middle Triassic, is relatively richer. It is resoluble into broadly two phases. The older, corresponding to Anisian, is referable to the *thiergartii–vincetinense* phase (Fig. 2). This assemblage is comparable to that of the Anisian recognised in the nearby L4-96 and is compositionally similar to that established in the Alpine Anisian of Italy and Hungary (Brugman and Visscher, 1988 and Brugman, 1986). The taxa are fairly similar to those of the categories 'B'-'G' and include pollens of *Leavigatosporites* sp., *Aratrisporites* sp. and *Cycadopites* sp. These are regarded hygrophytic (Visscher and Van der Zwan, 1981). A very few forms of categories 'K', 'L' and 'O' of xerophytic affinities also are present. The younger phase with a palynofossil assemblage referable to ?Ladinian age exhibits close affinities to *plurianulatus – novimundanus* phase. Its taxa, which include *Lunatisporites* sp., *Triadispora* sp. and *Stellapollenites* sp., seem referable to the categories K-O. A few representing categories B, C, E and G also are present. It may be thus observed that this phase includes a mixed assemblage of hygrophytic and xerophytic types. It is thus evident that the hygrophytic elements indicating humid environments thrived during the Anisian. These were taken over by relatively drier and mixed types during the ?Ladinian as may be inferred from the considerable presence of xerophytic categories (K, L and O) along with those of hygrophytic habitat.

Palaeovegetation

The palaeovegetation appears to have been fairly varied. Presence of *Platysaccus* sp. and *Alisporites* sp. (Pteridosperms or seed ferns) indicate prevalence of coniferous vegetation (Clement–Westerhof, 1974; Al Ameri, 1990 and Baldoni, 1991). *Aratrisporites* sp., could have been contributed by shrubby Lycopsida plants. *Cycadeles/Bennettitales* also seem to have been present.

Palaeoenvironment

The data available from the PUC 'B' sequence is largely inconclusive. The sedimentary succession dominated by the quartz-arenites with scarce to rare levels of shales has till date not yielded any palynofossils or fossil fauna diagnostic or indicative of marine or transitional environments. The gross characteristics, such as, grain size, overall composition, traces of fresh feldspars, detrital micaceous content, presence of oxidised–mottled shales, micaceous siltstones, normal graded bedding, planar cross bedding and interlaminated arenites and shales seem to indicate non-marine environments and possible prevalence of colder climates.

PUC 'A' sequence is lithologically more heterogenous. Shales are relatively very common. The overall lithologic suite and palynologic as well as fossil faunal assemblage indicate deposition under largely non-marine environments as is suggested by the presence of oxidised, mottled and variegated shales, detrital micaceous content carbonaceous-coaly matter, at times microconglomeratic contents in arenites, arenite-shale interlaminations, slumps, frequent alternations of very coarse and fine grained arenites and graded bedding etc. The more conclusive evidences for prevalence of non-marine environments, however, are offered by the palynofossils (Fig. 3; Appendix I) and presence of pyritized plant remains. This is further supported by the occurrence of branchiopods, fossil fish scales and fish tooth. The branchiopods, especially the *Lioesthria* sp., "probably indicate a non-marine environment such as presence of fresh water ponds or saline lakes" (M.C. Keen, personal communication 1993).

Occurrences, though rare, of *Veryhachium* sp. and *Microhystridium* sp. at a few levels seem to suggest occasional prevalence of some marine influence, or these few acritarchs are reworked older material.

Provenance

The sandstones of PUC 'B' and PUC 'A' comprise mainly strained quartz. Feldspars are very rare and those present are usually fresh and include alkali feldspars. The detritus, in general, is subrounded and

moderately sorted. Chert and meta quartzite, quartz-schist, argillite and orthoquartzite rock fragments are present. The heavy mineral suite mainly comprises stable minerals, such as zircon, tourmaline, rutile and sphene and some of these are distinctly recycled. All these characteristics indicate that these sandstones were derived from acid igneous and low grade quartz rich metamorphic rocks fairly deficient in feldspars. Presence of recycled grains suggests derivation from sedimentary rocks. The basement met at Rakb High (Fig. 1) comprises mainly quartz rich granites and in all probability, it contributed most of the detritus. Contributions from the Amal Platform region cannot be ruled out.

The presence of recycled grains of quartz, zircon, rutile and tourmaline bespeak significant contributions from pre-existing older sedimentaries, such as Gargaf Quartzite, Amal Sandstone and even the quartz-arenites of PUC 'B' sequence. This is further evidenced by presence of reworked Palaeozoic palynomorphs such as *Dactylofusa* sp., *Multiplicisphaeridium* sp., *Apiculiretusisporites* sp., *Cymatiosphaera* sp., *Dictyotidium* sp., *Leiofusa* sp., *Retusotriletes* sp., *Hymenozonotriletes* sp., *Dibolisporites* sp., *Verricosisporites* sp., and *Calyptosporites* sp. etc. (Bindra Thusu, personal communication–1993, Thusu, 1993).

CONCLUSIONS

1. The thick sandstone sequence, met in the subsurface of Maradah Trough and classified into Pre-Upper Cretaceous (PUC) 'B' and 'A' units comprises mainly quartz-arenites with subordinate shales and siltstones . The PUC 'A' sequence is classified into four units on basis of lithologic variations and log characters. Each of the four units significantly thickens towards the Rakb High adjoining the western margins of Maradah Trough.

2. The PUC 'B' unit is tentatively dated as Precambrian to Cambrian and the PUC 'A' unit is inferred to be of Middle Triassic (Anisian and ?Ladinian) age on basis of palynofossils.

3. The PUC 'B' sandstones seem largely non-marine. They may also include some fluvioglacial deposits. In general, the PUC 'A' sequence evolved under largely non-marine environments possibly with occasional mild marine influence towards the eastern parts of Maradah Trough. The palaeoclimates were mainly hygrophytic during the Anisian but changed to mixed hygrophytic-xerophytic during the ?Ladinian.

4. The Maradah Trough was assymetrically active with enhanced negative tectonism along the fault separating it from the Rakb High during evolution of the Middle Triassic sequence.

5. The provenance for arenites of PUC 'B' and 'A' units largely comprised feldspar deficient acid igneous and low grade quartzose metamorphic rocks. Contributions from recycling of pre-existing older sedimentaries, which might include Gargaf Quartzite, Amal Sanstone and even the quartz-arenites of PUC 'B' sequence, are significantly displayed by the arenites of PUC 'A' sequence.

ACKNOWLEDGEMENT

The authors are grateful to Mr. M. Idris, General Manager, and Mr. El Bakai and Mr. Salem Suleiman, Supervisors, Petroleum Research Centre, for help and permission to publish, to Dr. M.C. Keen, Glasgow University, U.K., for identification of fossil faunal assemblages in core samples from wells B2 and B3-96 and to Drs. M. Busrewil, M. Salem and A. Sbeta, Professors, Department of Geology, University of Al Fateh, Tripoli, Libya, for valuable comments. Thanks are due to Mr. Khalifa Shebani, for the well logs and samples.

APPENDIX 1

Selected palynofossils in PUC 'B' and PUC 'A' sequences, Maradah Trough, Sirt Basin, Libya.

Palynomorphs are arranged according to their *principal* distinguishing features.

Pre-Upper Cretaceous 'A' sequence
Azonate smooth trilete spores.

Leavigate.
Calamospora spp.
Punctatisporites ssp.
Deltoidospora spp.
Concavispora sp.
Todisporites marginalis.

Muronati.
Cyclotriletes–Convulutispora complex
Convolutispora spp.
Uvaesporites spp.
?Sellospora rugoverrucata.

Smooth monolete spores.
Laevigatosporites spp.

Sculptured monolete spores.
Aratrisporites spp.

Monosaccoid pollen.
Ovalipollis pseudoalatus
Stellapollenites thiergartii

Alete bisaccoid pollen.
?Voltziaceaesporites heteromorphus
Alisporites–Falcisporites complex
Platysaccus papilionis

Platysaccus queenslandi
Vitreisporites pallidus

Monolete, dilete and trilete bisaccoid pollen.
Argustisulcites grandis
Triadispora crassa
Triadispora plicata

Teaniate bisaccoid pollen.
Teaniate bisaccoid pollen
Lunatisporites noviaulensis

Asaccate
Inaperturate pollen.
Partitisporites novimundanus morphon

Colpate pollen.
Enzonalasporites ssp.
Cycadopites spp.
Monosulcites spp.

Acritarchs
Micrhystridium spp.
Veryhachium spp.

Miscellaneous
Cyanophytic tubes.

Pre-Upper Cretaceous 'B' sequence
?Leiosphaeridia spp.
?Kildinella ripheica.

REFERENCES

Adloff, M.-C., Massa, D. and Vachard, D., 1986. Trias de Tripolitaine (Libye). Nouvelles donnés biostratigraphiques et palynologiques. *Rev Inst. Fr. Petrole*, **41**, 27–72.

Al-Ameri, T.K., 1990. Palynological evidence for Middle Triassic age, palaeoenvironments and sedimentary provenance of sediments in Bore-hole 5/8, Western Iraq Desert. *Rev. Palaeobot. Palynol.*, **65**, 267–274.

Bacelle, L., and Bosellini, A., 1965. Diagramme per la stima visiva della composizione percentule nell rocce sedimentarie. Ann. Univ. di Ferrara, N.S., *Sez IX. Sci. Geol. Palaeont.* **1**, (3), 59–62.

Baldoni, A.M., 1992. Palynology of the Lower Leftpan Formation (Upper Cretaceous) of Barranca de Los Perros Chubut Province, Argentina, Part I – Crytogam spores and gymnosperm pollen. *Palynology*, **16**, 117–136.

Banerjee, S., 1980. *Stratigraphic Lexicon of Libya. Ind. Res. Cent.*, Tripoli, 300 P.

Barr, F.T., and Weegar, A.A., 1972. *Stratigraphic Nomenclature of Sirte Basin, Libya. Petrol. Explor. Soc. Libya*, 179 P.

Baudet, D. 1988 Precambrian palynomorphs from northeast Libya In: El Arnauti A., Owers, B. and Thusu, B. (eds), *Subsurface Palynostratigraphy of Northeast Libya.* Garyounis University Publication Benghazi, Libya, 17–27.

Bellini, E., and Massa, D., 1980. A stratigraphic contribution to the Palaeozoic of the southern basins of Libya. In: Salem, M.J. and Busrewil, M.T. (eds), *The Geology of Libya*, London Academic Press, **II**, 3–56.

Brugman, W.A., 1986. A *Palynological Characterisation of the Upper Scythian and Anisian of the Transdanubian Central(Hungary) and the Vincentinian* Alps(Italy). Thesis University of Utrecht (unpublished).

Brugman, W.A., Eggink, J.W., and Visscher, H., 1985. Middle Triassic (Anisian-Ladinian) palynomorphs. *J. Micropalaeontology* **4**, 107–112.

Brugman, W.A. and H. Visscher, 1988. Permian and Triassic palynostratigraphy of northeast Libya. In: El Arnauti, A., Owens, B. and Thusu, B. (eds), *Subsurface Palynostratigraphy of Northeast Libya*, Garyounis University Publications, Benghazi, 157–171.

Clement-Westerhof, J.A., 1974. In *situ* pollen from gymnospermous cones from the Upper Permian of the Italian Alps – a preliminary account. *Rev. Palaeobot. Palynol.*, **17**, 63–73.

Eem, J.G.L.A. van der, 1982. *Palynological Investigations in the Ladinian and Lower Karnian of the Western Dolomites, Italy.* Thesis University of Utrecht, The Netherlands (unpublished).

Geochem, 1980. *Source Rock Evaluation Reference Manual.* Geochem Laboratories, U.K.

Gilbert, C.M., 1949. Cementation of some California Tertiary reservoir sands. *J. Geol.* **57**, 1–17.

Gilbert, C.M., 1954. Sedimentary Rocks, In: *Petrography* (Edited by Williams, H., Turner, T.J. and Gilbert, C.M.). San Francisco, W.H. Freeman & Co. 251–384.

Karr, R.K., Kieser, G., and Jain, K.P.., 1972. Permo-Triassic subsurface palynology from Libya. *Pollen et Spores*, **XIV** (4), 389–453.

Krumbein, W.C., 1941. Measurement and geologic significance of shape and roundness of sedimentary particles. *J. Sediment. Petrology* **11**, 64–72.

Massa, D., and Delort, T., 1984. Evolution du bassin de Syrte (Libye) du Cambrien au Cretace basal. *Bull. Soc. Geol. Fr.* **XXVI** (6), 1087–1096.

Mouzughi, A.J. and Taleb, 1981. Tectonic elements of Libya (1:2.000.000). National Oil Corporation of Libya.

Roberts, J.M., 1970. Amal Field, Libya In: Halbouty, M.T. (ed.) Geology of Giant Petroleum Fields. *Mem. Am. Assoc. Petrol. Geol.*, **14**, 438–448.

Schurman, W.M.L., 1977. Aspects of Late Triassic palynology. 2. Palynology of the "Gres et Schiste à Avicula contorta" and "Argilles de Levaillois" (Rhaetian) of northeastern France and southern Luxemburg. *Rev. Palaeobot. Palynol.* **23**, 159–253.

Siever, R., 1959. Petrology and geochemistry of silica cemented sandstones in some Pennsylvanian sandstones In: Silica in sediments. *Soc. Econ. Palaeon. Min.*, Special Publication no. **7**, 55–79.

Staplin, F.L., 1969. Sedimentary organic matter, organic metamorphism and oil and gas occurrence. *Bull. Can. Soc. Petrol. Geol.*, **17**, 47–66.

Taylor, J.M., 1950. Pore space reduction in sandstones. *Bull. Am. Assoc. Petrol. Geol.* **34**, 701–717.

Terry, R.D., and Chillinger, G.V., 1955. Summary of "Concerning some additional aids in studying sedimentary formations by M.S. Shvestov". *J. Sediment. Petrology*, **25**, 229–234.

Thompson, A., 1959. Pressure solution and porosity. In: Silica in sediments. *Soc. Econ. Palaeont. Min.*, Special Publication. no. 7, 72–110.

Thusu, B., 1993. Implication of the discovery of reworked and in-*situ* Late Palaeozoic and Triassic palynomorphs on the evolution of Sirt Basin, Libya. 1st Symposium of Sedimentary Basins of Libya. (Geology of Sirt Basin), Tripoli, Libya. (Abstract). p. 40.

Thusu, B., Van der Eem, J.G.L.A., El Mehdawi, A., and Bu-Argoub, F., 1988. Jurassic – Early Cretaceous Palynostratigraphy in northeast Libya. In: El Arnauti A., Owens B. and Thusu B., (eds) *Subsurface Palynostratigraphy of Northeast Libya.* Garyounis University Publications, Benghazi, 171–214.

Van der Zwan, C.J., 1980. Aspects of Late Devonian and Early Carboniferous palynology of Southern Ireland. 2 Palynology of Devonian-Carboniferous transition sequences with special reference to the Bantry Bay area, Co. Cork. *Rev. Palaeobot. Palynol.*, **30**, 165–286.

Visscher, H., and Van der Zwan, C.J., 1981. Palynology of the Circum Mediterranean Triassic. Phytogeographical and Palaeoclimatological implications. *Geol. Rundschau.*, **70**, 625–634.

PRJ, Vol. 8 (January 1996); P. 61–66, 4 FIGS, 1 TABLE.

Models for the Hydrogen-bonded Water Molecules to the Chemisorbed Oxyhydroxyl Layer on the Chromium Surface

A.S. Al-Taie*

نماذج إرتباط جزئيات الماء على طبقة الأوكسي هيدروكسيل الممتزة كيميائياً على سطح الكروميوم

علي سلمان الطائي

لقد إستعمل المطياف الضوئي الألكتروني الحديث لدراسة حزم الإنبعاث الألكتروني بواسطة الأشعة السينية وفوق البنفسجية في الفراغ الخارق المنبعث من تعرض سطح الكروميوم النظيف إلى بخار الماء أولاً ، وسطح الكروميوم المعرض إلى الأوكسجين مسبقاً ثم إلى بخار الماء ثانياً في درجات حرارة تتراوح بين 80 K إلى 623 K

في المراحل الأولى للإمتزاز وجد أن جزئيات بخار الماء تتفكك حال إمتزازها على الطبقة الأولى لذرات السطح مكونة طبقة من الأوكسي هيدروكسيل وجزيئات الماء المتأصرة تناسقياً من خلال ذرات الأوكسجين على المراكز غير المشبعة للسطح .

أما جزئيات بخار الماء فانها تمتز فيزيائياً عند تعرض السطح لأكثر من طبقة من خلال تكون أواصر هيدروجينية مع طبقة الأوكسي هيدروكسيل الممتزة كيميائياً .

فسرت نتائج هذه الدراسة باقتراح ميكانيكية ونماذج لجزئيات الماء الممتزة بواسطة أواصر هيدروجينية على طبقة الأوكسي هيدروكسيل بين درجات حرارة تتراوح بين 80 K و 298 K .

Abstract *XPS and UPS Photoelectron Spectroscopy techniques (Anoble ESCA-5 Spectrometer which permit pressure from* 1–10^{-11} Torr*) have been used to investigate water vapour interaction with clean and pre-oxygen exposed chromium surface in the temperature range* 80–623 k.

Initially at low exposure ($\sigma <$ monolayer), the interaction of water vapour with clean chromium surface is dissociative at active site of chromium atoms through the formation of an adsorbed oxyhydroxyl layer together with molecular water which is coordinately bonded to the unsaturated site, via the oxygen which strongly held.

The second layer which represents the physically adsorbed layer occurs at higher than one monolayer coverage through water molecules hydrogen bonded to the chemisorbed oxyhydroxyl layer. Models and the mechanism of the dehydroxylation of this layer when the exposed surface warmed to room temperature, have been suggested by the monitoring of the XPS and UPS spectra.

INTRODUCTION

The interaction of water vapour with clean metal surfaces has been studied and characterized by XPS and UPS in the past decade and the behaviour of the interaction can be summarized in general by three categories.

Firstly, molecular adsorption at low temperature takes place with no evidence for any interaction at room temperature.[1-5] Secondly, dissociative adsorption at room temperature gives chemisorbed oxygen and molecularly adsorbed water. In the third category dissociation of the water, molecule is only partial and surface hydroxyl species dominates.[6-11]

In each case of these studies, the oxygen species

*Department of Chemical Engineering, Al-Fateh University P.O. Box 13589, Tripoli, G.S.P.L.A.J.

with $O_{(1s)}$ binding energy between that of chemisorbed oxygen and adsorbed water molecules was assigned to the hydroxyl groups.

In this work, the Photoelectron spectroscopy (XPS) was used to determine surface concentrations of oxygen, hydroxyl and water molecules through monitoring the $O_{(1s)}$ spectral regions, while the (UPS) provided information about the nature of the bonding of the adspecies to the substrate.

Experimental

Spectra from polycrystalline chromium surface were obtained by using a Vacuum Generators model ESCA-5 Spectrometer, fitted with a VGQ7 mass spectrometer for use in monitoring the gas phase[12] during evacuation and thermal treatment. Details of the spectrometer, sample preparation mounting base pressures and operating conditions together with data quantification can be found in previous publications.[13-15]

Fig. 1 shows a series of $He_{(1)}$ spectra for various exposure of H_2O-vapour to clean surface at 80 K, then subsequent heating of the substrate to 623 K,

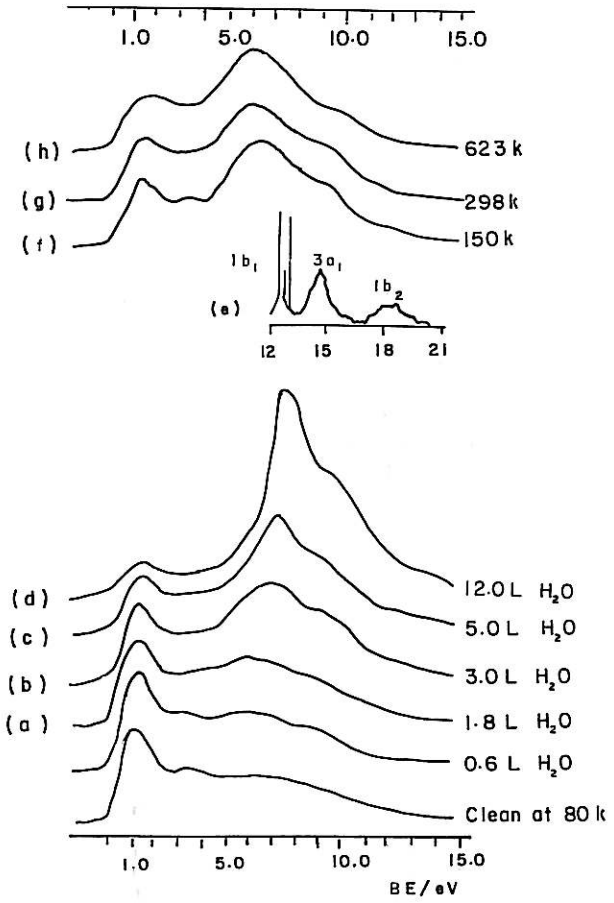


Fig. 1. $He_{(1)}$ spectra for the interaction of H_2O–vapour with a clean chromium surface at 80 k together with the gas phase spectrum of H_2O, and subsequent heating the adlayer to 623 k.

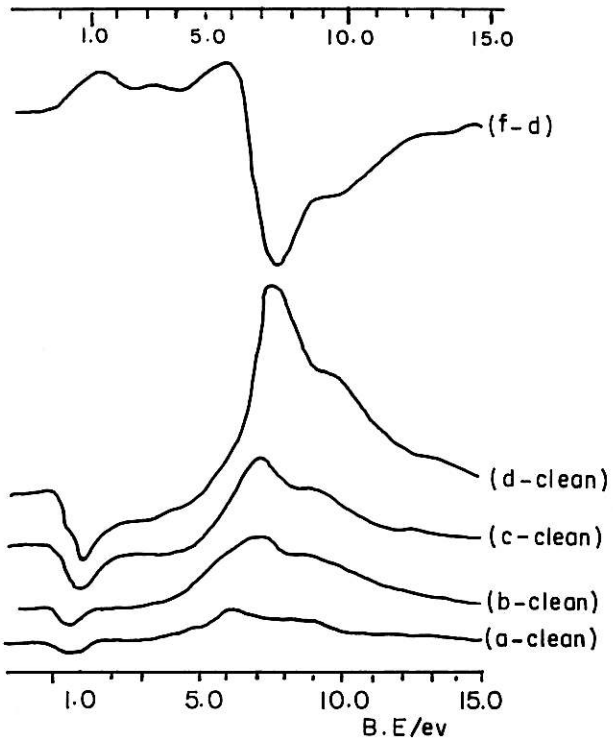


Fig. 2. Shows some of the difference spectra corresponding to figure 1.

together with the gas phase,[12] while Fig. 2 shows some of the difference spectra corresponding to Fig. 1.

The three valence orbitals of the H_2O molecules are $1b_1$, $3a_1$ and $1b_2$, the $1b_2$ provides the bonds between the hydrogen and oxygen holding the molecule together while the $3a_1$ bond between the two hydrogens gives the water about 109° bend,[12] and the $1b_1$ is the non-bonding oxygen orbital of pure 2p character.

The clean surface exhibits an intense band at about 1.0 ev with a second weak feature at 2.5 ev below the fermi level from the 3d level.

Slight changes in the $He_{(1)}$ spectra due to initial interaction of water vapour with clean surface are first observed, which resulted in the development of bands at 5.5 and 9.0 ev figure 1 and clearly in the corresponding difference spectrum (a-clean) Fig. 2.

On increasing the exposure, a more intense band at about 7.0 ev developed with increase of intensity and width of the band at 9.0 ev, at the same time the band at 5.5 ev is still seen from the profile of the 7.0 ev to lower binding energy. With more addition of water vapour, the band at 7.0 ev becomes narrower and is shifted to 7.3 ev and at the same time a weak third band emerged at 13.0 ev with the attenuation of the d-band.

From the difference spectra and by comparison with the gas phase spectrum, there are three regions, 4.5 to 5.5, 6 to 9.0 and 9 to 13.0 ev. The 4.5 to 5.5 ev region is assigned to emission from the $0_{(2p)}$ orbital of the chemisorbed oxygen from observations of the

interaction of clean chromium with oxygen.[15] The second region 6.0 to 9.0 ev is composite, being made up to emission from the $O_{(2p)}$ surface hydroxyl and the $1b_1$ orbital of molecularly adsorbed water at about 7.3 ev,[16-18] and the third region which is also composite, is made up of emission from the hydroxyl (at 9.5 ev) and emission from the $3a_1$ orbital of molecularly adsorbed water at 13.0 ev.

DISCUSSION

Initially, at low exposure ($\sigma <$ monolayer), the interaction of H_2O-vapour with clean surface is dissociative at the active site of chromium atoms through the formation of an adsorbed oxyhydroxyl layer, together with molecular water which is coordinately bonded to the unsaturated sites via the oxygen atom which is strongly held.

The curve-fitting $O_{(1s)}$ spectral region shows three components peaks at 530.1 (due to chemisorbed oxygen), 531.7 (due to chemisorbed hydroxyl species), and 533.5 ev (due to molecular water) respectively.

The $He_{(1)}$ spectra corresponding to this range of coverage shows a band mainly in regions one and two as shown in Fig. 1(a,b), and the difference spectra (a-clean) (b-clean) in Fig. 2, which mainly shows the band due to chemisorbed oxygen atoms (O_{2p}) and chemisorbed hydroxyl species,[16-18] whereas the $1b_2$ orbital from the molecularly adsorbed water in the third region is very weak indicating that water molecule does not have its integrity on the surface with this range of exposure.

The second layer which represents the physically adsorbed layer occurs at higher than one monolayer coverage through water molecules hydrogen bonded to the chemisorbed oxyhydroxyl layer which cannot be distinguished from the OH species of the chemisorbed layer by XPS or UPS techniques (strong hydrogen bonding interaction $O^{\delta}.....H-OH$). This occurs at low temperature between molecularly adsorbed water and surface oxygen.[1,19]

The second type of physical adsorption is represented by H_2O – molecules which are hydrogen bonded to the chemisorbed layer through hydrogen atoms and weakly bonded to the surface through oxygen atom. These two types of physical adsorption may be illustrated by models (1) and (2) respectively.

On increasing the coverage ($\sigma = 2.6$) the main changes are the increase in the intensity of $O_{(1s)}$ at 533.5 ev with a shift in the B.E. to 534.0 ev, the $He_{(1)}$ spectrum, Fig. 1 and 2 shows the bands of the condensed molecular water at about 7.3, 9.5 and 13.0 ev respectively.

As the adlayer is warmed to 150 k, most of the $O_{(1s)}$ intensity at 534.0 ev disappears with a shift to 533.5 ev and a little increase in the intensity of $O_{(1s)}$ at 530.1 and 531.7 ev, with a total concentration of oxygen adlayer left on the surface 2.1×10^{15} atom. cm^{-2} ($\sigma = 1.3$).

The corresponding $He_{(1)}$ spectrum showed disappearance of the molecular orbitals from regions two and three with a shift in the bands of $1b_1$ and $3a_1$ at 7.3 and 9.5 ev to lower binding energy and much wider than before, with gained intensity at 5.5 ev. The layer which is desorbed at 150 k represents the condensed water.[20]

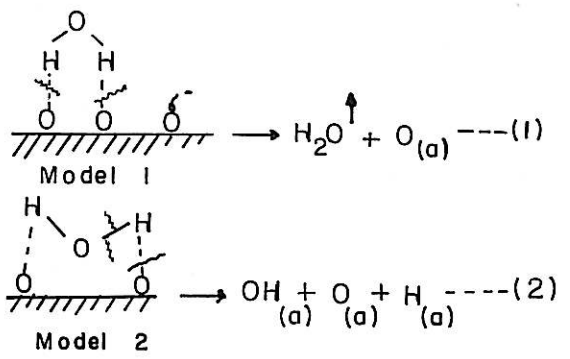
On further warming the substrate to R.T. 298.0 K the intensity of the $O_{(1s)}$ at 530.1 ev increased by half what is lost from the intensity at 531.7 and 533.5 ev respectively (Table 1).

Table 1. Surface concentrations of chemisorbed oxygen, hydroxide and water from the curve-fitted data of XPS-spectra

Treatment	$\sigma \times 10^{-15}$ *of* $O_{(1s)}$ *chemisorbed hydroxide*	$\sigma \times 10^{-15}$ *of chemisorbed hydroxide*	$\sigma \times 10^{-15}$ *of water*
1.8 L H_2O at 80 k	0.070	0.120	0.123
3 L H_2O at 80 k	0.080	0.480	0.590
6 L H_2O at 80 k	0.20	0.650	1.270
12 L H_2O at 80 k	0.160	1.050	2.982
Warmed to 150 k	0.360	1.360	0.441
Warmed to 210 k	0.540	0.970	0.237
Warmed to 298 k	0.880	0.640	0.120
Warmed to 623 k	1.410	0.170	0.075
30 L H_2O on clean at 298 k	0.500	0.20	—
400 L H_2O at 298 k	1.110	0.50	0.219
Heated to 623 k	1.390	0.27	0.154
Addition of 750 L H_2O over at 298 k	1.390	0.627	0.430
12 L O_2 clean at 298 k	1.50	—	—
12 L H_2O at 298 k	1.120	0.834	0.149
3672 L H_2O at 298 k	1.150	1.05	0.285
Heated to 623 k	1.870	0.282	0.112

The suggested explanation of this observation may be by dehydroxylation through the breaking of hydrogen bonding to desorb water molecules and addition of chemisorbed oxygen atoms to the surface (model 1), through the breaking of oxygen hydrogen bond and hydrogen bond toward the chemisorbed oxygen to form chemisorbed hydroxyls on the surface, chemisorbed oxygen atoms and hydrogen atoms (model 2).

During the heating of the substrate from 298 to 623 k, the decrease in the concentrations of hydroxide and H_2O species at 531.7 and 533.5 ev is paralleled by an increase in the chemisorbed oxygen component at 530.1 ev, which clearly indicated that the decomposition proceeds through the dehydroxylation of chemisorbed hydroxide and dehydrogenation of the coordinative water molecule, the suggested mechanism is:



$$H_2O_{(a)} \rightarrow H_2O\uparrow + O_{(a)} \quad ---(1)$$

$$OH_{(a)} + O_{(a)} + H_{(a)} \quad ----(2)$$

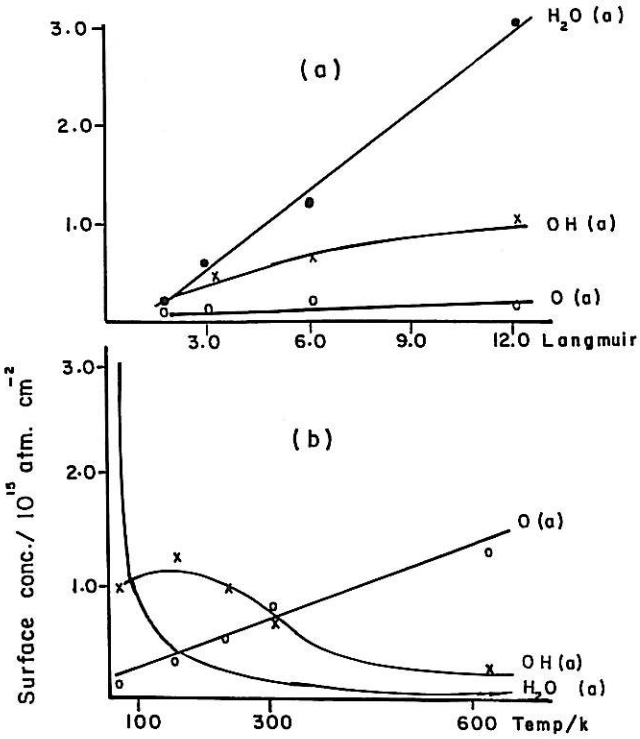


Fig. 3. Shows the variation of (α) oxygen species, $O_{(a)}$ and $H_2O_{(a)}$ concentrations with the exposure at 80 k, (b) $O_{(a)}$ $OH_{(a)}$ and $H_2O_{(a)}$ with temperature of the substrate.

$$OH_{(a)} \rightarrow O_{(b)} + \tfrac{1}{2}H_{2(g)}, \quad (3)$$

$$H_2O_{(a)} \rightarrow O_{(b)} + H_{2(g)}. \quad (4)$$

We assigned $O_{(b)}$ on the basis of the core level investigation, which shows that the bulk oxidation started at *R.* Temperature and no bulk oxidation below that temperature.

The hydrogen adatoms may be subsequently recombining and desorbing as molecular hydrogen,[18] where the dehydroxylation takes place above room temperature through desorption of hydrogen gas.[4]

When the clean surface is exposed to H_2O-vapour at room temperature, the $O_{(1s)}$ spectral region after about half monolayer exposure, shows two wide components (from curve-Fit) with about 0.5 ev shift to higher binding energy, and the corresponding $He_{(1)}$ spectrum shows a development of three bands, when the up-take increase in one monolayer coverage the $O_{(1s)}$ component at 534.5 ev increases with a comparable increase in the intensity of the other components at 530.5 and 532.3 ev, respectively.

From these observations, the interaction of H_2O vapour with a clean surface at 298 k occurs by initial dissociation of water to chemisorbed oxygen atoms, followed by hydroxide and the water to form a layer of chemisorbed species, with higher concentration of chemisorbed oxygen atom on the surface than that at 80 k interaction.

On heating the substrate to 623 k, the mechanism of the activation is through the dehydroxylation and dehydrogenation of the hydroxyls and coordinative water molecules as mentioned before.

When this surface is cooled to 298 k, the addition of water vapour resulted in dissociation to hydroxyl and coordinative water adsorption without any change in the concentration of the $O_{(b)}$ at 530.1 ev. This confirmed that during the heating of the adlayer regeneration of the active metallic surface sites by incorporation of the chemisorbed oxygen atoms in to the bulk occurs and the adsorption of water vapour at 298 k leads to dissociation to hydroxyls and coordinative bonding water on the metallic site.

When the clean surface is pre-oxygen exposed at 298 k (σ = one monolayer), and then followed by H_2O-vapour, surface hydroxylation takes place and the concentration of the hydroxyls which is formed equal to twice the loss in the concentration of chemisorbed oxygen at low temperature and when the exposure of H_2O-vapour increased to 367 L, there was no change in the concentration of the chemisorbed oxygen and the only change is the increase in the concentration of the hydroxyls and water species. During the heating of the adlayer to 623 k, dehydroxylation occurs through desorption oxygen atoms to the surface (Fig. 4 which shows the desorption features from the hydroxyl and water bands).

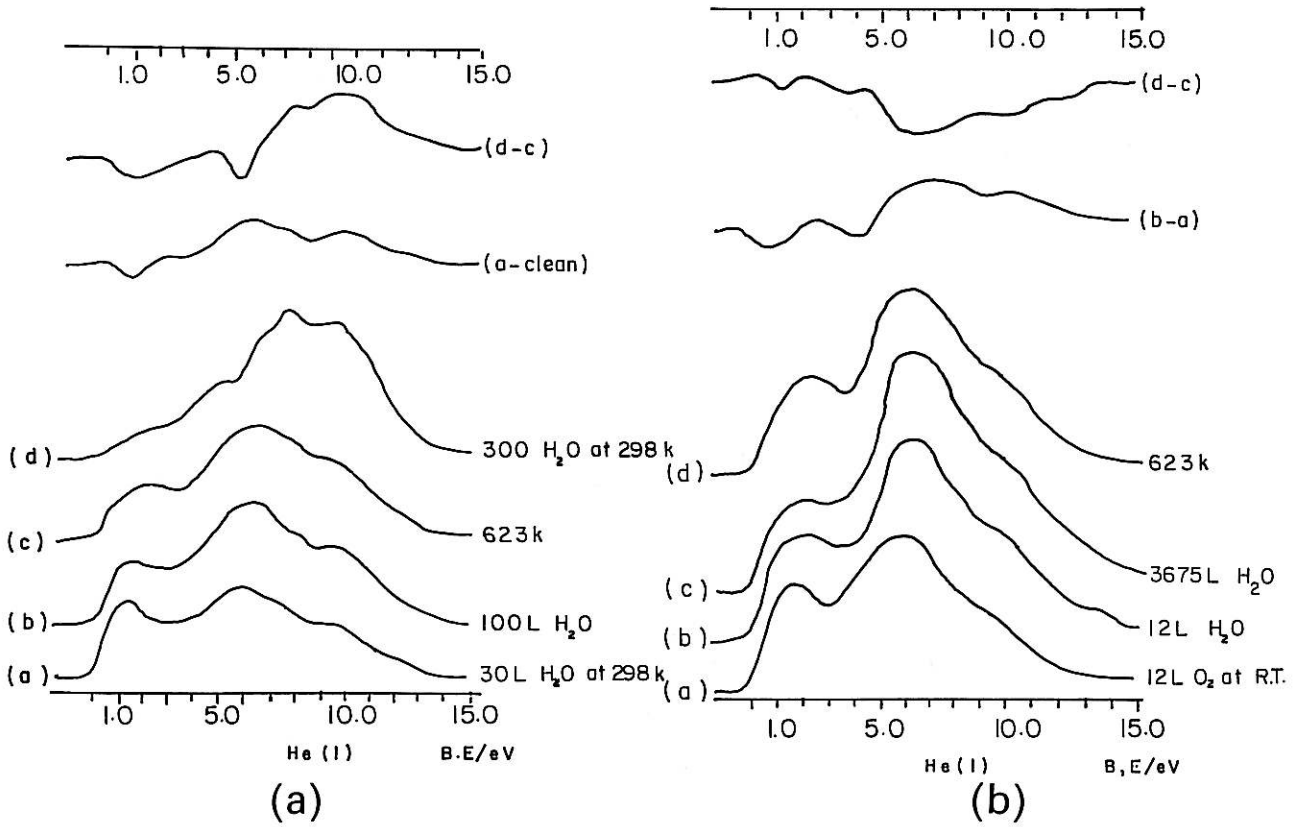


Fig. 4. (a) $He_{(1)}$ spectra for clean chromium surface exposed to H_2O–vapour, then heating the surface to 300L H_2O at 298 k. (b) $He_{(1)}$ for the partial oxidised surface with H_2O – vapour and heated to 623 k.

The suggested mechanism is that the Cr–O surface has active oxygen adatoms that have not developed the ionicity associated with the $Cr-O^{2-}$ bond on the surface (may be chemisorbed oxygen species on the surface) hydroxylated through hydrogen bonding to water molecules which are already coordinated to unsaturated metallic site, or may be decomposition of water molecule into a mixed adlayer of hydrogen atoms and surface hydroxyls on the active site, and then subsequently the hydrogen adatoms bonded to the chemisorbed oxygen adatoms from hydroxyl species; this mechanism can be illustrated by the following equations:

$$O_{(a)} + H_2O \xrightarrow{298\,k} O\ldots\ldots H\text{–}OH, \tag{5}$$

$$H_2O \xrightarrow{\text{active site}} OH_{(a)} + H_{(a)}, \tag{6}$$

$$O_{(a)} + H_{(a)} \rightarrow OH_{(a)}, \tag{7}$$

The dehydroxylation process is:

$$O\ldots\ldots H\text{–}OH_{(a)} \xrightarrow{623\,k} 2O_{(b)} + H_{2(g)}, \tag{8}$$

or

$$2OH_{(a)} \xrightarrow{623\,k} 2O_{(b)} + H_{2(g)}. \tag{9}$$

ACKNOWLEDGEMENT

The author wishes to thank Prof. Roberts, M.W. and Dr. Carely, A.F., of School of Chemistry and Applied Chemistry, University of Wales, Cardiff, U.K. for their helpful and valuable discussions.

REFERENCES

1. Au, C.T., Breza, J. and Roberts, M.W., 1979, *Chem. Phys. Lett.*, **66**, 340.
2. Fisher, G.B. and Fland, J.L., 1980. *Surf. Sci.* **94**, 446.
3. Miller, J.N., Lindau, I. and Spices, W.E., 1981. *Surf Sci.* **111**, 595.
4. Au, C.T., Roberts, M.W. and Zhu, A.R., 1982. *Surf. Sci.* **115**, L 117.
5. Marini, C. and Harn, K., 1983. *Surf. Sci.* **126**, 279.
6. Atkinson, S.j., Brundle, C.R. and Roberts, M.W., 1974. *Faraday Disc. Chem. Soc.* **58**, 62.
7. Norton, P.R., Tapping, R.L. and Goodale; J.W., 1977. *Surf. Sci.* **65**, 13.
8. Roberts, M.W. and Wood, P.R., 1977. *J. Electron Spectros* **11**, 431.
9. Gimzewski, J.K., Affrossman, S., Gibson, M.T., Watson, L.M. and Fabizn, D.J., 1979. *Surf Sc.* **80**, 298.
10. Moyes, R.b. and Roberts, M.W., 1977. *Catalysis* **49**, 216.
11. Padalia, B.D., Gimzewski, J.K., Affrossman, S., Lang, W.C., Watson, L.M. and Fabizn, D.J., 1976. *Surf. Sci.* **61**, 468.
12. Turner, D.W., Baker, C., Baker, A.D. and Brundle, C.R., 1970.

Molecular Photoelectron Spectroscopy, Lond. Wiley interscience.
13. Joyner, R.W., Roberts, M.W. and Yates, K., 1979. *Surf. Sci.* **87**, 501.
14. Roberts, M.W., 1980. *Advnces in Catalysis*, **29**, 55.
15. Al-Taie, Ali, S., 1991. *Iraqi J. of Chem.* **16**(2), 1.
16. Briggs, D., Connor, J.A., considine, M. and Hillier, I.H., 1977. *J. Electron Spectrosc.* **12**, 143.
17. Wachs, I.E., and Kelemen, S.R., 1981. *J. Catal.* **71**, 78.
18. Dwyer, D.J., Kelemen, S.R. and Kalder, A., 1982. *J. Chem. Phys.* **76**, 1832.
19. Zecchina, A., Coluccia, S., Gughielminotti, and Ghiotti, G., 1971. *J. Physical Chemistry* **75**, 2774.
20. Stuve, E.M., Madix, R.J. and Sexton, B.A., 1981. *Surf. Sci.* **111**, 11.

PRJ, Vol. 8 (January 1996); P. 67–73, 3 FIGS, 11 TABLES.

Evaluation of Sedra and Hamada Crude Oils for Manufacturing of Lube Base Stocks

Iftikhar Ahmad*, Adel Tuwil* and Salem Debbah*

تقييم خام السدرة والحمادة لتصنيع زيوت التزييت الأساسية

أفتخار أحمد ، عادل الطويل و سالم الدباح

تم إجراء عملية تقييم لزيوت الأساس لخامي نفط السدرة والحمادة من ناحية النوعية والكمية حيث تم تحضير وتقييم المتبقى عند الضغط الجوي العادي ($340^{+0}C$) بهدف الحصول على زيوت الأساس ذات التصنيفات المختلفة ، كما تم إجراء عملية تقطير أخرى للمتبقى ($340^{+0}C$) عند الضغط المخلخل والحصول على تسع قطفات لزيوت الأساس ذات مدى حراري مختلف. تم مقارنة خامي السدرة والحمادة من حيث مدى احتوائها على زيوت الأساس من الناحية الكمية والنوعية للقطفات قبل وبعد عملية نزع الشمع والمواد العطرية منها بغرض استخدامها للحصول على زيوت الأساس ، وتعرض هذه الورقة أيضاً إمكانية استخدام زيوت الأساس لخامي السدرة والحمادة.

Abstract *The potential of production of lube base stocks of Sedra and Hamada crude oils has been assessed both in terms of quality and quantity. Atmospheric residua ($340^{+}°C$) of these crude oils were prepared and evaluated for manufacturing of lube base stocks for different classes. The atmospheric residua ($340^{+}°C$) of these crude oils were further distilled into nine different fractions. The comparative yield and properties of raw cuts, dewaxed cuts and dewaxed-solvent extracted cuts were determined and evaluated for lube base stocks production. Suggestions of possible use of Sedra and Hamada lube base stocks are also presented.*

INTRODUCTION

The lubricant production in Libya is entirely based on imported lube base oils, bulk of which is in the viscosity range of intermediate (N 150, N 250), heavy (N 500) and bright stocks. As a result of this situation an attempt has been made to look into the likely availability of lube base stocks from Hamada and Sedra crude oils both in respect to yield and quality since these crude oils are processed in Az-Zawiyah refinery.

This paper presents comparative yield potential and available viscosity range of base stocks from Sedra and Hamada crude oils. This work also presents views on utilization aspects, based on the current developments in lubricant formulations and application aspects.

EXPERIMENTAL

Experimental work, reported herein, was carried out using Sedra and Hamada crude oil samples obtained from Az-Zawiyah refinery. Physico-chemical data of these crude oils are reported in Table 1. Sedra crude oil has API gravity 35.6 while Hamada crude oil has 40.0 API gravity. The characterization factors (K_{uop}) of Sedra and Hamada crude oils are 12.20 and 12.25, respectively.

Preparation of Atmospheric Residue

The atmospheric residue was prepared by distillation of crude oil through a distillation column, which is conforming to ASTM D2892 method, for atmospheric distillation to remove naphtha, kerosine and

*Petroleum Research Centre P.O. Box 6431, Tripoli, G.S.P.L.A.J.

Table 1. Characteristics of Sedra and Hamada crude oils

Test method	*Test description*	*Result*	
		Sedra crude	*Hamada crude*
ASTM D1298	Specific gravity at 15.6/15.6°C	0.8469	0.8249
ASTM D1298	API gravity	35.6	40.0
ASTM D1796	Water and sediment content	0.1	Traces
ASTM D129	Sulphur content	1.52	0.10
ASTM D97	Pour point, °C	3	−6
ASTM D445	Kinematic viscosity at 37.8°C, cSt	5.36	4.63
IP 143	Asphaltene content, wt.%	0.71	0.46
ASTM D189	Conradson carbon residue, wt.%	2.74	2.09
ASTM D482	Ash content, wt.%	Nil	0.0059
UOP 375	Characterisation factor	12.20	12.25
IP 77	Salt content, ppm	Nil	10.74

gas oil fractions boiling up to 340°C. The left over portion in distillation flask remains as atmospheric residue. The yield of atmospheric residue of Sedra and Hamada crude oils were found to be 50.26, and 48.56 wt.% respectively.

Preparation of Lube Distillate Cuts

Eight distillate cuts ranging from 340 to 550°C and vacuum residue of Sedra and Hamada crude oils were prepared by distillation of corresponding atmospheric residue (340$^+$°C) using a batch distillation apparatus made according to ASTM D1160 method. The position of cuts on composite TBP distillation curve up to 550°C is shown in Fig. 1. The boiling range and yield of these distillate cuts are presented in Table 2. The properties of distillate cuts of Sedra and Hamada crude oils are given in Table 3 and Table 4, respectively.

Deasphalting of Vacuum Residue

The vacuum residue (550$^+$°C) was propane deasphalted using a batch, four litres capacity extractor at

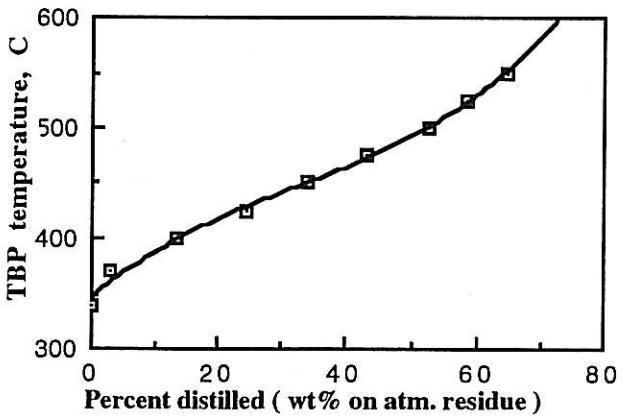


Fig. 1a. TBP distillation curve of sedra crude oil.

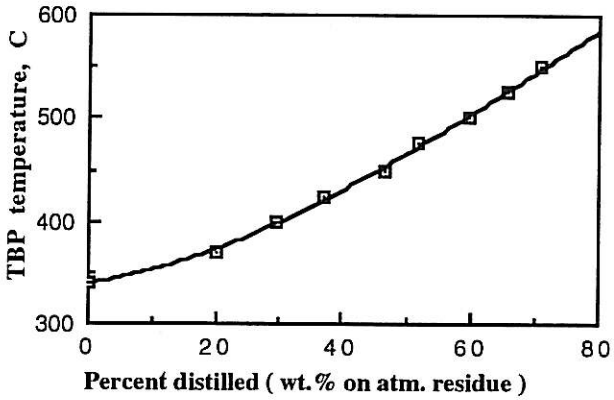


Fig. 1b. TBP distillation curve of Hamada crude oil.

60°C. The ratio of solvent (propane) to oil was used as 5:1 by volume. The deasphalted oil (DAO) was separated from the solvent initially in the extractor and subsequently by evaporation with a nitrogen purge at 150°C. The yield of oil and asphalt was found 11.34 and 23.12 wt.% on atm. residue, respectively for Sedra crude oil while the yield of oil and asphalt for Hamada crude oil was found as 8.28 and 20.69 wt.% on atm. residue, respectively.

Processing of Distillate Cuts and Deasphalted Oils (DAO)

Distillate cuts and deasphalted oils were processed according to the following steps:

Step 1: Dewaxing (to improve the low temperature properties)
Step 2: Solvent extraction (to improve viscosity index and quality)

The above sequence may be altered during the process design.

Dewaxing

A mixture of methyl ethyl ketone (MEK) and toluene in the ratio of 70:30 by volume was used for dewaxing of all distillate cuts. Dewaxing temperature was 12±2°C and the ratio of the solvent to feed was maintained as 3:1 by volume. The chilled solvent was mixed with the preheated feed and cooled to −12°C with agitation. The mixture was allowed to stand for about 2 hours and then filtered using No. 4 sintered glass filter. The wax cake was washed three times with the solvent and the extract was stripped out of the solvent in a rotary vacuum separator. The wax cake was stripped out from the filter and weighed to determine the yield of the slack wax. The yields of oils after dewaxing are reported in Table 2. The properties of dewaxed oils of Hamada and Sedra are given in Tables 5 and 6, respectively.

Table 2: Yields of raw and processed cuts of Hamada and Sedra crude oils

Hamada crude oil				*Sedra crude oil*			
Distillate cuts correspond to atm. distillation (°C)	*Yield on atm. residue (wt.%)*			*Distillate cuts correspond to atm. distillation (°C)*	*Yield on atm. residue (wt.%)*		
	Raw cut	*Dewaxed cut*	*Dewaxed and solvent extracted cut*		*Raw cut*	*Dewaxed cut*	*Dewaxed and solvent extracted cut*
340–370	20.05	18.97	14.24	340–355	2.87	2.53	1.70
370–400	9.55	8.77	5.61	355–395	10.58	8.88	6.36
400–425	7.35	6.64	4.50	395–421	10.82	9.08	5.66
425–450	9.74	8.72	6.10	421–450	9.63	8.03	5.26
450–475	5.15	4.63	3.28	450–475	9.21	7.70	5.23
475–500	7.72	7.02	5.16	475–500	9.49	8.17	5.49
500–525	6.26	5.68	4.35	500–525	5.77	5.01	3.36
525–550	5.21	4.74	3.74	525–550	6.13	5.33	3.54
550+ (deasphalted oil)	8.28	6.83	5.02	550+ (deasphalted oil)	11.34	9.55	7.36

Table 3. Properties of raw distillate cuts of Hamada crude oil

Distillate cuts correspond to atmospheric distillation (°C)	*Specific gravity at 15.6/15.6 °C*	*API gravity*	*Kin. viscosity at 40°C*		*Kin. viscosity at 100°C*		*Pour point (°C)*	*Total sulphur (wt.%)*
			(cSt)	*(SUS)*	*(cSt)*	*(SUS)*		
340–370	0.8588	33.3	8.47	53.6	2.25	33.7	3	0.25
370–400	0.8698	31.2	12.8	69.0	2.96	36.1	12	0.23
400–425	0.8768	29.9	18.4	91.1	3.67	38.4	21	0.28
425–450	0.8833	28.7	29.4	139	4.69	41.7	27	0.34
450–475	0.8916	27.2	86.0	399	8.88	55.4	36	0.39
475–500	0.9004	25.7	—	—	11.5	64.6	39	0.23
500–525	0.9034	25.1	—	—	13.8	73.2	39	0.28
525–550	0.9118	23.7	—	—	19.6	96.8	42	0.30
550+ (deasphalted oil)	0.9415	18.8	—	—	44.8	210	57	0.50

Table 4. Properties of raw distillate cuts of Sedra crude oil

Distillate cuts correspond to atm. distillation (°C)	*Specific gravity at 15.6/15.6 °C*	*API gravity*	*Kin. viscosity at 40°C*		*Kin. viscosity at 100°C*		*Pour point (°C)*	*Total sulphur (wt.%)*
			(cSt)	*(SUS)*	*(cSt)*	*(SUS)*		
340–355	0.8599	33.1	7.93	51.9	2.28	33.8	12	0.57
355–395	0.8709	31.0	12.1	66.4	2.86	35.7	18	0.60
395–421	0.8788	29.5	15.8	80.6	3.46	37.7	27	0.61
421–450	0.8857	28.3	25.7	122	4.52	41.1	30	0.65
450–475	0.8956	26.5	—	—	6.45	47.3	39	0.69
475–500	0.9075	24.4	—	—	9.31	56.8	42	0.72
500–525	0.9175	22.7	—	—	13.4	71.7	45	0.73
525–550	0.9295	20.7	—	—	21.9	107	51	0.81
550+ (deasphalted oil)	0.9318	20.4	—	—	38.4	181	60	—

Table 5. Properties of dewaxed distillate cuts of Hamada crude oil

Distillate cuts correspond to atm. distillation (°C)	*Specific gravity at 15.6/15.6 °C*	*API gravity*	*Kin. viscosity at 40°C*		*Kin. viscosity at 100°C*		*Viscosity index*	*Pour point (°C)*	*Total sulphur (wt.%)*
			(cSt)	*(SUS)*	*(dSt)*	*(SUS)*			
340–370	0.8580	33.4	7.84	51.5	2.18	33.4	71	−6	0.26
370–400	0.8719	30.8	11.9	65.6	2.74	35.3	50	−6	0.27
400–425	0.8831	28.7	20.6	100	3.78	38.7	45	−6	0.29
425–450	0.8921	27.1	34.7	163	4.97	42.6	44	−6	0.31
450–475	0.8987	25.9	61.8	287	7.04	49.2	57	−6	0.31
475–500	0.9073	24.5	129	598	10.8	62.1	52	−6	0.32
500–525	0.9124	23.6	222	1028	15.3	79.1	56	−9	0.34
525–550	0.9185	22.6	419	1941	21.7	106	49	−6	0.36
550+ (deasphalted oil)	0.9239	21.7	1524	—	54.9	257	78	0	0.73

Table 6. Properties of dewaxed distillate cuts of Sedra crude oil

Distillate cuts correspond to distillation (TBP) (°C)	*Specific gravity at 15.6/15.6 °C*	*API gravity*	*Kin. viscosity at 40°C*		*Kin. viscosity at 100°C*		*Viscosity index*	*Pour point (°C)*	*Total sulphur (wt.%)*
			(cSt)	*(SUS)*	*(cSt)*	*(SUS)*			
340–355	0.8709	31.0	8.00	52.1	2.21	33.7	72	−6	0.45
355–395	0.8869	28.0	14.0	73.5	2.97	36.4	38	−6	0.54
395–421	0.8949	26.6	20.0	97.8	3.64	38.6	31	−9	0.64
421–450	0.9028	25.2	30.4	143	4.72	42.1	52	−6	0.68
450–475	0.9128	23.5	65.1	302	7.15	49.9	52	−6	0.73
475–500	0.9198	22.3	112	520	9.79	58.9	49	−6	0.81
500–525	0.9258	21.3	191	886	13.1	71.1	39	−9	0.84
525–550	0.9299	20.7	285	1322	17.5	88.6	52	−9	0.88
550+ (deasphalted oil)	0.9317	20.4	1457	6749	51.3	242	72	+3	0.52

Solvent Extraction

The majority of lubricating oil refining technologies use furfural, phenol and N-methyl-pyrrolidone (NMP) as a solvent. It is generally known that the thermal stability of furfural is low, while phenol has undesirable safety and health aspects. NMP is considered more advantageous, for it is non toxic, its physical and chemical characteristics are more favourable, and it dissolves the aromatics more selectively than either phenol or furfural. The main characteristics of the most widely used solvents: phenol. furfural and NMP are given in earlier publication (Ahmad *et al.*, 1995; Gardos *et al.*, 1982).

Keeping all these points into consideration dry NMP was selected as solvent for extraction to improve viscosity index and quality of the base oil. The conditions used for solvent extraction are shown in Table 7. The dewaxed oil (50 ml) and an appropriate amount of NMP solvent were mixed and agitated at 55 to 58°C for 20 minutes. The mixture was allowed to stand for 30 minutes to settle down. The upper layer (raffinate) containing the product was separated and stripped using initially a rotary vacuum evaporator and subsequently using a stream stripper. GLC analysis of the oil was performed which indicated that the solvent content has been reduced to traces in the base oil. The yield and properties of the oil after solvent extraction are tabulated in Tables 2, 8 and 9, respectively.

Table 7. Conditions used for solvent extraction of dewaxed oil

Solvent oil ratio	2:1
Temperature, °C	55–58
Number of stages	1
Extraction time, min.	20
Settling time, min.	30

DISCUSSION

The atmospheric residua (340$^+$°C) of Hamada and Sedra crude oils was distilled using a batch distillation apparatus made according to ASTM D1160

Table 8. Properties of processed (dewaxed and solvent extracted) distillate cuts of Hamada crude oil

Distillate cuts correspond to atm. distillation (°C)	*Spec. gravity at 15.6/15.6 °C*	*API gravity*	*Kin. viscosity at 40°C*		*Kin. viscosity at 100°C*		*Viscosity index*	*Pour point (°C)*	*Flash point (°C)*	*Total sulphur (wt.%)*	*Conradson carbon residue (wt.%)*
			(cSt)	*(SUS)*	*(cSt)*	*(SUS)*					
340–370	0.8371	37.5	7.55	50.6	2.11	33.2	66	−6	164	0.07	0.0225
370–400	0.8537	34.2	12.3	67.1	3.06	36.4	108	−6	180	0.03	0.0270
400–425	0.8607	32.9	21.1	103	4.00	39.5	73	−6	196	0.05	0.0271
425–450	0.8685	31.4	26.5	126	4.66	41.6	87	−6	210	0.11	0.0271
450–475	0.8755	30.1	52.9	246	6.66	48.0	69	−6	232	0.21	0.0273
475–500	0.8830	28.7	93.6	434	9.40	57.1	69	−6	258	0.18	0.0791
500–525	0.8871	28.0	155	718	13.1	70.6	71	−9	282	0.09	0.1026
525–550	0.8908	27.3	257	1191	17.7	88.8	68	−6	292	0.06	0.3427
550+ (deasphalted oil)	0.9076	24.4	994	—	44.1	207	82	0	>300	0.55	0.8529

Table 9. Properties of processed (dewaxed and solvent extracted) distillate cuts of Sedra crude oil

Distillate cuts correspond to atm. distillation (°C)	*Spec. gravity at 15.6/15.6 °C*	*API gravity*	*Kin. viscosity at 40°C*		*Kin. viscosity at 100°C*		*Viscosity index*	*Pour point (°C)*	*Flash point (°C)*	*Total sulphur (wt.%)*	*Conradson carbon residue (wt.%)*
			(cSt)	*(SUS)*	*(cSt)*	*(SUS)*					
340–355	0.8548	34.0	8.89	55.0	2.43	34.5	90	−6	166	0.11	0.033
355–395	0.8585	33.3	12.5	67.8	2.85	35.9	57	−9	178	0.14	0.054
395–421	0.8663	31.8	16.5	83.4	3.37	37.7	57	−6	188	0.17	0.089
421–450	0.8745	30.3	20.2	98.7	3.97	39.7	84	−6	218	0.25	0.070
450–475	0.8845	28.5	47.3	220	6.56	48.0	86	−6	231	0.30	0.150
475–500	0.8896	27.6	72.6	337	8.67	55.1	89	−6	250	0.33	0.068
500–525	0.8948	26.6	125	580	11.8	66.2	78	−6	274	0.39	0.064
525–550	0.8976	26.1	176	816	15.1	78.8	83	−6	295	0.45	0.094
550+ (deasphalted oil)	0.9110	23.8	937	4340	43.5	205	85	+3	248	0.42	2.080

method. The eight distillate cuts ranging from 340 to 550°C were prepared and vacuum residue was also collected. The vacuum residue (550$^+$°C) obtained from Hamada crude oil and Sedra crude oil, was then separately propane deasphalted and the oil contents were collected. They were found to be 8.28 wt.% and 11.34 wt.% on atmospheric residue for Hamada and Sedra crude oils, respectively. The deasphalted oil and other distillate fractions were subjected to dewaxing and solvent extraction. The properties of oils obtained after treatment are given in Table 8 for Hamada crude oil and Table 9 for Sedra crude oil. The plot of mid wt.% of yield versus kinematic viscosity at 40°C of processed oils is shown in Fig. 2 and Fig. 3 for Hamada and Sedra crude oils respectively. The yields of different grades of base stocks have been calculated and the cut range corresponds to these yields were calculated and presented in Table 10.

The distillate fractions after processing (dewaxing and solvent extraction) had viscosity index 66–108 in case of Hamada crude oil and 57 to 90°C in case of Sedra crude oil, and pour point −6 to −9°C in

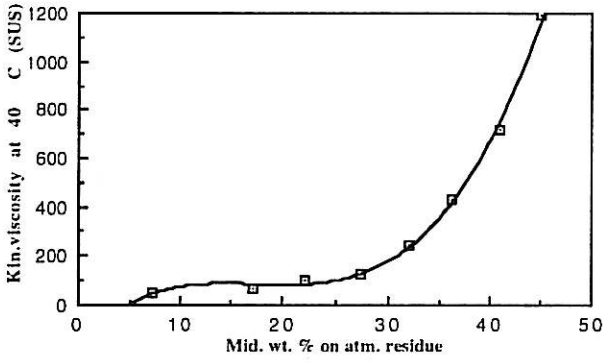


Fig. 2. Kin viscosity versus mid wt.% of yield of processed base oil of hamada crude oil.

case of both Hamada and Sedra crude oils. The deasphalted oils obtained from vacuum residua after dewaxing and solvent extraction had pour point 0°C in case of Hamada crude oil and +3°C in case of Sedra crude oil. The viscosity index (VI) of processed oils obtained from Hamada and Sedra crude oils are lower than the required in specifications of finished

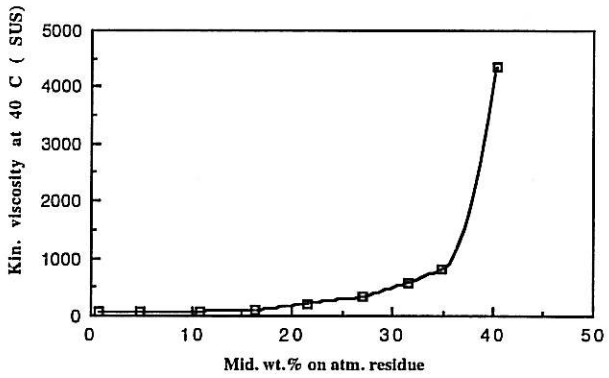


Fig. 3. Kin viscosity versus mid. wt.% of yield of processed base oil of sedra crude oil.

Table 10. Distillation range and yield of different class of base oils

Base oil	*Distillation range (°C)*		*Yield on atm. residue (wt.%)*		*Yield on crude oil (wt.%)*	
	Hamada crude	*Sedra crude*	*Hamada crude*	*Sedra crude*	*Hamada crude*	*Sedra crude*
Base stock for light lubricants	340–449	340–442	46.04	31.50	22.36	15.83
N 150	449–466	442–478	2.60	6.60	1.26	3.32
N 250	—	478–505	—	4.50	—	2.26
N 500	466–550	505–550	14.58	8.10	7.08	4.07
Bright stock	550+	550+	5.02	7.36	2.44	3.70

engine oils. Therefore, further processing or addition of a suitable additive of viscosity index improver is required to produce good quality engine oil from these base lube oils. Material balance of the yields of lube base stocks, wax content, aromatic content and asphalt content are given in Table 11. The yields of base stock to produce light viscosity range lubricants were found to be 46.04 wt.% on atm. residue (22.36 wt.% on crude) in case of Hamada crude oil and 31.50 wt.% on atm. residue (15.83 wt.% on crude) in case of Sedra crude oil. Recent reports in the literature (Singh *et al.* 1985) indicate that base oils of lower viscosity are required by the automotive sector to meet the need of fuel efficient multigrade lube oils. However, the volatility of such base oils need to be carefully controlled to avoid excessive oil consumption. These reports further indicate that friction modifiers have been found to respond best in low viscosity oils.

The above trends make the situation favourable towards the use of lube base stocks from Hamada and Sedra crude oils since the major potential of these oils are in lower viscosity range. The volatility

Table 11. Material balance of the process

Product	*Yield on atm. residue (wt.%)*		*Yield on crude (wt.%)*	
	Hamada crude	*Sedra crude*	*Hamada crude*	*Sedra crude*
Base oil for light viscosity lubricants	46.04	31.50	22.36	15.83
N 150	2.60	6.60	1.26	3.32
N 250	—	4.50	—	2.26
N 500	14.58	8.10	7.08	4.07
Bright stock	5.02	7.36	2.44	3.70
Wax content	3.72	8.56	1.81	4.30
Aromaticextract	7.35	9.22	3.57	4.63
Asphalt	20.69	23.12	10.05	11.62

Losses were calculated to be 1.04 wt.% on atm. residue in case of Sedra crude oil.

characteristics of these base oils can be improved by careful control of vacuum unit operation so that produced oils have less low boiling materials.

Although it is difficult to make any firm statement on the application aspect of formulated lubricants from Hamada and Sedra lube base stocks in the absence of any performance data, however, it is possible to state that it appears possible to formulate multigrade oils like 20W50, 20W40, and alike with the combination of the following:

(a) By the use of modern additive package of enhanced viscosity index increasing power.
(b) By the use of synthetic base oils as components in the base oil blend.

CONCLUSIONS

1. Obtained evaluation results indicate that Hamada and Sedra crude oils can be used to produce different grades of lube base stocks but the viscosity index of these base oils was found between 66 to 108 in case of Hamada crude oil and 57 to 90 in case of Sedra crude oil. Therefore, a suitable additive of viscosity index improver is required to produce good quality engine oil from these base lube oils.
2. Production potential of a substantially large amount (46.04 wt.% on atmospheric residue; 22.36 wt.% on crude oil in case of Hamada crude oil and 31.50 wt.% on atmospheric residue; 15.83 wt.% on crude oil in case of Sedra crude oil) of lube base stocks lies in the light viscosity range. Such type of base oils, according to the recent trends, can be used in the formulation of fuel efficient, multigrade motor oil along with the proper additive package and synthetic lubricants.

ACKNOWLEDGEMENT

The authors are thankful to the staff of the Industrial Processing Department of the Petroleum Research Centre for preparation of lube cuts and determining their properties. The authors are also thankful to PRC management for providing facilities and encouragement.

REFERENCES

Ahmad, I., Tuwil, AA., Buseiffi, M., Dabah, S. and Balat, A., 1995. Possibility of manufacturing lube base stocks from Brega crude oil. *Petrol. Res. J.*, **7**, 101–106.

Gardos, G., Kovacas, M., Szabo, T.K., Denes, F. and Miko, F., 1982. Investigation on energy conserving lubricating oil producing processes, *Hung. J. Ind. Chem.*, **10**, 257–266.

Singh, H., Gupta, P.C., Anwar, M., Chaudhry, G.S., Kishore, K., Kaushik, R.S., Kumar, M.M. and Lal, M., 1985. Possibility of manufacturing lube base stocks from BH crude. *Petrol. Asia J.*, 7, 150–157.

PRJ, Vol. 8 (January 1996): P. 75–78, 2 FIGS, 3 TABLES.

Production of Glycerine by Tungstate Catalyzed Oxidation of Allyl Alcohol by Hydrogen Peroxide: a Kinetic and Mechanistic Study

Iftikhar Ahmad* and Masood Degam*

دراسة تركيب وحركية أليل الكحول مع فوق أكسيد الهيدروجين في وجود التنجستات كعامل حفاز لنتاج الجلسرين

أفتخار أحمد و مسعود دغيم

تمت دراسة حركية ومكانيكية الحصول على الجلسرين من أليل الكحول بواسطة فوق أكسيد الهيدروجين في وجود تنجستات الصوديوم كعامل مساعد. كان التفاعل من الدرجة الأولى بالنسبة إلى أليل الكحول والعامل المساعد ومن درجة الصفر بالنسبة إلى فوق أكسيد الهيدروجين.

أما بالنسبة لحركية تكوين الجلسرين فهي عملية أكسدة أليل الكحول إلى جليسيدول ومن ثم إلى جلسرين وهي تعتمد على تأثير الملح وأحلاله لحركية تكوين الجليسيدول وهي عملية ترتكز على الضاحية القطبية (الكتروفيلك). وقد تم حساب طاقة التنشيط وكانت 68.9 (كيلوجول/مول$^{-1}$).

Abstract *The kinetics and mechanism of formation of glycerine from allyl alcohol by hydrogen peroxide in the presence of sodium tungstate as catalyst have been studied. The reaction is first order with respect to allyl alcohol and catalyst and zero order with respect to hydrogen peroxide. The mechanism of formation of glycerine is considered to be through epoxidation of allyl alcohol to glycidol and then hydrolysis of glycidol to glycerine. Based on substituent and salt effects the mechanism of formation of glycidol is believed to be concerted with considerable polar (electrophilic) character. The energy of activation has been calculated to be* 68.9 kJ mol^{-1}.

INTRODUCTION

Glycerine is a chemical which enjoys wide use in industry because of both its chemical and physical properties. Its major use as a chemical is in the manufacture of alkyds resins. Glycerine is also used in drugs, cosmetics, tobacco, food and beverages, explosives, manufacture of cellophanes and polyethers. Glycerine is produced as a by-product in soap industry. It is also produced (Lowenheim and Moran, 1975) synthetically as petrochemical from propylene via either allyl chloride or acrolein as intermediates. Another possible synthetic route of manufacturing of glycerine is from the oxidation of allyl alcohol by hydrogen peroxide using tungstic acid or its salt as catalyst. This paper describes the kinetics and mechanism of the formation of glycerine from allyl alcohol by hydrogen peroxide using sodium tungstate as catalyst.

EXPERIMENTAL

All the chemicals used were of B.D.H. (Analar) grade. Hydrogen peroxide was standardized (Kolthoff *et al.*, 1969) by permanganate method and allyl alcohol was standardized using bromate-bromide procedure (Lucas and Pressman, 1938). The ionic strength of the reaction mixture was maintained by the addition of sodium perchlorate. The pH of the reaction mixture was adjusted by addition of perchloric acid solution. In the kinetic runs, the concen-

*Petroleum Research Centre P.O. Box 6431, Tripoli, G.S.P.L.A.J.

tration of hydrogen peroxide was measured colorimetrically (Reichert *et al.*, 1939, Ahmad and Degam, 1991).

The kinetics of the reaction was followed by monitoring the concentration of hydrogen peroxide. Every run was at least 90% complete. After the reactants had reached thermostat temperature, the reaction was started by addition of hydrogen peroxide. The kinetics were followed by examining 5 ml aliquots of the reaction mixture for hydrogen peroxide content. The aliquots were added to a test tube which already contains 10 ml distilled water and 5 ml titanium sulphate solution to stop the reaction. Optical density of this solution was measured at 420 nm and the concentrtion of hydrogen peroxide was read from a calibration graph.

The concentration of glycerine was measured quantitatively by using gas chromatographic technique. Chrompack Packard Gas Chromatograph (model 439) equipped with flame ionization detector (FID) was used. The column was 10 m long and packed with the material used for analysis of acohols. Nitrogen was used as carrier gas. The yield of glycerine at pH 3.0 was found to be 95%. The presence of glycidol as an intermediate was also detected by pyridinium chloride-pyridine method (Jungnickel *et al.*, 1953).

RESULTS AND DISCUSSION

The progress of the reaction was followed by examining the concentration of hydrogen peroxide at different time intervals. The isolation method was applied for determining the kinetics of the reaction. In all experiments the concentration of allyl alcohol was at least fifteen times higher than the concentration of hydrogen peroxide. The disappearance of hydrogen peroxide in kinetic run obeys a simple zero order reaction. The plots of concentration of hydrogen peroxide versus time were good straight lines and their slope yields k_{obsd}. The pseudo-zero order rate constants (k_{obsd}) were found to be independent of the concentration of hydrogen peroxide. The results are reported in Table 1. The average k_{obsd} was found to be $3.45 \times 10^{-7} \pm 0.012 \times 10^{-7}$ mol dm^{-3} sec^{-1}.

The order of reaction with respect to sodium tungstate (catalyst) was determined by varying its concentration and keeping all other variables constant. The plot of k_{obsd} against the concentration of sodium tungstate was a straight line (Fig. 1) which passes through the origin. This shows first order dependence of rate on catalyst (sodium tungstate) concentration and it also confirms that there is no reaction in the absence of sodium tungstate. Similarly, the dependence of rate on allyl alcohol concentration was determined by varying its concentration while keeping all other variables constant. The observed pseudo-zero-order rate constants (k_{obsd}), when divided by allyl alcohol concentration, gave a constant value (Table 2). This shows that the order of reaction with respect to allyl alcohol is first order.

Table 1. Pseudo-zero order rate for tungstate catalyzed formation of glycerine from allyl alcohol by hydrogen peroxide

$[H_2O_2] \times 10^3$ (*M*)	$k_{obsd} \times 10^7$ (mol dm^{-3} sec^{-1})
2.50	3.45
3.00	3.47
3.50	3.44
4.00	3.46
4.50	3.45
5.00	3.44

$[Na_2WO_4] = 5.00 \times 10^{-4}$ M; [Allyl alcohol] = 0.10 M; Temp., 40°C; pH = 3.0; $\mu = 50.00 \times 10^{-4}$ M.

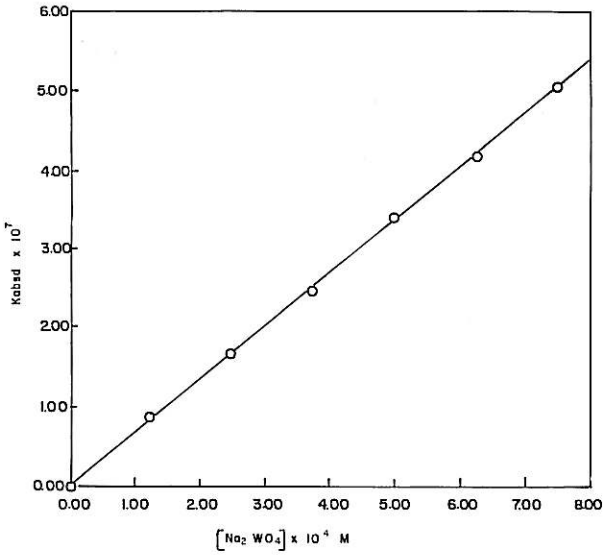


Fig. 1. First order dependence of rate on catalyst concentration $[H_2O_2] = 4.00 \times 10^{-3}$ M [Allyl alcohol] = 0.10 M pH, 3.0; Temp., 40°C.

Table 2. First order dependence of rate on allyl alcohol concentration for the formation of glycerine by hydrogen peroxide using sodium tungstate as catalyst

[*Allyl alcohol*]	$k_{obsd} \times 10^7$ (mol dm^{-3} sec^{-1})	$\frac{k_{obsd}}{[Allyl\ alcohol]} \times 10^7$
0.10	3.45	34.5
0.15	5.19	34.6
0.20	6.88	34.4
0.25	8.63	34.5
0.30	10.40	34.7
0.35	12.10	34.6

$[H_2O_2] = 4.00 \times 10^{-3}$; $[Na_2WO_4] = 5.00 \times 10^{-4}$ M; Temp., 40°C; pH = 3.0; $\mu = 50.00 \times 10^{-4}$ M.

In aqueous solutions tungstate gave tungstate anions by the following equation

$$WO_4^{2-} + H_2O \rightleftharpoons HWO_4^- + {}^-OH. \quad (1)$$

Preliminary studies have shown that the formation of glycerine from allyl alcohol is through the intermediate glycidol (epoxy allyl alcohol). Secondly at our experimental conditions, hydrogen peroxide does not bring about the formation of glycerine from allyl alcohol without the catalyst and the catalyst alone (without hydrogen peroxide) as well fails to bring about the formation of glycerine. These observations suggest that hydrogen peroxide oxidizes tungstic acid anion into peroxytungstic acid anion which then brings about the epoxidation of allyl alcohol to glycidol. The glycidol hydrolyses at low pH values and gives glycerine as the final product.

$$HWO_4^- + H_2O_2 \rightarrow HWO_5^- + H_2O. \quad (2)$$

It has been reported earlier (Beg and Ahmad, 1975) that the HWO_5^- is the active species for epoxidation reactions in such system. The most probable mechanism is as follows

$$CH_2{=}CH{-}CH_2OH + HWO_5^- \underset{k_2}{\overset{k_1}{\rightleftharpoons}}$$

(intermediate complex), (3)

(intermediate complex)

$$\xrightarrow{k_3} CH_2{-}CH{-}CH_2OH + H_2O, \quad (4)$$

$$\underset{\backslash\ /}{\overset{}{O}}$$

$$CH_2{-}CH{-}CH_2OH \xrightarrow{\text{Hydrolysis}}$$

$$\underset{\backslash\ /}{\overset{}{O}}$$

$$HOCH_2{-}CH(OH){-}CH_2OH$$

(Glycerine), (5)

$$\text{Rate of reaction} = k_3\,[\text{intermediate complex}]. \quad (6)$$

Applying steady-state approximation of the concentration of intermediate complex, we get

$$k_1\,[CH_2{=}CH{-}CH_2OH][HWO_5^-] - k_2\,[\text{intermediate complex}] - k_3\,[\text{intermediate complex}] = 0, \quad (7)$$

$$[\text{intermediate complex}] = \frac{k_1[CH_2{=}CH{-}CH_2OH][HWO_5^-]}{k_2 + k_3}. \quad (8)$$

Substituting the concentration of intermediate complex from equation (8) into equation (6), we get

$$\text{Rate of reaction} = k[CH_2{=}CH{-}CH_2OH]\,[HWO_5^-], \quad (9)$$

where

$$k = \frac{k_1 k_3}{k_2 + k_3}.$$

Since the formation of peroxytungstic acid anion from tungstic acid anion is assumed to be instantaneous and complete, equation (9) can be written as

$$\text{Rate of reaction} = k'[CH_2{=}CH{-}CH_2OH]\,[Na_2WO_4]. \quad (10)$$

This explains the order of reaction with respect to allyl alcohol, catalyst and hydrogen peroxide. Hence

$$\text{Rate of reaction} = k_{obsd}, \quad (11)$$

where

$$k_{obsd} = k'[CH_2{=}CH{-}CH_2OH]\,[Na_2WO_4]. \quad (12)$$

Increasing in ionic strength did not affect the reaction rate. This was confirmed by changing the ionic strength of the medium by addition of sodium perchlorate solution from 50.00×10^{-4} M to 300.00×10^{-4} M and determining the rate of reaction (k_{obsd}). In all the cases k_{obsd} was found to be the same within reproducibility limit of the experiments. The reaction rate of crotyl alcohol was performed under the same conditions as for allyl alcohol given in Table 1. In place of 0.10 M allyl alcohol, crotyl alcohol of the same concentration was used to observe the substituent effect of methyl group on reaction rate. The average value of k_{obsd} was found to be 3.84×10^{-7} mol dm^{-3} sec^{-1}. The faster oxidation rate of crotyl alcohol compared to that of allyl alcohol under identical conditions shows that the presence of methyl group at the double bond is rate enhancing. This points to an electrophilic addition which is generally observed in the corresponding reaction of olefins with organic peracids and in other three-centered additions (Swern, 1957). The salt effects and the methyl substituent effect described above give an insight into the nature of the transition state of the oxygen transfer from peroxytungstic acid anion to the double bonds of the olefinic substrate as described elsewhere (Ahmad and Degam, 1991). The mechanism of the reaction is given in Fig. 2.

The reaction was studied at six different temperatures ranging from 35°C to 60°C, and the results are given in Table 3. The plots of log k_{obsd} against recip-

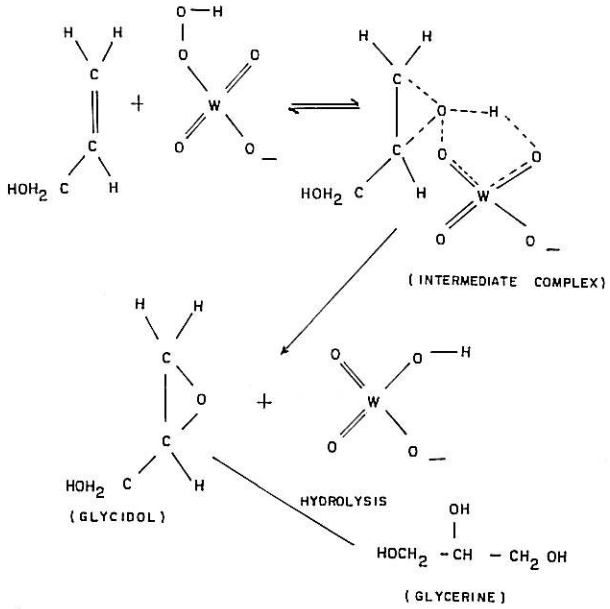


Fig. 2. Mechanism of the reaction.

Table 3. Dependence of rate on temperature

Temperature	$\frac{1}{T}\times 10^3$	$k_{obsd}\times 10^7$	$7+\log k_{obsd}$
308	3.25	2.18	0.3385
313	3.19	3.45	0.5378
318	3.14	4.87	0.6875
323	3.10	7.01	0.8513
328	3.05	11.22	1.0499
333	3.00	15.85	1.2000

$[H_2O_2]=4.00\times 10^{-3}$ M; $[Na_2WO_4]=5.00\times 10^{-4}$ M; [Allyl alcohol] = 0.10 MpH = 3.0; $\mu=50.00\times 10^{-4}$ M.

rocal of temperature gave a straight line. The energy of activation was calculated from the slope of the plot to be 68.9 kJ mol^{-1}.

ACKNOWLEDGEMENT

The authors are thankful to PRC management for providing facilities, encouragement and permission to publish this work.

REFERENCES

Ahmad, I. and Degam, M., 1991. The comparative catalytic activities of tungstate and molybdate ions in the epoxidation of maleic anhydride by hydrogen peroxide. *Petrol. Res. J.*, **3**, 53–56.

Beg, M.A. and Ahmad, I., 1975. Kinetics and mechanism of the epoxidation of fumaric acid with aqueous hydrogen peroxide catalyzed by sodium tungstate or sodium molybdate, *J. Catal.*, **39**, 260–264.

Jungnickel, J.L., Peters, E.D., Polgar, A., Weiss, F.T., Proskauer, E.S. and Weissberger, A., 1953. *Organic Analysis.* Wiley Interscience, New York, **1**, p. 136.

Kolthoff, M., Sandell, E.B., Meehan, E.J. and Stanley, B., 1969, *Qualitative Chemical Analysis.* 4th ed., Macmillan Co. Collier Macmillan Ltd., London.

Lowenheim, F.A. and Moran, M.K., 1975. *Industrial Chemicals*, 4th ed., John Wiley and Sons, p. 430.

Lucas, H.J. and Pressman, D., 1938. Determination of unsaturation in organic compounds by means of mercury catalysed reaction with standard bromate-bromide. *Ind. Eng. Chem., Anal. Ed.*, **10**, p. 140.

Reichert, J.S., McNeight, S.A., and Rudel, H.W., 1939. The colorimetric method of determination of hydrogen peroxide. *Ind. Eng. Chem., Anal. Ed.*, **11**, p. 194.

Swern, D., 1957. *Organic Reactions, Organic Peroxides*, John Wiley and Sons, New York, **2**, p. 378.